Final Technical Report DFID-FRP Project no. R7991

Annex 2:

Hydrological measurement protocol for montane cloud forest

Arnoud Frumau, Conrado Tobón, and Sampurno Bruijnzeel

28 February 2006

Part I: Introduction

I.1. General background

Tropical montane catchments carrying so-called cloud forests are widely considered to be prime suppliers of large volumes of high-quality streamflow. As the term cloud forest implies, these forests tend to be subjected to frequent or even persistent fog incidence. The fog is not only thought to represent an extra input of water to the ecosystem but also to suppress evaporation. As a result, for similar rainfall conditions amounts of streamflow emanating from cloud forest areas can be expected to be higher than the water yield from forests situated below the main cloud belt. Depending on the definition of what constitutes a cloud forest, and the methodology used for mapping their distribution, ecologically defined cloud forests have been estimated to make up only 1.4% of the world's remaining tropical forests but a recent climatically-based inventory indicated that as much as 12% of remaining tropical forest can be considered to be cloud-affected[1] (see Mulligan 2005 for details).

Hydrologically speaking, the inner workings of cloud forest ecosystems (of which various types can be distinguished that are found under progressively wetter and cooler climatic conditions) are only poorly documented and understood. There are several reasons for this. Firstly, many cloud forests are found in comparatively inhospitable places such as remote mountain ridges and summits or very steep slopes. In addition, many sites receive high rainfall amounts next to being frequently enshrouded in low cloud, making for excessively wet conditions. This presents major logistical difficulties for the execution of modern-day hydrological process research with its ample use of electronic equipment for measuring and recording climatic and other hydrological variables. Last but not least, fog is notoriously difficult to quantify whereas the windy conditions prevailing in many cloud forest areas (especially away from the equatorial tropics) present a further complicating factor when trying to determine areal rainfall inputs in complex mountainous terrain.

In short, closing the water balance for montane catchment areas with cloud forest is a major challenge. Yet, the need for reliable hydrological information on the hydrological functioning of tropical uplands is arguably greater than ever before. Populations in the lowlands (as well as in the uplands themselves) are rising steadily and are placing increasingly greater demands on natural resources. Fears have been expressed that the conversion of cloud forest to pasture or annual cropping may lead to diminished annual and seasonal water yields due to the loss upon forest removal of the extra amounts of cloud water stripped by tall forest vegetation.

In view of the nearly complete absence of reliable data on the hydrological consequences of converting cloud forest the project '*Hydrological impacts of converting tropical montane cloud forest to pasture, with initial reference to northern Costa Rica*' was initiated in spring 2002 with financial support from the Forestry Research Programme of the Department for International Development of the U.K. (FRP project no. R7991). Field measurements were conducted in cloud forests and pastures on the windward (Atlantic) side of the Sierra de Tilarán in northern Costa Rica between June-July 2002 and July-August 2004 by a multi-national research team led by the Vrije Universiteit Amsterdam and hosted by the Instituto Tecnológico de Costa Rica (Cartago).

After an initial description of the hydrological cycle in montane cloud forest and defining the main terms of the water balance, this report continues to describe in some detail the methods and equipment used (and partly developed) by the project to quantify the cloud forest catchment water budget under the prevailing climatic and topographic conditions. The methodological descriptions offered below are divided over four main sections relating to the quantification of: (i) rainfall and fog water inputs; (ii) energy budget and evaporation components; (iii) soil water dynamics and soil physical characteristics, and (iv) streamflow patterns and totals. An overview of the actual site locations and a listing of equipment used by the project is given in the Appendix.

[1] For maximum readability references to the literature are largely omitted in the general parts of this document. A list of further reading material is offered at the end.

In each section various approaches to quantifying a certain variable are introduced and the reasons outlined for adopting or adapting a particular method or piece of equipment to achieve optimum performance under the prevailing wet and windy conditions. Some examples are given of how the various data can be processed and presented in suitable formats for further use by third parties. A summary of the main results obtained by the project is given in the Final Technical Report for the project whereas further details will be published in a series of scientific papers planned for submission by project team members in the course of 2006.

Finally, it is pertinent to note that accurate quantification of catchment water inputs and outputs becomes more difficult as the scale of study increases because many of the water budget components are highly spatially variable and not readily interpolated from a few point measurements. Although spatial issues are addressed to some extent in the present document, the reader is referred to Annex 3 (distributed hydrological modeling at the operational catchment scale) and, particularly, to chapters 2 and 4 in Annex 4 (idem at local to national scale) to the Final Technical Report on the overall project.

I.2 The hydrological cycle in a cloud forest ecosystem

The principal components of the general forest hillslope hydrological cycle are shown in Figure I.1.

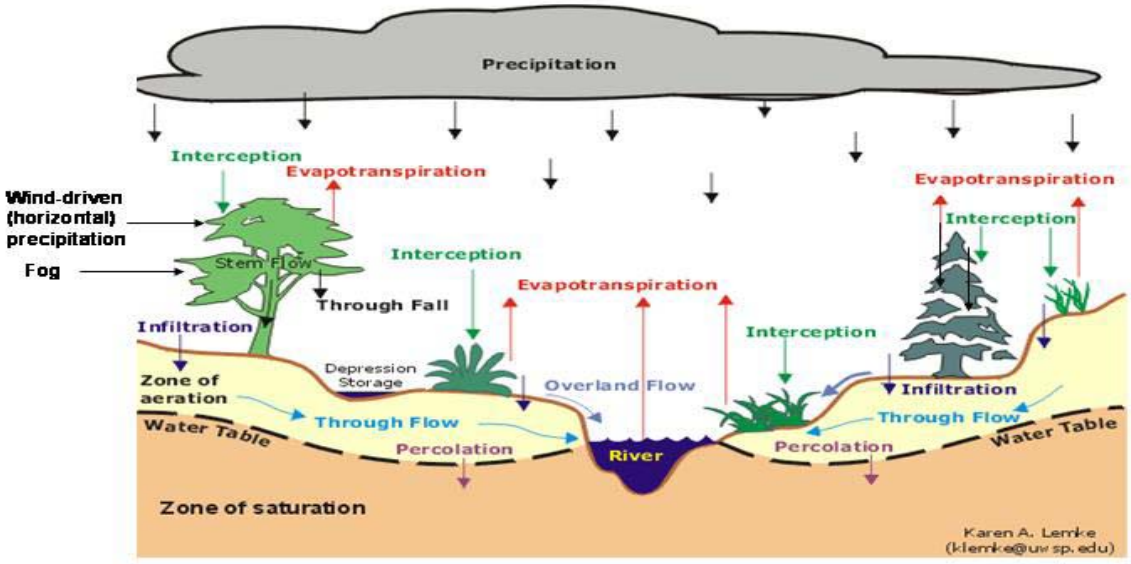

Figure I.1. *Conceptual representation of the cloud forest hydrological cycle.*

Rainfall *(P)* is the most important input of water to most forests, but in coastal or montane fog belts so-called 'occult' precipitation (i.e. cloud water / fog not picked up by an ordinary rain gauge, *CW*) can be important too. Under particularly windy conditions part of the occult precipitation arriving horizontally (or parallel to the surface) may also consist of wind-driven rain. Where no distinction can be made between fog and horizontal rain, the term horizontal precipitation (*HP*) is used below to denote the sum of the two occult precipitation components.

A small proportion of the precipitation reaches the ground without touching the canopy ('direct' or 'free' throughfall). Another (usually small) part flows down along branches and stems as stemflow *(Sf)*. A considerable portion of the precipitation hitting the canopy evaporates back into the atmosphere

during and shortly after the storm (interception loss, *Ei*), while the remainder reaches the forest floor as crown drip. Because it is impractical to separate direct throughfall and crown drip, the two are usually lumped and simply referred to as throughfall *(Tf)*. The sum of throughfall and stemflow is often termed net precipitation and normally substantially smaller than *P* because of interception losses unless there are significant contributions by occult precipitation (*CW* and/or *HP*).

If the intensity of net precipitation falling on sloping ground exceeds the capacity of the soil to absorb the water, the excess runs off as 'Hortonian' or 'infiltration-excess' overland flow *(HOF)*. Given the generally high absorption capacity of the organic-rich topsoil in most forests, this type of flow is rarely observed in undisturbed forest unless there is an unusually dense clayey substrate or an excessive concentration of stemflow.

A considerable part of the net precipitation infiltrating into the soil is taken up by the roots of the vegetation and returned to the atmosphere via transpiration *(Et)*. The term evapotranspiration *(ET)* is often used to indicate the sum of transpiration (evaporation from a dry canopy), interception loss (evaporation from a wet canopy) and evaporation from the litter and soil surface *(Es)*. The latter term is usually small, especially in dense forests where little radiation penetrates to the forest floor, humidity is maintained at high levels and ventilation is limited.

If not obstructed by an impermeable layer in the soil, the water not taken up by the vegetation will move to the groundwater table via vertical and lateral downslope percolation and then flow laterally to the nearest stream as groundwater feeding the 'baseflow' or 'delayed' flow of the stream (Figures I.1 and I.2).

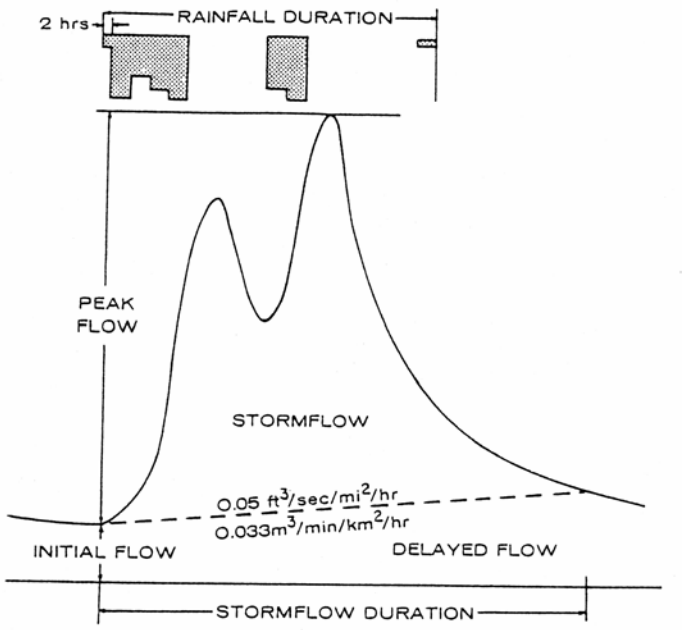

Figure I.2. *Definitions of baseflow (delayed flow), stormflow (quickflow) and peak flow.*

Alternatively, the percolating water may be deflected upon meeting impermeable subsoil or rock. Such slow, laterally draining 'throughflow' helps to maintain the typically wet zones found around headwater streams, thereby augmenting the stream's baseflow. During rainfall, infiltrated water may take one of several routes to the nearest stream channel, depending on the soil's hydraulic conductivity profile with depth, slope form and steepness, and the spatial distribution of soil moisture already present. 'Saturation overland flow' *(SOF)* is caused by rain falling onto an already saturated soil, as typically occurring in hillside depressions or on concave footslopes near the stream (Figure I.1).

More widespread hillside *SOF* (i.e. outside the riparian zone and depressions) has been observed sometimes during intense rainfall in the tropics in places with an impeding soil horizon at shallow depth. Rapid lateral throughflow during storms ('subsurface stormflow', *SSF*) usually represents a mixture of 'old' (i.e. already present in the soil before the rain) and 'new' water traveling through 'macropores' and 'pipes'. Due to the contributions by *SOF*, *SSF*, and in extreme or disturbed cases also *HOF*, streamflow usually increases rapidly during rainfall. The increase above baseflow levels is called 'stormflow' or 'quickflow' whereas the highest discharge is referred to as 'peak flow' (Figure I.2). Peak discharges may be reached during the rainfall event itself or as late as a few days afterwards, depending on catchment size and steepness, soil depth and water content, and the duration, intensity and quantity of the rainfall. The total amount of streamflow discharged from a catchment area over a certain period of time (usually a month, season or year) is called 'water yield' (expressed in mm).

I.3 General methodological considerations

When trying to assess the effect of land cover change on amounts of streamflow, a 'direct' comparison of flows from catchments with contrasting vegetation covers can be problematic for several reasons. First, there may be complications caused by local contrasts in rainfall, radiation and wind, or ungauged underground transfers of water from one catchment to another (leakage *L*). The same applies to a comparison of flows from a single catchment before and after a change in cover. The classic response to such problems has been the 'paired catchment experiment' in which the streamflow from two (usually adjacent) catchments of comparable geology, topography, exposure and vegetation are expressed in terms of each other (using regression analysis) during a 'calibration phase' (Figure I.3). Once a robust baseline calibration relationship has been obtained, one of the catchments is subjected to manipulation of its cover (e.g. clear-felling) while the other catchment remains undisturbed as the 'control'. Throughout this 'treatment' phase, streamflow from both catchments continues to be monitored. Any effects of the treatment are evaluated by comparing the actually measured flow totals from the manipulated catchment with the flows that would have occurred if the catchment had remained undisturbed. This is usually achieved by inserting streamflow totals determined for the control catchment into the calibration relationship (Figure I.3).

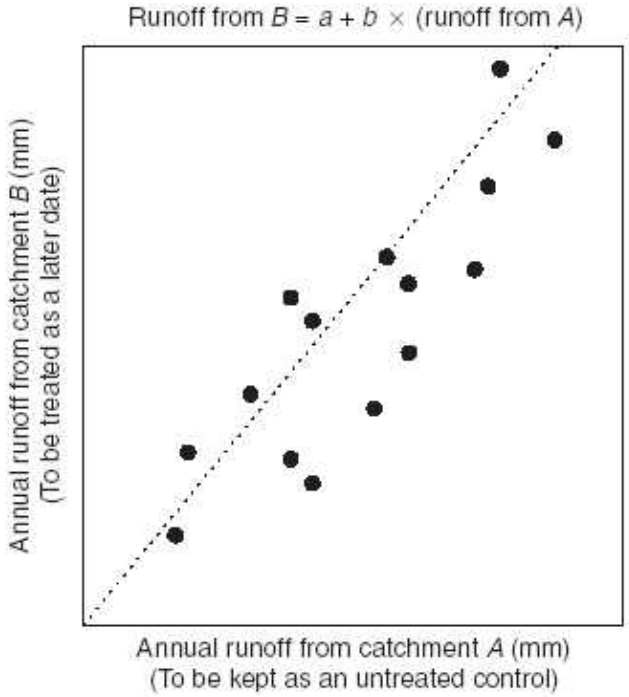

Figure I.3. *The paired catchment technique*

Although a more rigorous assessment of the hydrological impacts can be obtained in this way than in the case of a 'direct' comparison of flows, the tacit underlying assumption is that differences in leakage between the two catchments remain unchanged with time, regardless of catchment cover status. Also, to avoid unjustified extrapolation of the calibration relationship to accommodate extremes in streamflow during the treatment phase (e.g. due to excessive rainfall or drought), it is imperative for the calibration period to include both wet and dry years. This makes the paired catchment method a time-consuming (typically >5 years) and thus expensive affair. More importantly, the method is essentially a 'black-box' requiring additional hydrological process research to reveal the relative importance of different causative factors to explain the observed changes in streamflow. After all, without such process knowledge, results cannot easily be applied outside of the test catchments, where climatic or land conditions may be somewhat different.

Last, but not least, it is virtually impossible nowadays to obtain permission for the catchment-wide experimental felling of old-growth tropical forest, and even more so in countries where montane forest conservation and ecotourism are high on the agenda. All this, plus the limited resolution afforded by the paired catchment approach (usually more than 20% vegetation cover change required for effects on streamflow to be detectable in small headwater catchments), has led to a general decline in the number of such studies in the last few decades and to increased emphasis on computer simulations.

Therefore, a *process-based, bottom-up approach was adopted in which the successive hydrological processes that together determine amounts of streamflow (rainfall, fog water interception, wet canopy evaporation, infiltration, soil water uptake, vertical and lateral drainage) were quantified (and modeled as required) separately*.

The general annual water balance equation for a catchment in the cloud belt reads:

$$P + HP = ET + Q + \Delta S + L$$

where:

P = rainfall (areal)
HP = (near-) horizontal rainfall and fog stripped by the vegetation
ET = evapotranspiration
Q = streamflow
ΔS = change in soil water and groundwater storages (+ or -)
L = apparent underground catchment leakage (or gain).

All values are expressed in mm $year^{-1}$.

Furthermore: $ET = Et + Ei + Es$

where *Et* = evaporation from a dry vegetation surface (transpiration or soil water uptake); *Ei* = evaporation from a wetted vegetation surface (interception evaporation); and *Es* = evaporation from the bare soil (negligible in dense vegetations).

Finally: $Q = Qb + Qs$

where *Qb* = baseflow (groundwater outflow between rain storms) and *Qs* = stormflow (the increased discharge during and shortly after rain storms, often also called 'quickflow'; see also Figure 2).

By describing the various hydrological processes mathematically and defining the respective feedback mechanisms in a quantitative manner it becomes possible to predict the behaviour of the vegetation under different climatic conditions. By also selecting catchment areas with year-round flow and streams that have incised into solid bedrock, and measuring groundwater levels and subsoil hydraulic conductivities, one should be able to minimize the risk of obtaining biased streamflow results, also because independent estimates of vegetation water use can be made (e.g. using micro-meteorological or plant physiological techniques). In other words, once all measurable components of the catchment water budget (i.e. all gains and losses) are quantified, the deep leakage term *L* can be evaluated by solving the water budget equation for *L*. Thus, after correcting for contrasts in deep leakage losses between catchments, the flows from forested and cleared catchments can be compared more reliably than would be possible through a 'direct' comparison.

An important complication rendering the application of the catchment water budget approach less than straightforward under the climatic conditions prevailing in many cloud forest areas is the following. The combination of strong winds and low rainfall intensities tends to produce substantial amounts of 'horizontal precipitation' in the form of wind-driven rain that, like fog, largely bypasses traditional rain gauges. Indeed, the very high runoff to rainfall ratios – as well as throughfall to rainfall ratios - that have been reported for some cloud forest areas may well reflect such unmeasured wind-driven rainfall inputs instead of high fog water inputs *per se*, as is commonly assumed. In addition, such wind-affected precipitation inputs can be expected to vary enormously in space due to variations in site exposure, the presence or absence of intercepting obstacles (e.g. tall trees vs. short grass) and slope steepness.

Thus, the success or failure of the catchment water budget approach in wet and windy cloud forest headwater areas hinges on the proper quantification of spatial patterns of rainfall and fog water inputs, and much attention has to be paid to develop methods to measure and predict these adequately.

Part II. Quantifying rainfall and fog inputs in a cloud forest setting

II.1 Introduction of terms

Precipitation in liquid form consists of **rain** or **drizzle**. Rain consists of water droplets exceeding 0.5 mm in diameter, with terminal velocities exceeding 200 cm/s. Drizzle consists of smaller, more uniformly distributed water droplets of 0.1 - 0.5 mm (associated terminal velocities 25-200 cm/s) that appear to float while they follow the prevailing air currents. Unlike fog droplets, which tend to remain in suspension until scavenged by vegetation or other objects upon passage of the foggy air, drizzle falls to the ground. Drizzle is usually produced by low stratus clouds and is frequently accompanied by low visibility and fog. **The amount of precipitation** is usually measured with a fixed **rain gauge** and expressed in millimetres of water depth at a given point over a specified period of time[2]. **The intensity of rainfall** may be classified as: i) 'light' (<2.5 mm/hr, ii) 'moderate' (2.5 - 7.5 mm/hr), and iii) 'heavy' (> 7.5 mm/hr). In addition, for each class the maximum rate of fall should be no more than a tenth of its upper limit in six minutes. **The intensity of drizzle** is usually classified as: i) light (<0.3 mm/hr), ii) moderate (0.3 - 0.5 mm/hr), and iii) heavy (>0.5 mm/hr. When precipitation equals or exceeds 1 mm/hr, most if not all of the precipitation usually consists of rain.

The very presence of a rain gauge within the wind field has a **distorting effect on the flow of the air** above the gauge orifice and measured amounts will need to be corrected for this. In addition, **precipitation often falls at an angle** (measured from the vertical) due to wind, with drizzle being more susceptible to wind effects than rain, due to the smaller inertia of the associated droplets. The greater the inclination of the rain, the more the catch will represent an underestimation of 'true' rainfall. A further complication is introduced when such inclined precipitation falls onto complex mountainous terrain. Slopes facing the inclined rainfall will tend to catch much more precipitation than do slopes 'facing away' from the rain.

After introducing several types of rain gauges, the various corrections of measured rainfall that need to be applied to estimate 'true' rainfall under the wet and windy conditions prevailing in many cloud forest areas are discussed in some detail in the sections below. However, because it is difficult in practice to separate fog water (i.e. wind-driven cloud) from near-horizontal wind-driven rain, we will first define fog and introduce the **concept of potential precipitation**.

Fog is a cloud formed or lying on the ground and is defined by international agreement as being associated with a **visibility less than 1,000 m**. Cloud fragments which fill low spots or hollows in the terrain are patchy fogs that do not fit the visibility requirement. The visibility reduction in fog depends on the concentration of cloud condensation nuclei and the resulting distribution of droplet sizes. The liquid water content (*LWC*) of fog is related to visibility, although in a highly non-linear manner. Fog with very low visibility does therefore not necessarily have a higher LWC than fog with higher visibility. Cloud droplets are generally 1 - 20 µm in diameter. This allows fog and low cloud to hang seemingly suspended in the air and to be transported by modest winds and turbulence. For consistency with the definitions of rain and drizzle, fog is defined here in terms of its droplet size and corresponding terminal velocity in still air. Fog is comprised of **droplets with diameters of less than 100 µm** and a settling velocity lower than 25 cm/s, with small droplets reducing visibility more efficiently than larger droplets do.

The fog interception efficiency of vegetation differs for tall (forest, trees) and short (pasture, crops) vegetations. Thus, the actual amount of fog caught depends on the duration and *LWC* value of the fog, the prevailing wind speed, and the trapping efficiency of the vegetation. In windy tropical montane areas or coastal fog belts that are frequently immersed in cloud, the extra amount of fog water stripped can be significant, therefore. Various approaches towards measuring fog will also be discussed below.

[2] Strictly speaking, any minor amounts of dew and fog settled onto the gauge orifice during still conditions are included in a measurement by a rain gauge. Although the main pathway to the surface is by contact with surface irregularities, this atmospheric water falls under gravity too (albeit at a very slow rate) and hence classifies as precipitation.

T**he total liquid water** in the atmosphere thus may consist of rain, drizzle and/or fog and may precipitate onto a surface or stay in suspension, depending on droplet size, wind speed and atmospheric turbulence. The **potential precipitation** ($\mathbf{P_{pot}}$) at a given point in space may be defined as the potential water depth reaching a plane that is orientated perpendicularly to the average trajectory direction of the water drops over a specified period of time. The vertical component of this potential water depth is measured as precipitation (**P**) by a conventional rain gauge (cf. section III.2.1). This measurement must be considered as being *non-conservative* because of its dependence on wind speed and hence site exposure. The horizontal component of the potential precipitation, **horizontal precipitation** (**HP**), can be measured with a passive fog gauge as described in section II.2.2 below. This latter measurement is the integration (summation) of: (i) the horizontal component of the inclined precipitation, (ii) horizontal wind-driven precipitation (**WDP**), and (iii) fog (**F**). The potential precipitation (P_{pot}) and its effective angle can be derived from measurements of *P* and *HP* (including fog), using simple trigonometry (Figure II.1 and section II.4.3.2 below).

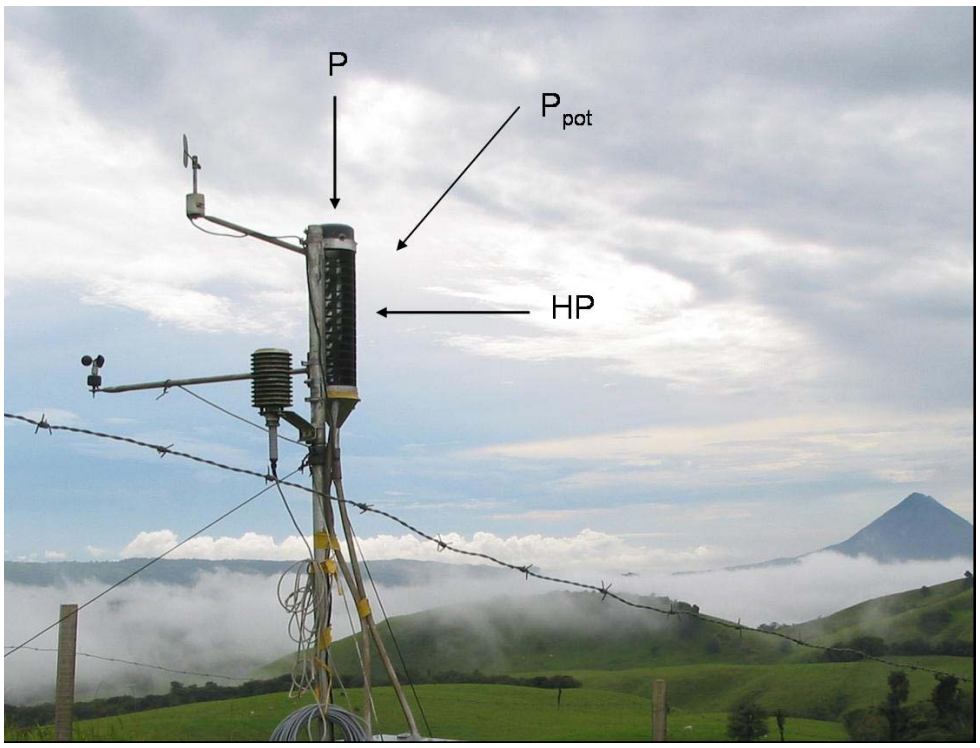

Figure II.1. *Inclined rainfall and its vertical and horizontal components as measured by a modified Juvik-type gauge.*

P_{pot} can be considered a *conservative* parameter in the case of inclined precipitation (assuming negligible phase changes). This is acceptable for small spatial scales. Amounts of horizontal potential precipitation consisting of fog and / or wind-driven rain, on the other hand, depend on local wind speeds, with higher wind speeds producing larger fluxes. As such, these are site-specific. Large differences in space and time as well as with height above the surface exist for horizontal fluxes. As a first estimate, a measurement of potential precipitation at a single measurement site is assumed to represent the mean spatial potential input for a small catchment. Knowledge of the precipitation angle then allows calculation of the input to differently orientated slopes (section II.4). Wind speeds, turbulence and flow direction (geographic direction as well as upward or downward components) all modify the precipitation angle and as such detailed information about the air flows in the area is desirable, especially for slopes with orientations that differ from the slope where the point measurement is made.

II.2 **Instrumentation for the measurement of precipitation and fog**

Instrumentation for measurement of rainfall and fog varies widely and no universal standard is clearly defined. The commission of Instruments and Methods of Observation (CIMO) of the World Meteorological Organization (WMO) aims at the global standardization of meteorological observations and improving the long-term quality of the measurements. Although a standard for meteorological observations is preferred for weather prediction purposes the instrumentation of most research projects will be specific to the project's objectives. This holds even more in the case of remote, wet and windy cloud forest sites. The following sections describe the instrumentation used or developed within the current project for the quantification of precipitation, fog, throughfall and stemflow (see also Appendix for details on specific instruments). The various quality checks and corrections applied to the measurements are described in section II.4 below.

II. 2.1 *Precipitation*

A rain gauge measures the amount of liquid or solid (in the case of snow) precipitation on a horizontal plane (*P*, mm) over a set period of time (ranging from minutes to hours, days, months or a year). Types of rain gauges include manually read **standard rain gauges** and **ground-level** (**buried pit) collectors**, as well as **recording gauges** or **tipping bucket gauges**. Each type has its specific advantages and disadvantages for collecting rainfall data. The standard rain gauge consists of a funnel attached to a graduated cylinder that fits into a larger container. There are more than 50 types of manual, national standard rain gauges in use around the world. These differ considerably in design, shape, size and material. The orifice area varies from 7 to 1,000 cm^2, although most gauges have an area of 100-200 cm^2. Materials used for the gauges are primarily galvanized iron sheets and copper but PVC plastic is popular as well. The installation height varies between countries from 0.2 to 2.0 m but some 90 countries use installation heights of 1 m and less. A height of 30 cm abouve ground level was used in the current project. Several types of gauges have some form of permanent windshield, the most widely used of these is the Alter shield. The standard rain gauge provides a point rainfall estimate over a specified time period (most often one day, with the gauge usually emptied in the early morning).

The **standard rain gauge** (totalizer, Figure II.2) used in the current project had an orifice of 100 cm^2 on top of a 12 cm diameter PVC pipe (25 cm high and closed cap fitted at the bottom). A graduated cylinder (250 ml) was placed inside and read daily every early morning. A metal holder with a downward vertical pin welded onto it was pushed into the ground to hold the gauge securely in place and the orifice in level position. Standard gauges were used throughout as a reference and back-up for the recording gauges described below. In addition, a series of totalizer gauges was used to assess the spatial variability of rainfall in pasture areas, something that is not as easily achieved in areas carrying tall forest as access above the canopy is usually limited to one or two sites at best. Wind-shielding can be applied to reduce the sensitivity of wind-losses of the gauge. Locally purchased plastic baskets were tested as a cheap and easy alternative to more expensive commercially available shields (Figure II.2; see also section II.4.1).

Spherical rain gauges have been advanced in recent years as an alternative approach to quantify rainfall under windy conditions. Spherical gauges of two different designs (described originally by Chang and Flannery, 2001) were constructed and installed on a tower above the forest canopy during the later stages of the project (March – June 2005) for comparative purposes (Figure II.3). The two gauges have been designed in such a way as to present the same effective orifice surface, regardless of the precipitation angle. In theory, therefore, spherical should provide a measurement of potential precipitation. However, it is to be expected that the non-pervious spherical gauges also cause distortion of the air flow around and above them and therefore the collected water volumes would represent an underestimation. In addition, the effective gauge orifice of 316 cm^2 valid for vertical precipitation needs to be corrected for the partly open structure of the lower half of the sphere which presents a reduction in effective gauge surface with increased precipitation inclination (section II.3.2).

Figure II.2. *Left-hand panel: Different types of rain gauges installed on top of a 25 m high scaffolding tower extending above the cloud forest (canopy height 20-22 m). From left to right: standard manual gauge, Campbell ARG100 automatic rainfall recorder, custom-built VUA rainfall recorder, and shielded standard rain gauge. Right-hand panel: Custom built VUA recording gauge with tipping bucket and data-logger installed inside a pvc-box with funnel fitted on top.*

Figure II.3. *Spherical rain-gauge experiment. Installation on top of the tower (left) and detailed view of spherical gauges using cylinders (right top) and vanes (right bottom). Also shown (centre) is a modified Juvik cylindrical fog gauge used for the evaluation of potential precipitation.*

Recording rain gauges provide important additional information on rainfall characteristics such as rainfall intensity (and variations therein during storms) and event duration. The temporal resolution of the recorder depends on the type of gauge but it is often set at hourly values. In the current project **tipping bucket-type recording gauges** such as the ARG100 (Campbell Scientific Inc, 0.2mm resolution) and the custom-built VUA-gauge (Vrije Universiteit Amsterdam, 0.07mm resolution) were used (Figure II.2). The latter recorder had an orifice of 510 cm^2 to allow for greater measurement resolution. Technical specifications of the ARG100 and similar rainfall recorders can be found at www.campbellsci.com, whereas the VUA-type can be constructed from locally purchased orifices (plastic or preferably metal funnels) and tipping buckets (e.g. WS7048, www.lacrossetechnology.fr).

The resolution of the rainfall measurement depends on the combination of orifice and tipping bucket size (cf. Figure II.6 below). A resolution of at least 0.2 mm is preferred, although the choice depends on the data-recording capacity and data-retrieving scheme as well. The number of 'tips' of the tipping bucket system counted **per minute** need to be recorded by a watertight data logger. The project employed numerous recorders (type Tinytag-Plus TGPR-1201, Gemini Data loggers Ltd., UK, www.geminidataloggers.com) that were placed at the measurement location itself (Figure II.2 right-hand panel and Figure II.4). In addition, programmable multi-channel data loggers such as the CR23X and CR10 manufactured by Campbell Scientific Inc. (www.campbellsci.com) were used at locations where rainfall was recorded along with other weather variables or soil moisture content (Figures II.4 and II.5).

Figure II.4. *The CR10X-datalogger of Campbell Scientific (top left), the Tinytag single channel puls datalogger (top right) and power supply by batteries charged in turn by solar panels (bottom).*

Figure II.5. *CR23X-datalogger for automatic data recording (left). An AM416 relay multiplexer is used to increase the number of input channels to the data logger (right).*

Calibration of tipping buckets

All tipping buckets were calibrated in the laboratory and in the field about 15-20 times by recording the number of tips generated by pouring a pre-set volume of 280 ml of water into a funnel at a controlled flow rate (Figure II.6). Typical flow rates were 1-11 ml/min which is equivalent to 1.0-11.0 mm/hr for a gauge orifice of 100 cm^2. The WS7048 tipping bucket employed by the project has a 4 ml capacity according to the manufacturer but it was found to vary between 3.51 and 4.60 ml among the 27 tipping buckets tested. It was assumed that these calibrations are also valid for flow rates outside the specified range as no significant differences were found between the extremes of the tested flow rates. The tipping bucket capacity of the ARG100 recording gauge (0.2 mm) was verified through *in situ* calibration (adding preset volumes of water to the gauge).

Figure II.6. Left: Calibration of tipping buckets (type WS7048) at the field laboratory Santa Elena, Costa Rica; centre: in situ calibration in the field; right: close-up of tipping bucket.

The calibrations were validated by comparing daily catches of the recording gauges with those of the standard gauges under conditions of low wind speed (<1.5 m/s) to minimize the influence of wind-induced losses. Wind losses for the selected records were negligible, as evidenced by the negligible differences in catch for shielded and unshielded standard gauges (cf. Figure II.2).

II.2.2 *Fog instrumentation*

A distinction can be made between qualitative (visibility) and quantitative (*LWC*) measurements of fog. Below, low-cost, passive fog gauges and a cloud-water spectrometer system are described, along with instrumentation for the determination of the onset and duration of fog.

Fog gauges have less than 100% efficient collection either due to fractional sampling of the air passing the gauge or by flow distortion around the gauge. As such, fog during precipitation-free periods is underestimated, especially for short intermittent fog events, because of additional losses by wetting of, and evaporation from the gauge surface. Little is known of the relative performance of the more widely used passive fog gauge types, particularly under the conditions of low-intensity rain and strong winds that are observed at so many cloud forest sites. Therefore, the collection efficiencies of the gauges used by the project were determined during fog conditions by comparison with the liquid water content as measured directly by a fog droplet spectrometer (section II.2.2.2). In addition, performance of the three gauge types was compared for conditions of low-intensity rain and strong winds. Three structurally different passive fog gauges (wire harp, Juvik-type, and Daube-type tunnel gauge) as well as modifications of these gauges were used in the current project (Figure II.7). These all diverted the collected water to tipping buckets that were similar to those used in most of the rain gauges described in the previous section.

Figure II.7. *Passive fog gauges, from left to right: rotating Daube tunnel gauge, wire harp, and modified Juvik-type fog gauge as installed on top of a scaffolding tower to allow measurements to be made above the cloud forest canopy*.

II.2.2.1 Passive Fog-gauges

Being the cheapest to construct, the **wire harp** was the fog gauge of choice at the beginning of the project and it was installed initially at all project sites (see Appendix for locations). Wire harps of 2500 cm^2 cross-sectional area using 0.8 mm diameter nylon strings (Nylon80 as used for fishing) spaced 2 mm apart were installed about perpendicularly to the main fog-carrying wind direction to measure fog. Because the gauges were not covered against precipitation, the catch also included horizontal precipitation (Figure II.7, right-hand panel). Both the effective cross-sectional area and fog-catching efficiency of the wire harp depended on the wind direction. The resolution varied but was typically 0.015 mm per tip for wind blowing perpendicularly to the screen.

During conditions of fog-only (i.e. no precipitation), the collection efficiencies of all three passive fog gauges were found to depend on wind speed, droplet size and fog *LWC*. However, the actual efficiency could be approximated from a linear relation against the horizontal cloud water flux (CWF) measured by the collector itself. For the wire harp:

$$C_{effWH} = 0.29 * C_t * CWF_{WH} + 0.14$$

where C_{effWH} is the collection efficiency of the wire harp, C_t is a time normalization factor equal to 30 divided by the sampling period in minutes, and CWF_{WH} is the cloud water flux measured by the gauge itself. The collection efficiency under fog conditions as derived for the wire harp was usually less than 0.30 (Figure II.8a) and much lower than for the more robust Juvik-type gauge (see below). In addition, the catch of the wire harp during conditions of wind-driven rain was strongly dependent on wind speed and decreased rapidly for wind speeds above 3-4 m/sec when droplets trapped by the device were blown off the strings again (Figure II.8b). Hence the wire harps were quickly replaced with a modified Juvik-based design (see below).

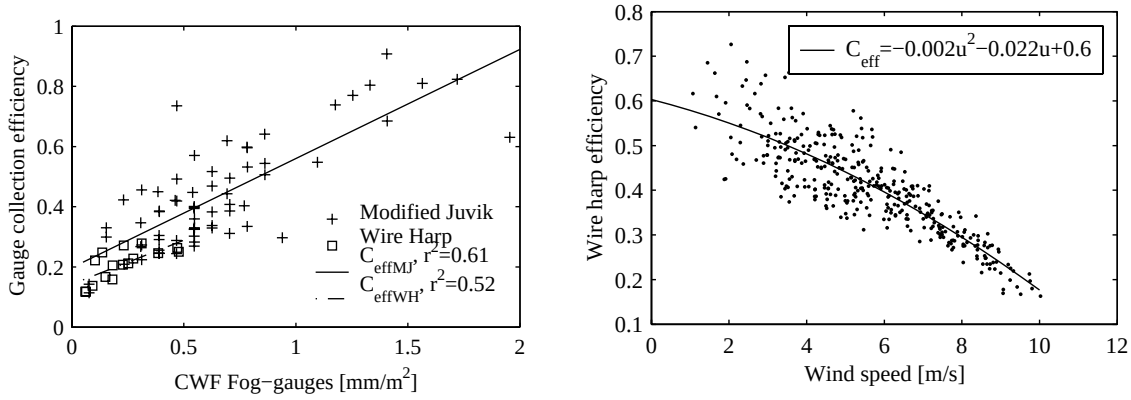

Figure II.8 (a) C*ollection efficiencies (relative to fog spectrometer value) for wire harp and modified Juvik gauge during conditions of fog-only.* (*b*) *Fog-collection efficiency of wire harp during conditions of wind-driven rain showing strong effect of wind on gauge performance.*

A Daube-type **tunnel gauge** is a two-stage gauge capable of separating horizontal precipitation *HP* into wind-driven rain (*WDP*) and fog (*F*). A rotational type can be used which aligns itself to the wind. Only one such gauge was used by the project for comparative purposes because of the high construction costs and size of the device. Any HP passing the 610 cm^2 intake orifice is separated into WDP (collected in the first stage by impaction on a 45° angle ramp inside the tunnel) whereas the smaller and lighter fog droplets are led further on to the second stage with two wire harps (625 cm^2) placed in series and having two rows of nylon strings each (Figure II.7).

The original **Juvik-type fog gauge** consists of a louvered cylindrical aluminium screen of 40.5 cm height and 540 cm^2 cross-sectional area (Phifer Shadescreen; see www.asmfg.com/shade.htm). The cylindrical screen catches any fog and/or rain falling at an angle. Although this gauge is sometimes equipped with a metal hat to prevent vertical rain from entering the gauge (Figure II.9), no attempt was made in the present case in view of the prevailing low-intensity rains and strong winds. Instead, the gauge was capped by a second funnel (100 cm^2) to allow the separate measurement of vertical rain (*P*) (cf. Figures II.1 and II.7 right). The measurement resolution of the modified Juvik gauge is 0.07mm for *HP* and 0.4 mm for *P*. As the gauge measures all precipitation components (i.e. *P* and *HP* including *F*) it can be considered a **potential precipitation gauge** (*sensu* Figure II.1) although it should be noted that the gauge does not separate fog from horizontal rain.

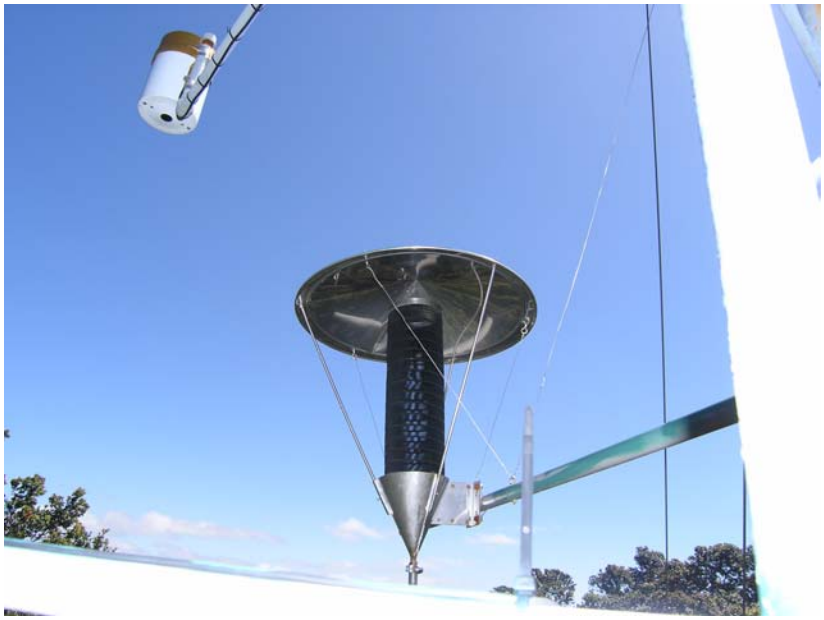

Figure II.9. *Classic Juvik fog gauge with hat to keep vertical rain out.*

The collection efficiency of the modified Juvik gauge during times of fog-only was much better than that for the wire harp (Figure II.8a) but very similar to that for the tunnel gauge:

$$C_{effMJ} = 0.36 * C_t * CWF_{MJ} + 0.2 \qquad \text{(modified Juvik gauge)}$$

$$C_{effTunnel} = 0.40 * C_t * CWF_{Tunnel} + 0.16 \qquad \text{(tunnel gauge)}$$

Whilst the maximum efficiency for fog-only of the wire harp was ca. 0.30, this was increased to ca. 0.80 for the modified Juvik gauge (Figure II.8a). Also, during conditions of wind-driven rain, the catch of the modified Juvik gauge proved to be independent of wind speed and unaffected by problems of water being blown through or off the gauge as was the case with the wire harp (cf. Figure II.8b). Furthermore, catches of wind-driven rain by the tunnel gauge and the modified Juvik gauge were equal, indicating 100% catch efficiency for the two devices regardless of wind direction (Figure II.10).

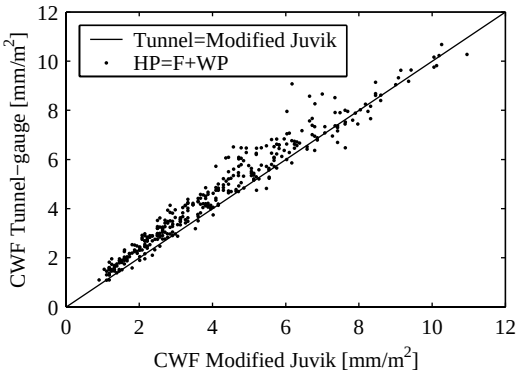

Figure II.10. *Amounts of horizontal precipitation collected by modified Juvik and tunnel gauge during conditions of wind-driven rainfall (including any fog).*

A further experimental modification of the Juvik gauge consisted of an additional cylindrical screen of 6.5 cm diameter placed inside the main cylindrical screen was tested at a windy pasture site. Although the catching surface of the gauge was increased by almost 50% for a similar cross-sectional area, no significant differences in collected amounts were obtained. Therefore, the modified Juvik-type gauge was adopted as the standard for further use in the project for the measurement of potential precipitation.

II.2.2.2 Cloud Droplet Spectrometer

A **cloud droplet spectrometer** (**FM-100**, Droplet Measurement Technologies Inc., Boulder, U.S.A.) determines the frequency distribution of fog droplets in air forced through a laser beam at a constant speed of 13 m/sec (Figure II.11a). The FM-100 allows the counting and characterization of cloud droplets with diameters between 2 and 50 µm in up to 40 particle size bins by the amount of light they scatter during their passage through the laser beam. It is assumed that the degree of light scattering by a particle is proportional to its diameter, its composition, and its shape. The *LWC* for each droplet size class is computed from the geometric mean volume of spherical droplets due to the log-normal distribution of the droplet-size count. The FM-100 spectrometer was in operation during the dry season of 2003 (February 20th - May 13th 2003) and used in conjuction with a sonic anemometer system measuring rapid fluctuations in vertical wind speeds, thereby allowing the direct evaluation of fog water deposition rates (Figure 11a). As indicated previously, the FM-100 measurements were also used for the derivation of the collection efficiencies of the various passive fog water collectors used by the project (section II.2.2.1).

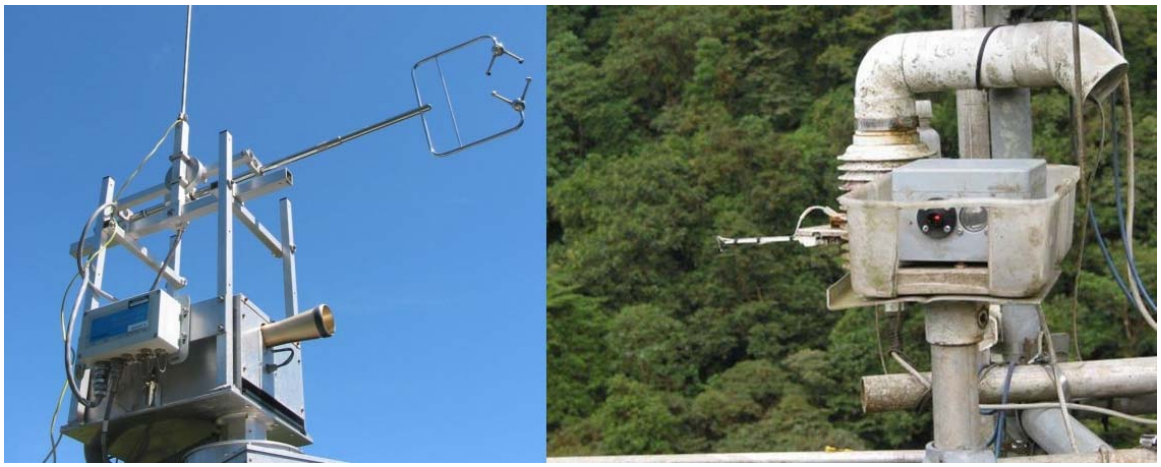

Figure II.11. (a) *Eddy-covariance set-up consisting of FM-100 cloud droplet spectrometer and Gill Solent sonic anemometer (top right).* (b) *Optical fog sensor (OFS-Mk2) placed inside a simple plastic box (cover temporarily removed) to protect laser window (red) and adjacent detector window from direct deposition of wind-driven droplets.*

II. 2.2.3 Optical fog sensor

An optical fog sensor (OFS-Mk2; Figure II.11b) measures the concentration of water particles (fog) in the air that limit visibility by detection of emitted laser light that is scattered back by the fog particles from a sensitive zone (1 cm^3) located about 30 cm ahead of the sensor. Visibility is related inversely to the instrument's voltage output. No backscattering generates a low instrumental output and therefore high visibility. The backscattered light also gives information about falling particles such as rain drops. Fog causes a DC signal in the sensor whereas falling particles produce small pulses as they pass the beam. A count of falling particles is therefore provided as well. Such information is helpful in separating periods of fog-only vs. fog-with-rain during fog gauge record analysis.

However, an indication of fog *LWC* values can only be obtained indirectly through insertion of a measured visibility record into a relationship linking visibility and *LWC.* Figure II.12 shows an example of such a relationship for fog recorded at Pico del Este, Puerto Rico.

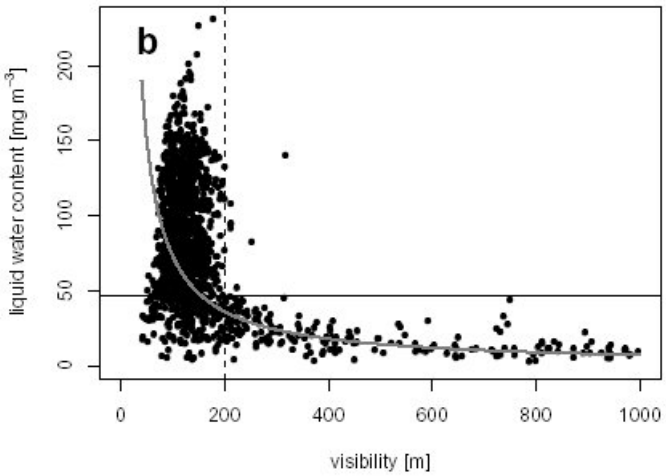

Figure II.12. *Relationship between visibility (m) and cloud water LWC (half-hourly averages) at Pico del Este, Puerto Rico. For visibility<200 m the LWC does not exceed 47 mg/m^3 in 95% of the cases*[3].

II. 2.2.4 Long-wave radiation balance

During times of fog a long-wave radiation sensor that is directed downward (Figure II.13a) effectively 'samples' the air passing underneath instead of the vegetation surface (as would be the case during clear conditions). At the same time the long-wave radiation sensor that is directed upward mainly detects the foggy air directly above it rather than the sky at large. It is therefore to be expected that the two sensors detect similar emitted long-wave radiation intensities because the temperatures just above and below the instruments are almost the same. Therefore, the onset and disappearance of a fog event (but not its density) can be detected as a near-neutral long-wave radiation balance (i.e. near zero). Long-wave radiation equipment is described in detail in part III of this document.

Figure II.13. *Eppley long-wave radiation sensors.*

[3] Unpublished data from W. Eugster et al.

II.3 **Throughfall and stemflow (net precipitation)**

II.3.1 *Throughfall*

Although passive fog gauges can be used to characterize an area's climate in terms of duration and frequency of fog occurrence, it would be wrong to equate the amounts of collected fog water to amounts actually captured by a live vegetation surface such as a cloud forest or rough grassland. Some kind of conversion factor is required that is site specific and thus needs to be derived on site.

In forested areas the amount of precipitation reaching the forest floor as crown drip (throughfall, *Tf*) and stemflow (*Sf*; cf. Figure I.1) is usually smaller than incident amounts of rainfall (*P*) because part of the intercepted rain is evaporated back into the atmosphere. Under such conditions, this rainfall interception *Ei* can be evaluated as the difference between gross (incident) and net rainfall:

$$Ei = P - (Tf + Sf)$$

However, in cloud forests, amounts of net precipitation (or crown drip) often exceed incident precipitation because of the (unknown) extra inputs contributed by cloud water and / or horizontal rainfall (*HP*). Under such conditions, interception evaporation can no longer be evaluated as the difference in gross and net precipitation and must be quantified using some other approach, if only because the equation now holds two unknowns (*Ei* and *HP*).

Because each forest represents a more or less unique situation that defies standardization, the classic approach of comparing gross and net precipitation for events or periods with and without fog or wind-driven precipitation at least has the merit of incorporating the influence of the structural characteristics of the forest under consideration. Where fog occurs in the absence of rainfall, a similar process of cloud water or fog interception (*F*) may be defined as:

$$F = E_{iF} + Tf + Sf$$

Because neither the actual amount of fog interception (*F*) nor that evaporated again from the wetted vegetation (E_{iF}) are easily quantifiable in a direct manner, a more practical approach is to equate net precipitation (P_{net}) during fog-only events to *net* fog interception F_{net}:

$$F_{net} = Tf + Sf = P_{net}$$

where the term fog interception now implies a *net gain* of water to the ecosystem.

In the more complex case of rainfall plus fog, separate knowledge of the total evaporation from the wetted vegetation (ΣE_l) is again required to solve the wet canopy water budget equation for *HP*:

$$P + HP = \Sigma E_l + Tf + Sf$$

In theory, this 'wet-canopy water budget equation' may be solved for *HP* (i.e. fog plus any horizontal rainfall) by measurement and/or computation of the remaining water balance terms. Below, the measurement of the two important terms **crown drip and stemflow** is discussed whereas in section II.4 the various corrections required for the proper estimation of *P* and *HP* at windy cloud forest sites will be dealt with in some detail. Finally, the evaluation of the wet canopy evaporation term E_l will be discussed in section III.2.3.

Crown drip or throughfall (*Tf*, mm) is usually measured using (numerous) **manual gauges and / or recording gutters** (Figure II.14). Manually measured throughfall gauges are essentially standard rain gauges placed beneath the tree canopy but they can also be custom-made from locally purchased funnels fitted on top of plastic containers. The gauge orifices need to be horizontal and to ensure their stable position on steep slopes the gauges are best placed in the type of steel holders described earlier in section II.2.1 for rain gauges. Empirical evidence suggests the use of at least 30 manual

gauges to obtain a representative spatial average estimate of *Tf* in most tropical rain forest types. The species richness of rain forests typically leads to tremendous spatial variability in crown structure and exposure to passing air, and therefore in highly variable drip and stemflow patterns, and any throughfall sampling scheme will need to take this into account. Of particular importance is the representative inclusion of so-called drip points, i.e. positions where throughfall becomes concentrated, often to the extent that *Tf* greatly exceeds incident precipitation.

Figure II.14, (a) *Manual throughfall gauge placed in metal holder.* (b) *Throughfall gutter connected to tipping- bucket recorder system.*

Manual gauges can be positioned along line transects (e.g. of 100 – 150 m length) or randomly in plots but to minimize the standard error of the average estimate it is recommended to regularly relocate the gauges in a random manner. Such a 'roving gauge' design offers the best guarantee to adequately sample the above-mentioned drip points. Where roving gauges and the accompanying site disturbance are less desirable, e.g. on steep slopes vulnerable to soil disturbance, a fixed gauge arrangement may be used as long as a sufficient number of gauges is employed. Trails connecting the various gauges may consist of steps made of slices of tree trunks covered with chicken wire to prevent them from becoming slippery, so as to avoid compaction of the surrounding surface.

Throughfall gutters may be constructed from stainless steel, aluminium or halved PVC pipes. In the present case, steel gutters of 4 m length and 30 cm width were used. These were placed at a 15° angle to facilitate drainage of the collected water into a pre-calibrated tipping bucket of 50 ml, giving a resolution of around 0.05 mm per tip (Figure II.14b). The number of tips of the bucket was counted each minute and recorded by a watertight pulse logger (Tinytag-Plus TGPR-1201) placed inside the tipping-bucket holder (Figure II.14b).

Recording throughfall gutters are useful in interception studies as they provide the temporal resolution required to gain insight into the dynamics of crown drip generation (evaporation, canopy storage and

drainage). This, in turn, is a *sine qua non* when modeling the interception process for future predictions of net precipitation. However, because the position of a throughfall gutter is normally fixed in space its catch is not necessarily representative of a forest's (or a plot's) average throughfall value as derived using numerous manual gauges (Figure II.15). Therefore, the temporal records of gutters need to be scaled up to the plot level using the results of the manual gauges before employing the temporal record in modeling exercises.

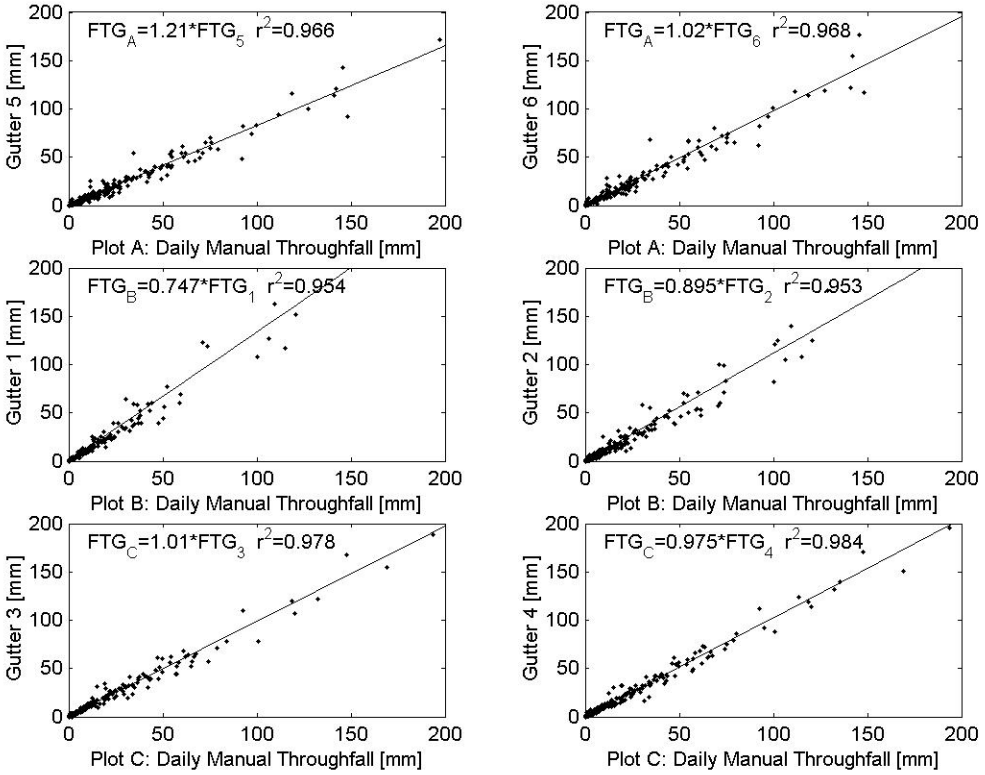

Figure II.15. *Throughfall amounts collected by fixed gutters may deviate considerably from average plot values as obtained with numerous manual roving gauges.*

To obtain a better idea of the spatial and temporal variability in net precipitation in cloud forest, several plots with different exposure to the prevailing winds and rain may be required. In the present case, three 1,000 m^2 plots (20 x 50 m) of contrasting exposure (called A, B and C in Figure II.16) were established for intensive measurements of crown drip (throughfall) and stemflow. Each plot was equipped with 20 manual throughfall gauges plus two recording gutters. The positions of the manual gauges were random whereas the recording gutters had a fixed position. Each plot was divided into 20 sub-plots or 'gauge areas' of 10 x 5 m each. Each gauge was appointed its own sampling area containing 50 possible sampling positions. A gauge was moved to a new location each week in a semi-random manner, choosing from the locations that had not been assigned yet. In this way all 50 positions were sampled after 50 weeks. The manual gauges were read daily. The measurements covered different precipitation conditions, i.e. events with rainfall only, fog only, or combined rain and fog, and for a range of wind speeds and rainfall intensities over a full seasonal cycle. The combined results shown in Figure II.15 further illustrate the degree of variation that may be encountered when comparing amounts of throughfall collected with individual gutters and a set of roving manual gauges, even within plots (e.g. A and B). Added variability comes from differences in species composition and, especially, exposure to rainfall and wind between plots (section II.4 below).

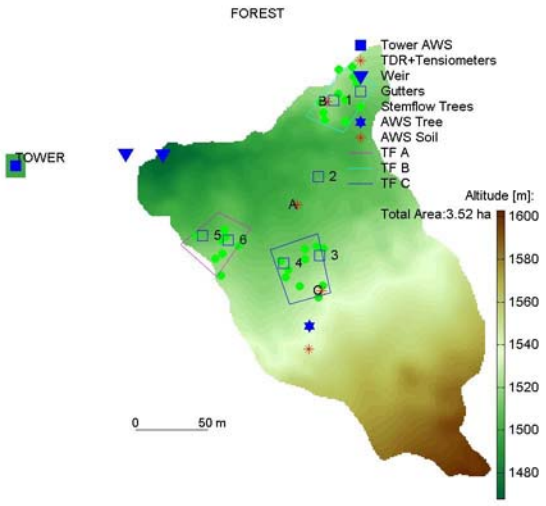

Figure II.16. *Instrumentation of the cloud forest catchment showing (inter alia) the location of three throughfall and stemflow plots A, B and C containing two gutters and 20 manual gauges each.*

An alternative sampling design that avoids the use of manual gauges (and thus frequent site visits or major soil disturbance) but still capable of sampling a sufficiently large surface area, is illustrated in Figure II.17. Here several long gutters are emptying their respective catches into a central tipping bucket system. The use of three of such automated set-ups is generally considered to give a good average estimate of throughfall although this lacks the degree of spatial information afforded by the use of a large number of manual gauges. Further comparison of the different approaches is desirable.

Figure II.17. *Assembly of several throughfall gutters emptying into a central tipping bucket system.*

To further increase one's insight into the processes governing crown drip, additional throughfall plots may be established underneath individual emergent (i.e. exposed) or rather more sheltered trees, in combination with studies of leaf wetness dynamics (using leaf wetness sensors), as well as the biomass and fog-absorption characteristics of mosses and epiphytes. The absorption and release of intercepted moisture (rain or fog) by mosses is very different from that by leaves and requires detailed experimental work. Figure II.18 illustrates the experimental approach followed in the present project and gives some preliminary results. The full integration of all processes determining crown drip spatial and temporal variability in cloud forest environments into a predictive model is still some way off, however, but could usefully employ detailed aerial photography from which to derive spatial variability in canopy topography and characteristics.

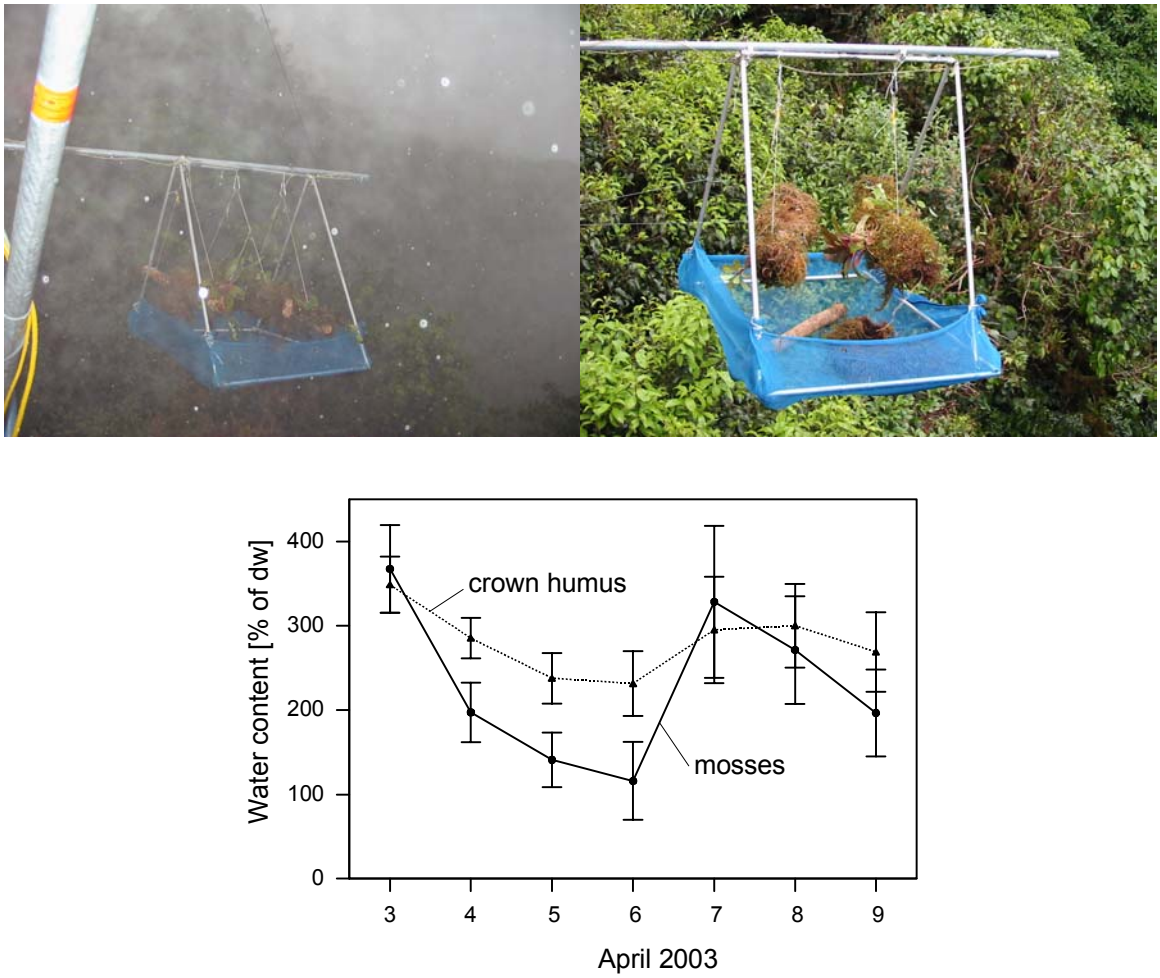

Figure II.18. *Within-canopy wetting and drying experiments of mosses and other epiphytes to derive their water uptake and release characteristics (top panels) and water contents of epiphytic mosses and crown humus as sampled in-situ within the inner crowns of dominant trees (bottom panel).*

In areas where cloud forest is replaced by pasture or crops the typical vegetation pattern is a mosaic of remnant forests surrounded by cleared areas. Some edges of these small woodlands will be more exposed to the prevailing wind and rain than others (Figure II.19). Studies of *Tf* in remnant cloud forest blocks will need to take the existence of a gradient away from the most exposed edge into account (Figure II.21). The experimental lay-out of *Tf* measurements in differently exposed secondary forest patches in the present project is given in Figure II.20. Apart from recording gutters use was made of 20 manual gauges per plot that were aligned in rows at various distances from the forest edge.

Figure II.19. *Cleared area in northern Costa Rica showing differently exposed cloud forest remnants.*

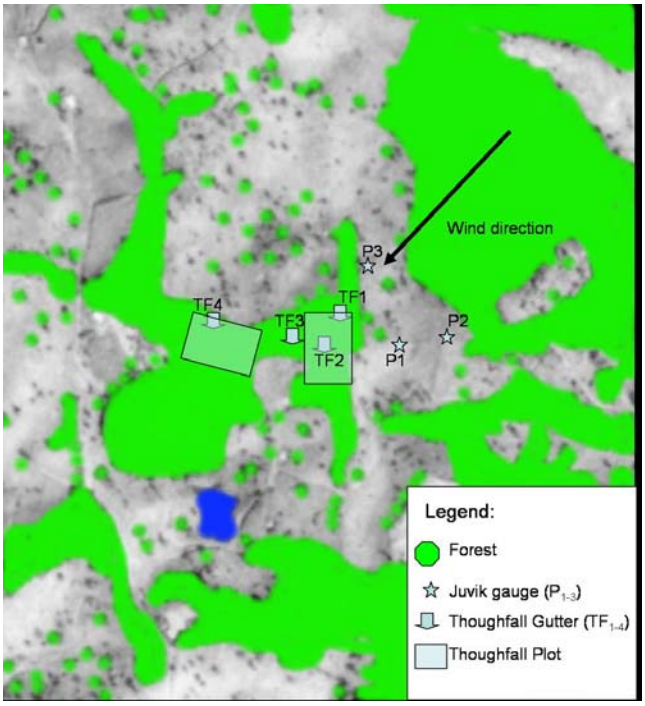

Figure II.20. *Experimental lay-out of throughfall measurements in secondary forest patches.*

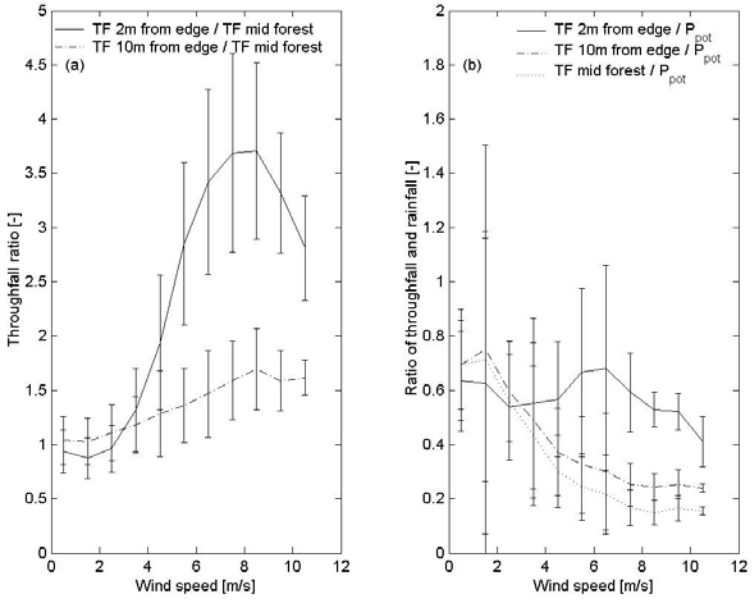

Figure II.21. *Throughfall patterns at increasing distances from the edge of exposed remnant cloud forest blocks surrounded by pasture exhibit a clear gradient.*

II.3.2 *Stemflow*

Stemflow (*Sf*) is usually measured by diverting the water running down the stem to a collector. In the present case silicon tubing was slit open lengthwise and attached in spiral fashion at 1.0-1.5 m height to the stems of 10 trees representing a range of diameter classes (Figure II.22). Any remaining voids between tubing and stem need to be sealed.

Areal *Sf* is expressed in millimetres of water whereas the results obtained for individual trees are given in litres. Conversion can be achieved in various ways. Either volumes per tree are divided by the projected crown area of that tree, or the stemflow of all trees within a bounded area of, say, 10 x 10 m is collected and the total volume divided by plot area. Naturally, by bulking stemflow volumes per plot, any information on contrasts in stemflow dynamics between species is lost. Alternatively, regressions may be derived that link *Sf* to rainfall on an event basis for dominant species. Total *Sf* volumes contributed per species can then be obtained by multiplication times the density of stems per hectare for each species. The overall volume for all species divided by plot, hillslope or catchment area then gives average *Sf* in mm.

Figure II.22. *Stemflow collector.*

An example of the computation of average stemflow for a montane forest in Puerto Rico is given in the following table. The disproportionately large contribution of palms in this particular forest (66% of total stemflow) is striking. Palms occur in many tropical cloud forests and their important contribution to stemflow should be taken into account when designing a stemflow sampling strategy.

Whilst stemflow is often negligibly small in tall cloud forests (typically <1% of incident rainfall), very high stemflow percentages have been reported for stunted ridge top cloud forests (up to 12-18% of rainfall). Under such conditions the proper quantification of stemflow assumes particular importance.

Table II.1. Estimated stemflow (Sf) per species in per cent of total rainfall of 2246 mm between 28 November 2000 and 5 November 2001 in the Bisley montane forest, Luquillo Mountains, Puerto Rico (after Holwerda *et al*., 2006).

Species	Tree density (no. / ha)	*Sf* (L/stem)	*Sf** (mm)	*Sf* (%)
Dacryodes excelsa	97[#]	589	5.7	0.3
Sloanea berteriana	382	332	12.7	0.6
Prestoa montana	123	5,000	61.5	2.7
Cecropia peltata	18	190	0.3	0.0
Other	743	-	-	0.5**
Total				

[#] trees with DBH>30 cm only.
* number of stems/ha times Litres/stem and divided by 10,000 to obtain mm of water.
** data obtained in previous study.

II.4 **Determining 'true' precipitation inputs in cloud forest areas**

II.4.1 *Introductory remarks*

Thorough quality checks of the precipitation and fog data obtained with the respective instruments described in section II.2 are needed in view of various potential sources of error (depending on the instrument under consideration). For example, volumes collected by rain-, fog- and throughfall gauges may be subject to errors related to evaporation of water from the gauges or splash-out of water from the funnel during intensive rainfall. In addition, instrumental tilting or damage, gauge overflow during extreme storms, or blockage of a funnel or gutter outlet by organic debris (e.g. leaves, insects) may occur, plus reading errors by field observers in the case of manually read gauges. Also, the shaking of a scaffolding tower connected via guy ropes to surrounding trees for added stability during heavy storms sometimes causes the tipping bucket system of rain- or fog gauges on the tower to tip before the bucket is filled completely. Frequent field checks generally prevent prolonged instrumental malfunctioning but the collected data still need to be rigorously checked and compared for inconsistencies.

In addition to these various (mostly random) errors, several more systematic errors may be distinguished. These include underestimation of precipitation, wind-driven rain and/or fog because of disturbance of the wind flow around the gauge (aerodynamic losses); underestimation of rainfall due to inclination of the rain (as opposed to vertically falling rain), and underestimation of rain falling on sloping ground (as opposed to horizontal terrain). The various corrections associated with each of these problems typical of wet and windy mountainous terrain are discussed in the following sections.

II.4.2 *Aerodynamically induced rainfall losses around the gauge ('wind loss')*

Underestimation of rainfall because of the distorted wind field above the gauge orifice can be an important source of error at windy sites (Figure II.23).

.

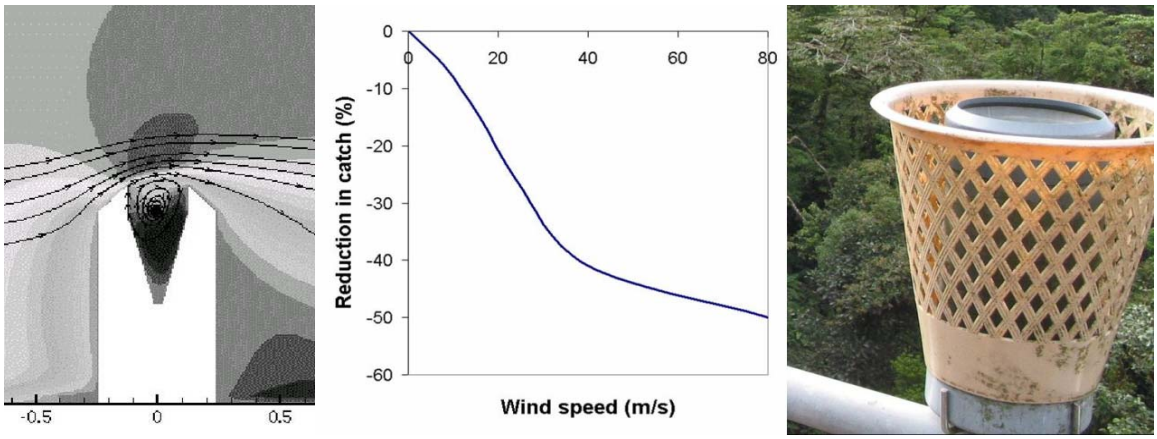

Figure II.23. *Wind-induced loss by turbulence and flow exceedance at the rim of a rain gauge (left); typical catch reduction pattern with increasing windspeed (centre); and simple gauge shield to reduce wind loss (right).*

The wind-induced error depends mainly on the size of the raindrops and the prevailing wind speed at the height of the gauge orifice. Several expressions to compute wind-induced rainfall losses exist in the literature, of which two widely used versions are discussed below before introducing the correction factors derived for the presently used gauge types in cloud forested terrain in northern Costa Rica.

For rain gauges in Scandinavia, Førland *et al.* (1996)[4] introduced a correction factor for wind-induced losses (k_f) to correct measured rainfall rates R (in mm/hr):

$$P_c = k_f P$$

where R_c is the corrected rainfall intensity (mm/hr). For liquid precipitation, k_f depends solely on rainfall intensity R and the wind speed at gauge height (U_g, m/sec) according to:

$$k_f = \exp(-0.0010 \ln(P) - 0.0122 U_g \ln(P) + 0.0343 U_g + 0.0077)$$

The correction factor (k_f) is calculated for each rainfall event or hourly record.

Yang *et al.* (1998) derived relations for wind-loss using several gauge designs for both snow and rain. Wind-induced losses were expressed as a catch ratio (k_g) to a reference and as a function of wind speed. The corrected rainfall P_c is given by $P_c = P/k_g$. Although Yang *et al*. claimed that a wide range of wind speed and catch ratio values were covered and that the correction equations are therefore likely to be valid for a wide range of environmental conditions, it is advisable to test this contention in individual cases when using a different gauge design or when experiencing rather special rainfall conditions, as in many tropical montane cloud forests.

As a first step towards improved point rainfall measurement a comparison was made in the current project between the catches of a shielded and unshielded standard rain gauge placed on a scaffolding tower above the cloud forest canopy (cf. Figure II.2). Using daily records from a period of 18 months an average wind-induced loss of 5.5% was derived. This is considered to be a minimum because the simple shielding that was applied probably did not prevent all aerodynamic losses whereas in addition several reading errors by the local observer could not be excluded.

Wind-induced losses were also studied in a nearby exposed pasture area using automatic rainfall recorders at two different installation heights, viz. at 2 m above ground level and close to the surface (0.5 m, with surrounding grass up to 0.3 m). The ARG-100 automatic rain gauge at 0.5m was found to have a negligible wind-induced loss compared with shielded and unshielded standard gauges at 0.2 m (cf. Figure II.2). The catch of the ARG-100 gauge at 0.5 m was taken as a reference, therefore. Wind-induced losses were determined for a modified Juvik gauge (Figure II.7) and a VUA gauge (Figure II.2) that were both installed at 2 m height, by comparing the respective catches with that of the ARG100. Events with an intensity >0.8 mm/hr at 0.5 m were used in the analysis. Mathematical relationships between catch ratio k_g and wind speed U were derived in a similar format to the ones obtained by Yang *et al*. (Figure II.24).

The results shown in Figure II.24 suggest that the Førland relation tends to underestimate the value of k at low wind speeds and overestimates it somewhat at higher wind speeds. The Yang correction model showed an inverse pattern of underestimation at low wind speeds and overestimation at higher wind speeds. Such results underscore the need for separate tests for locally used rain gauges and local climatic conditions. Interestingly, the dependency of the Juvik gauge on wind speed was slightly stronger than that derived for the VUA gauge.

However, application of the corresponding correction to the records of the modified Juvik gauges at other locations in the same overall area sometimes yielded unrealistically large corrections. In a montane environment where upward and downward wind components are important it is to be expected that any corrective expression derived for gauges at a particular slope is to some extent site specific. Further work showed that a better and more generally applicable expression was obtained when using the angle of the precipitation. The latter also incorporates the influence of wind speed and turbulence on rain droplets and therefore their susceptibility to being deflected around a rain gauge.

[4] see reference list at the end of this document.

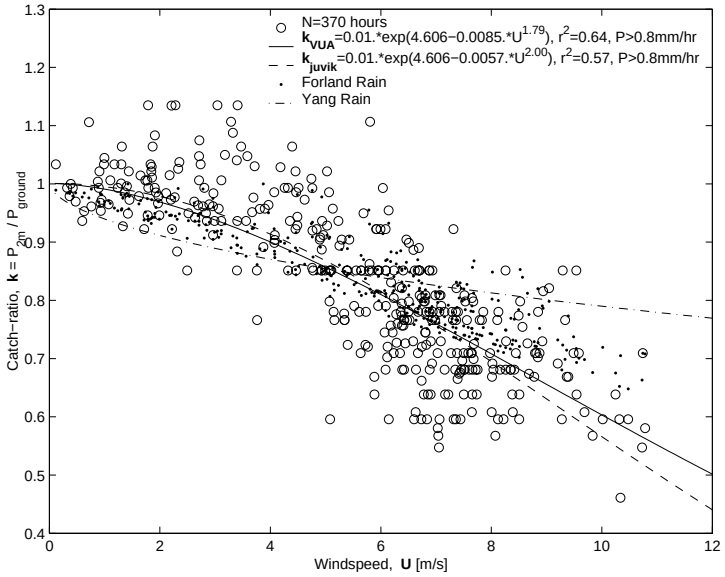

Figure II.24. Catch ratios of rainfall as a function of wind speed for a VUA- and a modified Juvik precipitation gauge at 2 m above ground level (San Gerardo pasture area, Costa Rica). Data points shown are for Juvik gauge only to avoid cluttering.

The catch ratio data were fitted to rainfall inclination data (derived themselves as described in the next two sections) instead of wind speed, using the same general mathematical format as before:

$$k_g = 0.01 \exp(4.606 - a_g \alpha^{b_g})$$

where α is the precipitation angle and a_g and b_g are gauge-specific coefficients. Values for a_g and b_g were 3.9191e-13 and 6.223, respectively, for the VUA gauge and 4.4406e-7 and 3.166 for the modified Juvik gauge. Again, the VUA gauge proved less sensitive to wind effects (i.e. less inclination) than the Juvik gauge (Figure II.25). The advantage of these expressions is that a significant correction only occurs for small droplets that are sensitive to changes in turbulence. In addition, large corrections are only applied to low precipitation intensities, thereby avoiding the unrealistically large corrections of precipitation totals obtained with earlier correction models (up to 45% of the annual total).

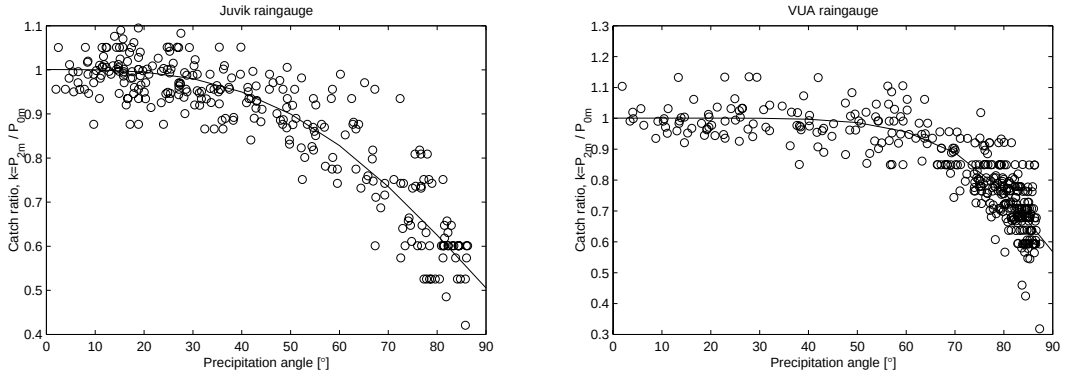

Figure II.25. Catch-ratio of rainfall as a function of incident precipitation angle (measured from the vertical) for the modified Juvik gauge (left) and the VUA recorder (right).

II.4.3 *Derivation of precipitation inclination*

Wind-induced losses of precipitation around the types of gauges used by the current project were estimated most realistically when using the angle of the incident rainfall as a proxy for wind speed. In the following, two approaches are described that can be used for the computation of rainfall inclination. The first of these is based largely on theoretical considerations whereas the second approach (pioneered by the project) derives the rainfall angle in a more direct manner by measuring the vertical and horizontal components of the precipitation.

II.4.3.1 Precipitation inclination from drop terminal velocities

Precipitation inclination is often derived from raindrop terminal velocity and wind speed. For each precipitation event, the median precipitation inclination angle can be calculated using relationships between precipitation intensity, droplet size, and terminal velocity of the droplets, in combination with wind speed as outlined below. The following account largely follows Sharon (1980).

The average precipitation inclination can be calculated from:

$$\tan(\alpha) = U / V_t$$

where α is now the precipitation inclination in degrees from the vertical, U the average horizontal droplet speed (approximated by the prevailing wind speed) and V_t the terminal fall velocity of the drops during an event. All forms of moisture that fall to the Earth's surface quickly establish an equilibrium between two forces working upon them, i.e. gravity (downward) and aerodynamic drag (upward). The resulting velocity is called the terminal velocity, or simply fall velocity (V_t). In the atmosphere droplets may be regarded as continuously adjusting their speeds to remain essentially in the terminal fall condition at all times. The terminal velocity of water droplets in still air can be computed from Stokes's law for drops smaller than 80 µm in diameter (D). Above that size, empirical values must be used.

The terminal velocity V_t (m/sec) of raindrops (>0.5 mm) is often calculated from their diameter D (mm) using:

$$V_t = 3.378 \ln(D) + 4.213$$

An alternative expression uses:

$$V_t = (-0.193 + 4.96D - 0.904D^2 + 0.0566D^3) \exp(z/20),$$

where z is the height in km and the factor exp(z/20) accounts for the decrease in density (and hence aerodynamic drag) with height in the atmosphere. Drops larger than 3 mm have a good chance of breaking up into smaller drops but the break-up probability increases rapidly for D >5 mm. Therefore, drops are rarely larger than 5 mm.

From the empirical terminal velocity derived from drop diameter and the average horizontal speed attained by the droplets (usually taken to equal the prevailing wind speed), the precipitation inclination for the event or sampling period can be computed by simple trigonometry. However, the *effective* terminal velocity depends on the *drop-size distribution* of the given precipitation or fog event and is often represented by the median droplet diameter (D_{50}), i.e. the diameter for which the total volume of all drops having greater diameters equals the total volume of all drops having smaller diameters.

The median drop size, D_{50} (mm) is often related to rainfall intensity, R (mm h^{-1}) according to:

$$D_{50} = a_d R^{b_d}$$

where the values of a_d (in hr) and b_d (dimensionless) are characteristic of precipitation type and therefore site-specific (see Van Dijk *et al.* (2002) for values obtained at different locations).

The value of D_{50} and thus of a_d and b_d can be expected to be smaller for the type of orographic precipitation found in many cloud forest situations than for convective storms in lowland areas. The values derived for rainfall intensities of 0.4 - 144 mm/hr in the classical (lowland) study by Laws and Parsons (1943) (a_d = 1.28 and b_d =0.173) were used in calculations of theoretical effective precipitation inclinations as a function of wind speed for different median drop diameters (Figure II.26).

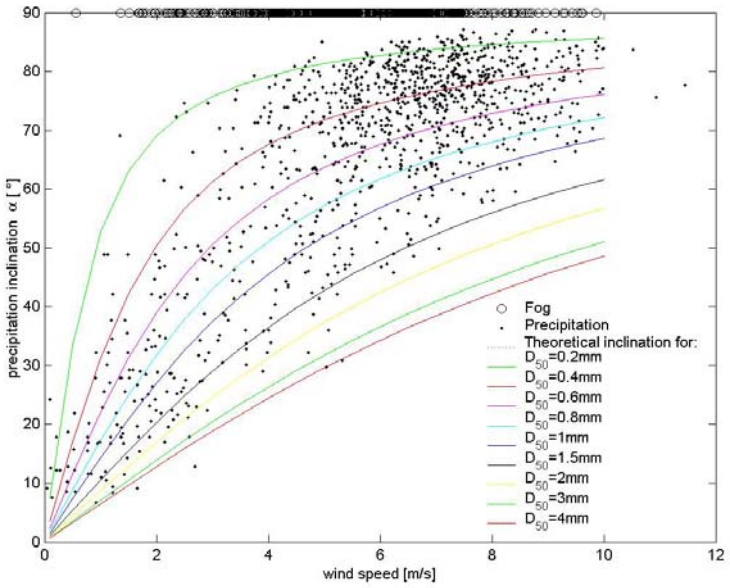

Figure II.26. Precipitation inclination as a function of wind speed. Lines represent theoretical relationships based on terminal velocities for different median droplet diameters. Dots represent measured inclinations (see next section).

II.4.3.2 *Precipitation inclination from measurements of P and HP*

An alternative and arguably more direct procedure to determine the precipitation angle was developed by the current project. The potential precipitation (P_p) may be defined as the potential amount of atmospheric water reaching a plane that is orientated perpendicularly to the average trajectory direction of the water drops over a specified period of time (section II.1). As such, it truly represents an upper limit (i.e. potential) to the amount of water that can enter at a point. Its vertical and horizontal components are represented by the amounts of vertical (P) and horizontal precipitation (HP) as measured by a modified Juvik gauge. As shown in Figure II.1, the angle of the precipitation can then be derived from P and HP using simple trigonometry after correcting P for wind losses (section II.3) and HP (in the case of fog-only) for gauge efficiency (Figure II.8a). Thus:

$$\tan(\alpha) = HP / P$$

where α is the precipitation inclination in degrees from the vertical. Furthermore:

$$P_p = \max(P/\cos(\alpha), HP/\sin(\alpha))$$

where P_p equals P in the case of vertical precipitation only, and P_p = HP in the case of fog-only.

The inclinations of incident precipitation derived from measured (and corrected) amounts of *P* and *HP* at the San Gerardo pasture weather station (see Appendix for location) are plotted against wind speed in Figure II.27. Precipitation angle proved to be related exponentially to wind speed, with the magnitude of the coefficient and exponent of the relationship being dependent on rainfall intensity (read: drop size). Various functions representing a range of rainfall intensities are shown in Figure II.27. These expressions allow precipitation inclinations to be estimated under similar environmental conditions from commonly available data, such as wind speed and precipitation intensity.

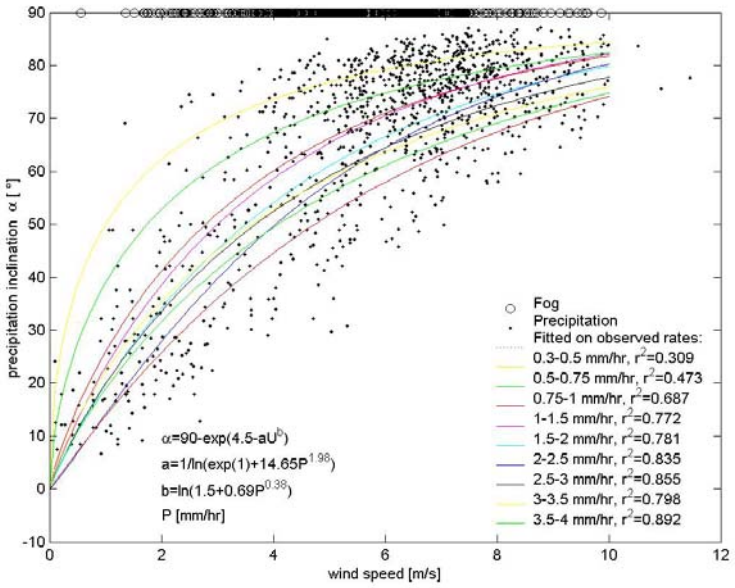

Figure II.27. *Precipitation inclination derived from measured amounts of vertical and horizontal precipitation vs. wind speed (points); also shown are fitted functions that relate wind speed and precipitation inclination for selected precipitation intensity ranges (lines).*

When comparing measured precipitation inclination values with the theoretical curves relating inclination to median drop size in Figure II.26 it becomes readily clear that the majority of the data falls within the curves derived for D_{50}-values of 0.2 and 2 mm. In addition, there is a concentration of data points in the upper parts of the graph representing windy conditions (> 5 m/sec) and drizzle-size drop diameters (0.2-0.4 mm). Interestingly, the theoretical inclination vs. wind speed relationship derived for droplet diameters of 0.2 - 0.4 mm (upper green line in Figure II.26) resembles that for rainfall rates of 0.3 - 0.5 mm/hr (yellow line in Figure II.27). Such low intensities are indeed typical for drizzle. Otherwise, the theoretically derived equations (based in turn on empirical relationships between median diameter and precipitation rate, e.g. $D_{50} = 1.28R^{0.17}$) seem to underestimate precipitation inclinations (Figure II.26), presumably because of an overestimation of droplet diameters. This can be explained by the fact that the empirical relation linking D_{50} and R was mainly derived for convective storms, whereas most precipitation events in the present study area (and indeed in many cloud forest areas) are primarily orographic in origin and thus characterized by smaller droplets. It follows that more representative estimates of precipitation inclination in areas with environmental conditions not too dissimilar to the present study area may be obtained using the relationships shown in Figure II.27.

The importance of knowledge of precipitation inclination is that it allows more accurate determination of precipitation inputs to topographically complex terrain if the spatial patterns of wind speed and topography are known. A basic assumption is that the potential precipitation as measured at a representative point is the same throughout the area of interest. The effective inclination then becomes a function of potential precipitation intensity and wind speed. The following section discusses the principles of correcting sloping rainfall in sloping terrain.

II.4.4 *Precipitation correction for sloping terrain*

Tipping bucket rain gauges are installed horizontally but the topography of most uplands is typically composed of differently orientated slopes. The intensity at which precipitation is intercepted by a slope depends on the angle of incidence relative to that slope, i.e. it is highest when precipitation falls normal to the surface, but becomes lower when the rain falls at an angle (Figure II.28). Because of the windy conditions prevailing in many cloud forest areas precipitation can be expected to fall at considerable angles for much of the time (cf. Figures II.26 and 27). Therefore, the actual precipitation incident to a slope will differ from that measured by a rain gauge. To correct for this effect, a trigonometric model was developed by Sharon (1980) on which most of the following account is based. The model allows the computation of precipitation intensity normal to a slope from conventional precipitation measurements when the azimuth and angle of the inclined precipitation can be accurately specified (Figure II.28).

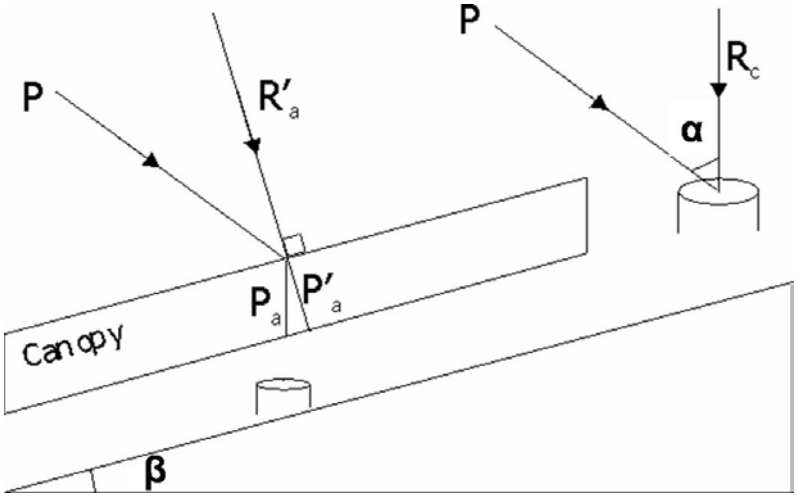

Figure II.28. *When rain falls at an angle α to a sloping surface with angle β, the intensity of rainfall intercepted by the sloping surface (P'_a) differs from that measured by a horizontal rain gauge (P_a).*

Precipitation depth along the normal to an inclined surface P'_a (mm) relates to measured precipitation depth P_a (or P_c after correction for wind losses) according to:

$$P'_a / P_c = (\cos(\beta) + \sin(\beta)\tan(\alpha)\cos(\Omega_a - \Omega_b))$$

where β is the inclination of the sloping ground, α the inclination of precipitation, Ω_a the slope aspect, and Ω_b the average direction of the wind, and therefore of the precipitation event. The vertical equivalent of P'_a reads:

$$P_a = P'_a / \cos(\beta)$$

which, in combination with the first relation gives:

$$f_c = P_a / P_c = 1 + \tan(\beta)\tan(\alpha)\cos(\Omega_a - \Omega_b)$$

where f_c is a correction factor applied to the gauge measurements after correction for wind-induced loss (P_c) to yield the 'true' quantity of rain incident to the slope P_a (Figure II.28). In case of a slope covered by a forest canopy it is assumed that the canopy surface runs parallel to the sloping ground and that it intercepts all precipitation incident to it (P'_a). Field applications of the various rainfall corrections at different scales can be found in Annexes 3 and 4 to the main Technical Project Report.

Part III. Energy budget and evapotranspiration components

III.1 Introduction and definition of terms

Evaporation (*E*) occurs when water is converted into water vapour by exchange of water molecules between air and a free water surface. It is the difference between two rates, a vaporization rate determined by temperature and a condensation rate determined by vapour pressure (Figure III.1). Evaporation continues as long as molecules (vapour) are removed from the evaporating surface by diffusion which keeps the vapour pressure above the evaporating surface low. Evaporation stops when the vaporization rate equals the condensation rate. The air is then said to be saturated. The vapour pressure at this equilibrium is called the saturation vapour pressure (e_s), which increases with temperature. The energy required to separate the molecules during evaporation (the vaporization) is called the latent heat of vaporization (λ) and decreases slightly with increasing water temperature.

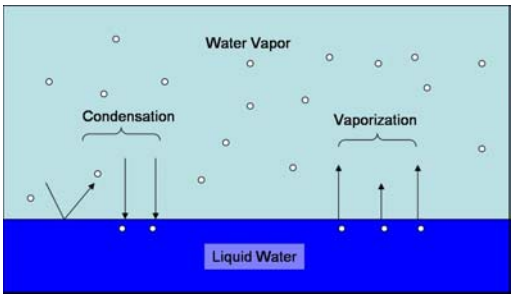

Figure III.1. *The evaporation process.*

Water may evaporate from a variety of surfaces, including vegetation and soils. When describing the evaporation from a vegetated surface it is helpful to make a distinction between wet and dry surface conditions because the associated evaporation rates are very different (see explanation below). The evaporation from wet vegetation is also called **interception** and may be defined as the capture of precipitation and fog by the plant canopy and its subsequent return to the atmosphere by evaporation. The process of water loss from plants through stomatal openings in the leaves takes place during dry canopy conditions and is commonly called **transpiration**. For a vegetated surface it is often difficult to distinguish between evaporation from a soil (E_s), wet vegetation (E_i) and transpiration (E_t). Therefore the composite term **evapotranspiration** (*ET*) is often used to denote the sum of the three components:

$$ET = (E_s + E_i) + E_t$$

The *rate* of evapotranspiration, evaporation or transpiration is normally expressed in millimetres of water per unit time. The rate expresses the amount of water lost from a surface in units of water depth. The time unit can be an hour, a day or an entire year in case a water balance is considered. The evapotranspiration rate expressed in energy units is called the **latent heat flux**, λE *[W/m^2]*.

The rate of evapotranspiration at any instant from the Earth's surface is controlled by four main factors:

1. **Energy availability**. The more energy available the greater the rate of evapotranspiration.
2. **The humidity gradient** away from the surface. The rate and quantity of water vapour entering the atmosphere both become higher in drier air.
3. **The wind speed** immediately above the surface. Wind enables water molecules to be removed from the surface and maintains a humidity gradient. This transport process by wind is known as **eddy diffusion**. Without transport the layer adjacent to the surface becomes saturated and evapotranspiration stops.
4. **Water availability**. Evapotranspiration cannot occur if water is not available.

In the absence of restrictions related to water availability (factor 4) at the evaporating surface, the amount of radiant energy (factor 1) captured at the surface is the dominant control of evaporation. Quantification of the **radiation balance** is therefore crucial to understanding and quantifying evaporation. However, the extent to which the energy available on the ground is actually used to evaporate water is determined by the processes controlling vapour diffusion through the air (factors 2 and 3). The transport of water away from each individual surface (leaf, soil) is represented in schematic form in Figure III.2. The transport occurs via the process of molecular diffusion *at the surface,* or *through the surface,* and by turbulent diffusion between the well-mixed atmosphere and the immediate vicinity of the surface. Each of these pathways is associated with a specific resistance against the process, viz. the boundary layer resistance (r_b), the stomatal resistance (r_{st}) (or the soil resistance (r_{soil}) in the case of soils), and the overall aerodynamic resistance (r_a), respectively (Figure III.2).

If the surface is considered as one big surface, e.g. a 'big leaf', instead of individual vegetation and soil surfaces, the individual stomatal, soil and boundary layer resistances are combined into a single **bulk surface resistance**, r_s. Thus, the diffusion of energy in the form of water vapour and sensible heat away from the plants or soil into the atmosphere can be represented by a network of resistances.

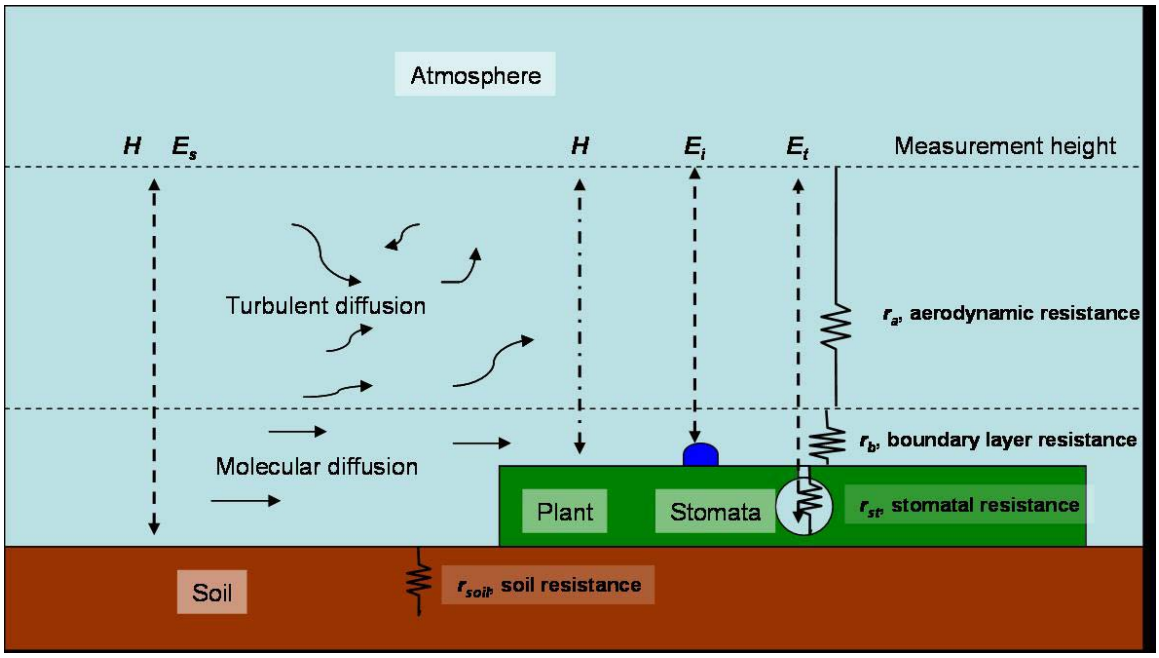

Figure III.2. *Schematic diagram showing the transfer of water vapour and heat into the atmosphere and the various resistances associated with the respective processes.*

Often a distinction is made between two different aspects of evapotranspiration: **potential evapotranspiration** (ET_p or *PET*) and **actual evapotranspiration** (ET_a). Potential evapotranspiration is a measure of the ability of the atmosphere to remove water from the surface through the processes of evaporation and transpiration assuming no control of soil water supply. Actual evapotranspiration is the quantity of water that is actually removed from a surface. These two types of evapotranspiration are considered mostly for practical purposes. Actual evapotranspiration is not easy to measure and often an **estimation of evapotranspiration** is made only, e.g. due to limited data availability. Several empirical methods have been developed to estimate *PET* and these are widely used in agrometeorology. Because such simplifications largely apply to short vegetation types like grassland and crops, they are of lesser importance in forest hydrology.

III.2 **Measuring evaporation**

There are numerous approaches and methods to quantify evaporation. Broadly speaking, a distinction can be made between two classes of methods, viz. (i) those quantifying the rate of liquid water losses, and (ii) those that measure the gain in water vapour by the atmosphere (Figure III.3).

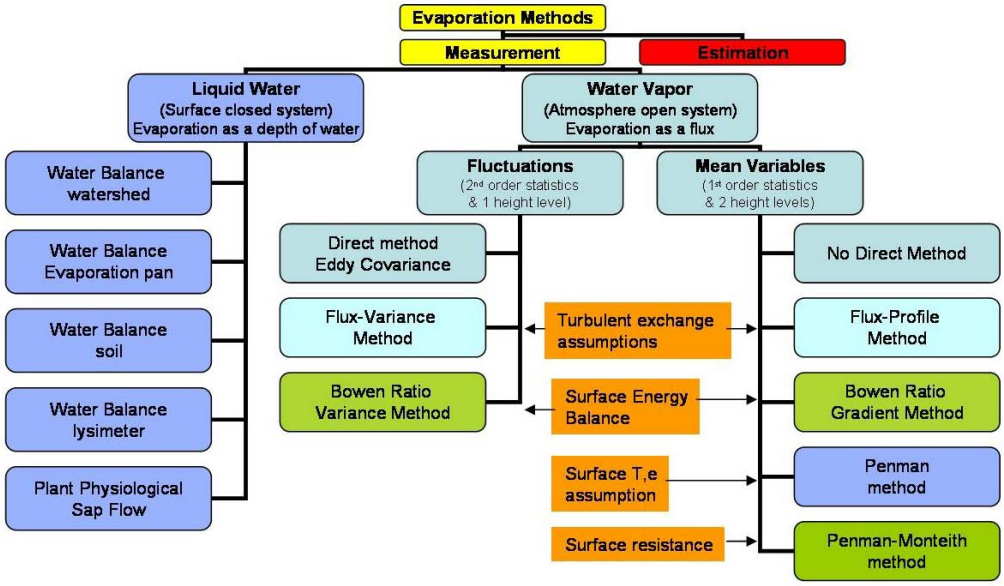

Figure III.3. *Schematic overview of evaporation methods.*

The first group of measurements either assumes or creates a closed system, such as a block of soil or lysimeter, or an entire catchment area, and deduces evaporation as the net loss of water from that closed system over a given time. Stated differently, these 'hydrological' approaches solve the **water budget** equation (section I.3) for evaporation by quantifying the remaining terms. All water balance measurements therefore share the problem that the error in the derived evaporation figure is an accumulation of the errors in the other measured variables. In addition, with the exception of weighing lysimeters, the time resolution afforded by the water budget method is typically in the order of a week or more rather than days which generally limits the application of the method to operational purposes. Finally, application of the water budget method is rendered extra complex in cloud forest terrain because of the problems associated with the proper quantification of water inputs (both precipitation and fog; sections II.2 and II.4) as well as ungauged subterranean losses. Summarizing, water budget approaches for the evaluation of evaporation from cloud forests are often doomed from the start and alternative approaches are required.

Plant physiological methods such as the measurement of **sap flow rates** in trees allow determination of the transpiration of the tree. Evaporation from dense forest surfaces where soil evaporation can be neglected consists primarily of transpiration and under such conditions sap flow approaches actual evaporation. Sap flow in a tree can be measured by various heat-flow techniques in which the temperature difference between a heated sensor and a reference sensor (both installed in the xylem of the tree) is a measure of sap flow velocity. Transpiration rates for individual trees are derived from sap flow velocity in combination with data on xylem cross-sectional area (giving total volume of sap flow in litres). The latter can be converted to millimetres of water by dividing this volume by the projected crown area of the tree. However, application of plant physiological methods in cloud forests is complicated for various reasons.

Firstly, the high diversity in tree species requires large numbers of replications and makes up-scaling to the stand level a complicated affair. More importantly, the very wet and foggy conditions in many cloud forests make for frequently wet canopy conditions during which transpiration comes to a halt. Finally, the very low atmospheric humidity deficits prevailing for much of the time (e.g. during fog) cause transpiration rates to be so low as to be sometimes undetectable. Sap flow techniques have had little application in cloud forests so far and further work is needed under a range of environmental conditions (e.g. high vs. low rainfall areas, different elevations).

Measurements of evaporation in the vapour phase most commonly assume that the atmosphere is an open system and a second group of methods therefore determines evaporation as an integration of the rate of flow of water vapour into the atmosphere through the turbulent boundary layer near the land surface (Figure III.2). As shown in Figure III.3, there are two broad classes of such **micro-meteorological techniques**, i.e. those based on measurements of gradients of mean variables such as temperature or humidity (1st-order statistics) and those based on measurements of fluctuations in these variables (2nd order statistics). Both general approaches rely on the fact that turbulent exchange is the dominant exchange mechanism within the near-surface atmosphere.

Application of any micro-meteorological method for the estimation of evaporation is not easy and requires high-quality equipment as well as technical expertise and back-up. In addition, they are best suited to flat terrain or uniform slopes of low gradient; conditions of atmospheric stability need to meet certain requirements, and the methods generally do not apply during rainfall. As such, applications of micro-meteorological methods to evaluate cloud forest evaporation in complex terrain have rarely been successful. Nevertheless, some of these techniques offer the possibility to measure actual rates of transpiration during conditions of a dry canopy. As shown later, this information can be used in an inverse manner to derive relationships between canopy resistance to evaporation and ambient weather variables such as humidity and radiation. This relationship can then be used during other times to compute evaporation when conditions are such that direct measurements are not possible.

In the following sections three methods that were selected by the present project to quantify evaporation from pasture and cloud forest will be discussed, viz. the eddy-covariance method, the Bowen-ratio flux-variance method, and the Penman-Monteith method.

III.2.1 *Eddy Covariance method*

The eddy-covariance method (ECV) is the preferred micro-meteorological technique on the grounds that it is a direct measurement of vertical fluxes of sensible (H) and latent heat (λE) by determination of the respective covariances $\overline{w'\theta'}$ and $\overline{w'q'}$. $\overline{w'\theta'}$ is the product of rapid fluctuations in vertical wind speed w (a measure of atmospheric turbulence) and in potential temperature θ whereas $\overline{w'q'}$ denotes the product of fluctuations in vertical wind speed and the specific humidity q of the air.

The latent heat (evaporation rate) and sensible heat fluxes are obtained from:

$$\lambda E = \rho\lambda\overline{w'q'}$$
$$H = \rho C_p \overline{w'\theta'}$$

where ρ is the density of air, λ the latent heat of vaporization, and C_p the heat capacity of air at constant pressure.

The ECV-method gives representative values for evaporation when the measurement takes place within the surface layer above the vegetation whereby it is assumed that no vertical flux divergence takes place with height above the surface. The method can be used to determine the roughness parameters employed by most micro-meteorological methods for the aerodynamic characterization of the behaviour of the surface and of the air flow. As such the method serves as a reference.

The fluctuations in wind speed, humidity and temperature may occur over a broad range of frequencies, some lasting for several minutes but others for only fractions of a second. Therefore, the sensors used to measure these fluctuations (i.e. *q'* and *w'*) must have a short response time. At the same time these sensors have to be co-located in order to measure the same moving air. Yet they should ideally be limited in size and be carefully positioned so as to avoid interference with the very movements of the air that they are to measure (Figure III.4).

Figure III.4. Left: *Sonic anemometer (Gill Solent Instruments, model R2).* Right: *wet- and dry-bulb thermo-couples plus feeding reservoir.*

Such rapid measurements are usually carried out using a **sonic anemometer** which samples the fluctuations in wind speed and temperature at a frequency of 20 Hz (Figure III.4) and additional instruments for the synchronous measurement of temperature and/or humidity (http://www.gill.co.uk). A sonic anemometer emits and receives sound waves along its three vertical axes and from this it derives the three-dimensional wind speed by combining the Doppler shifts in the three directions between emitted and received sound waves. The temperature is derived from the time elapsed between emission and reception of the sound wave as the velocity of sound waves is strongly influenced by temperature. The temperature measured by the sonic anemometer is usually corrected for humidity fluctuations because the velocity of sound also depends on atmospheric humidity. The typical averaging time is about half an hour. However, a clear 'spectral gap' is required for the separation between turbulent fluxes and larger-scale fluxes in the record. Where frequent clouds are passing the instrument the averaging time is ill-defined and the calculated fluxes are usually highly ambiguous. This represents a very serious limitation to the application of the technique in cloud forest environments since only the records obtained for relatively bright days can be used profitably. In addition, an array of corrections is required for use in sloping terrain (tilt corrections), for the presence of fluctuations that are smaller than the sampling frequency and for other types of frequency-response errors that fall outside the scope of the present document[5].

III.2.2 *Bowen-ratio energy balance flux-variance method (BREB-variance)*

Solar radiation (short-wave radiation) is received and reflected by the surface. In addition, environmental elements, i.e. the surface as well as the overlying air and clouds, all emit thermal energy (long-wave radiation). The balance between the various incoming and outgoing radiation components (net radiation) is the amount of available energy.

[5] See a.o. Garratt (1992), Van der Molen (2002) and Holwerda (2005) in the reading list.

Most of the available energy is used to heat the adjacent air (sensible heat flux *H*) and to evaporate water (latent heat flux λE). A small part of the energy is associated with heat transfer into the soil (*G*) or storage (*S*) in biomass or the air in between the vegetation. Finally, a small part of the energy is used for photosynthesis (*P*) (Figure III.5).

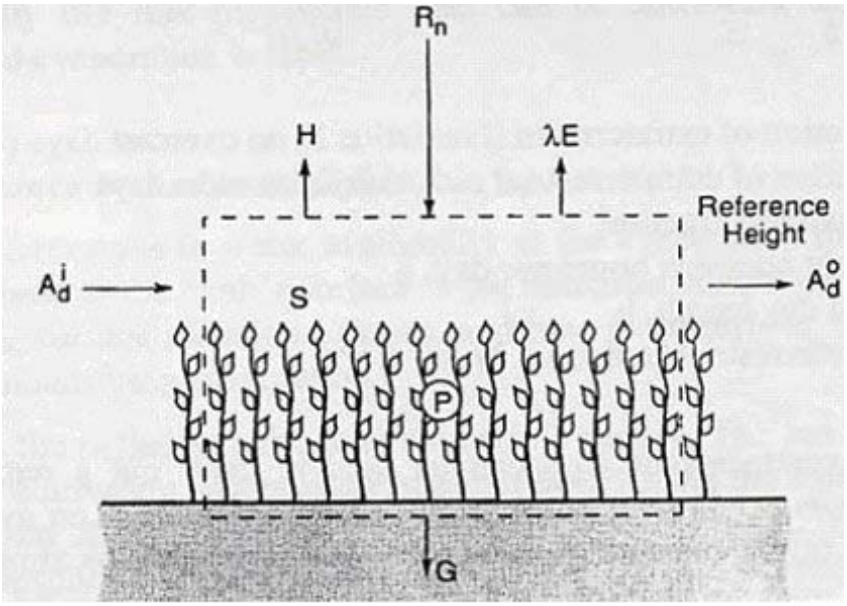

Figure III.5. *Energy balance components for a homogeneous surface cover*.

The radiation and energy balance at the surface can be written as follows:

$$R_n = R_s\downarrow + R_s\uparrow + R_l\downarrow + R_l\uparrow$$
$$R_n = H + \lambda E + G + S + P$$

The **radiation balance** or net radiation (R_n) is the summation of the incoming (↓) and outgoing (↑) short-wave (R_s) and long-wave (R_l) radiation components whereas the **energy balance** represents the balance between available energy at the surface and its partitioning between the various processes illustrated in Figure III.5, including heating of the air and evaporation. The remaining terms (*G, P* and *S*) normally make up only a very small portion of the total energy (<1-2% each). It should be noted that the surface is considered flat and homogeneous such that net amounts of horizontally advected energy (A_d) can be neglected (Figure III.5). In sloping terrain this is often not the case and provisions for this should be made in the calculations.

The **Bowen ratio** is defined as the ratio between sensible (*H*) and latent (λE) heat fluxes. Whilst it is often difficult to measure the two fluxes separately, this difficulty can be avoided by using their ratio (i.e. the Bowen ratio β) and combining it with the simplified energy balance to derive the following two expressions for *H* and λE, respectively:

$$H = \frac{\beta(R_n - G)}{\beta + 1}$$
$$\lambda E = \frac{(R_n - G)}{\beta + 1}$$

Because of the inherent similarities in the diffusion of water vapour and sensible heat, the Bowen-ratio energy-balance method is often less sensitive to changes in surface roughness and topography than several other micro-meteorological methods. Generally, as long as temperatures and humidity are not measured too close to the vegetation surface, and the surrounding area can be considered homogeneous, then the assumption of similarity is valid.

The Bowen-ratio may be derived from so-called flux-variance relations that describe the rapid fluctuations in air temperature and specific humidity. Expressed in simple mathemathical form:

$$\beta = \frac{H}{\lambda E} = \frac{c_p(\sigma_T)}{\lambda(\sigma_q)}$$

To evaluate the magnitude of λE, the Bowen-ratio variance method requires the measurement of the rapid fluctuations in temperature (represented by their standard deviation σ_T) and humidity (with standard deviation σ_q) at a single height above the vegetation surface. In addition, the quantification of net radiation and (ideally) the soil heat flux is needed as this defines the amount of available energy. Because the outcome of the method is highly dependent on the proper measurement of the fluctuations in temperature and humidity, the thermo-couples that are usually employed for this should be fast enough (cf. Figure III.4). The height of the measurement above the vegetation is important (preferably > 2m) as well because at greater heights the turbulent eddies of the air transporting heat and vapour tend to be larger whereas less transport takes place through smaller and more rapid fluctuations. Although thermo-couples (1 Hz sampling frequency) miss the smaller, more rapid fluctuations that are measured by sonic anemometers (20 Hz sampling frequency), the problem of frequency loss is eliminated to some extent by the use of the Bowen ratio. Nevertheless, the wet-bulb thermo-couple used for the measurement of humidity fluctuations is covered by a wick (Figure III.4). As a result, its response time is somewhat slower than that of the dry-bulb thermocouple and a correction is needed to account for this. Standard deviations of wet-bulb temperature are measured, but standard deviations of specific humidity are needed. The procedure to convert standard deviations of wet-bulb temperature into specific humidity uses the psychrometric formula[6].

III.2.3 *Bulk transfer or combination models of evaporation*

The principles of combined energy and atmospheric transport (or diffusion control) as applied in the Bowen ratio method are generalized in what is called the combination equation by taking the bulk transfer of heat and moisture between the surface and a reference height. The associated equations are called **bulk transfer equations** and describe the transport between the surface and a reference height in the atmosphere:

$$H = -\rho C_p \frac{\overline{T}_s - \overline{T}_a}{r_{aH}}$$

$$\lambda E = -\rho\lambda \frac{\overline{q}_s - \overline{q}_a}{r_{aV}}$$

where T_s is the so-called effective aerodynamic surface temperature, q_s the specific humidity at the surface and T_a and q_a the temperature and specific humidity at a reference level (often 2 m) above the surface. The aerodynamic resistances against upward transport of heat and vapour in the atmospheric surface layer are represented by the respective **bulk aerodynamic resistances**, r_{aH} and r_{aV} that are at work between the surface and the reference height.

[6] See e.g. Van der Molen (2002) and Holwerda (2005) for details.

The appropriate effective surface values for temperature and humidity as well as the parameterization of the bulk aerodynamic resistances depends on the representation of the surface in the respective models for the determination of sensible and latent heat fluxes. The more sophisticated versions of such models consist of multi-layer representations of a closed canopy, with sources of heat and moisture structured vertically. However, a single-layer representation of the evaporating surface is often the only feasible model for the determination of evaporation. Figure III.6 shows the schematic structure of single- and multi-layer combination models.

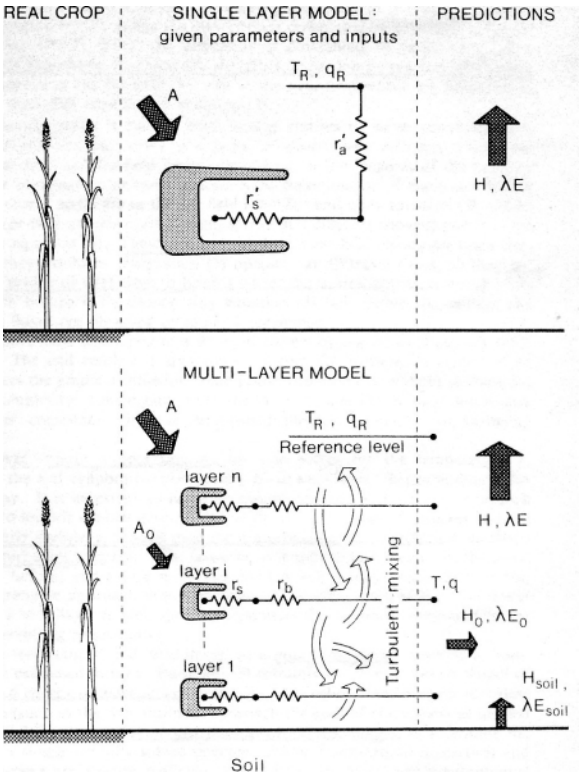

Figure III.6. *Schematic structure of single-layer and multi-layer combination models*[7].

The widely used **Penman and Penman-Monteith evaporation models** both use a single-layer representation of the surface. This surface is either a (hypothetical) flat, homogeneous free water surface (Penman) or a single 'big leaf' (Penman-Monteith). Water vapour (latent heat) is supposed to be released from the surface directly (free water) or through the numerous stomatal pores present in canopy leaves (big-leaf model). In the latter case, an additional resistance is included for the water vapour transport from within the leaf to the leaf surface, the so-called stomatal resistance, r_{sto}. The summed stomatal resistance for the entire vegetation surface is called **surface resistance**, r_s (i.e. bulk stomatal resistance; Figure III.6). A free water surface does not control evaporation rate as stomata do and r_s is zero. Note thar r_s also becomes zero for a vegetation surface that is fully wetted by rain.

The bulk transfer equations and the surface energy balance constitute a set of three equations with four unknowns (i.e. H, λE, T_s, and q_s). In a classical treatise, H.L. Penman introduced a simplification which eliminated the surface temperature from the equations through which he was able to describe the evaporation rate from a free water surface in terms of measurable parameters only. Assuming further that the resistances for heat and vapour transport are similar (i.e. $r_{aH} = r_{aV} = r_a$) - which is plausible for a free water surface where the sources for heat and vapour are identical - combination

[7] After Raupach and Finnigan (1988).

with the energy balance equation $H = R_n - G - \lambda E$ yields the well-known **Penman combination equation for evaporation from open water** (λE_0):

$$\lambda E_0 = \frac{\Delta(R_n - G) + \rho c_p VPD / r_a}{\Delta + \gamma}$$

where R_n (net radiation) minus G (ground heat flux) represents the available energy [W/m^2], *VPD* is the vapour pressure deficit of the air [mb] which is defined as the difference between saturated vapour pressure at ambient air temperature $e_{sat}(T_a)$ and the actual vapour pressure, $e_a(T_a)$; ρ is the density of air [kg/m^3], c_p the specific heat at constant pressure [J/(kg K)], r_a the bulk aerodynamic resistance to upward transport of vapour [sec/m) , λ the latent heat of vaporization [J/kg], γ the psychrometric constant [mb/K], and Δ the slope of the saturation-vapour pressure curve at ambient temperature T_a.

The Penman open water evaporation rate is often used as a reference to characterize a site's evaporation climate. By normalizing actual evaporation totals obtained for a specific vegetation type (e.g. grass or pine forest) at a particular location for local open water evaporation (i.e. ET_a / E_0), results obtained at different locations can be compared more easily.

Introduction of a surface control on the release of water vapour, i.e. describing evaporation from vegetation in single-layer models, adds the surface resistance r_s for latent heat transport defined earlier. The **Penman-Monteith combination equation** for a single big-leaf surface reads:

$$\lambda E = \frac{\Delta(R_n - G) + \rho c_p VPD / r_a}{\Delta + \gamma(1 + r_s / r_a)}$$

The amount of energy available for evaporation (R_n - G) applies to the net radiation (R_n) and soil heat flux (G) measured for the specific surface cover type under consideration. In addition, the two bulk resistances r_s (stomatal control) and r_a (aerodynamic control) need to be parameterized according to the surface (read: vegetation) type under consideration.

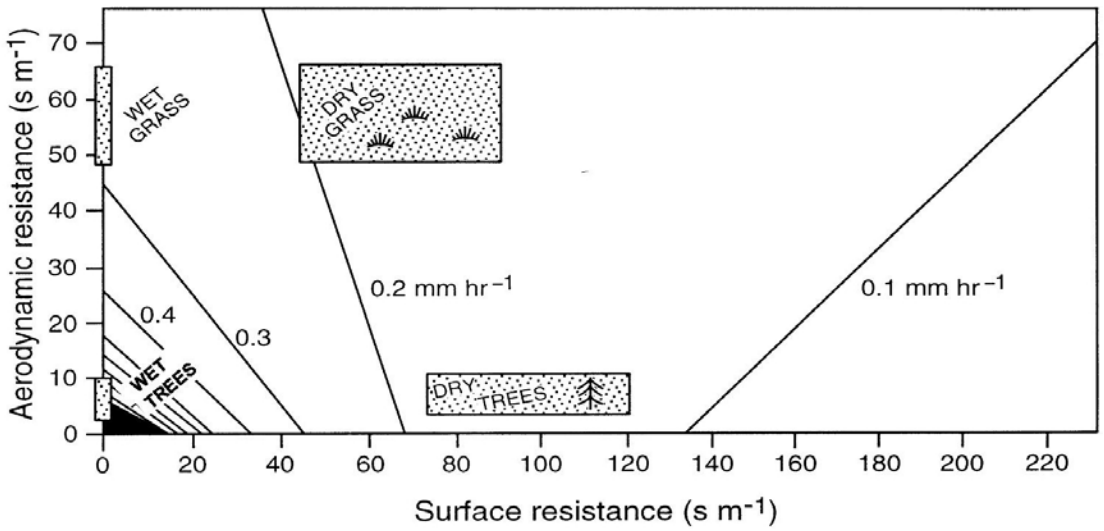

Figure III.7. *Illustration of the change in evaporation rates upon wetting of vegetation (Calder, 1990).*

As stated earlier, the value of r_s equals zero for a fully wetted surface. Under such conditions, the full Penman-Monteith equation reduces to:

$$\lambda E_{pm,wet} = \frac{\Delta(R_n - G) + \rho c_p VPD / r_a}{\Delta + \gamma}$$

As a result of the absence of stomatal control on evaporation during wet canopy conditions the associated evaporation rate becomes much enhanced and is governed largely by the magnitude of the vapour pressure deficit of the air (*VPD*) and bulk aerodynamic resistance r_a (Figure III.7).

Thus, the successful application of the Penman-Monteith equation for the prediction of actual evaporation from specific vegetation types hinges very much on the proper parameterization of the two bulk resistances r_s (bulk surface resistance) and r_a (bulk aerodynamic resistance). Their quantification is briefly discussed below.

Bulk resistance parameterization

As shown already in Figure III.6, a multi-layer model combines transport equations that are valid for each evaporating surface (leaf), whereby each leaf has a leaf stomatal resistance (r_{sto}) that accounts for the diffusion of water vapour from within the leaf to the leaf surface, plus a leaf boundary-layer resistance (r_b) that accounts for the diffusion of the water from the leaf surface to the surrounding well-mixed air.

In the case of a single-layer (big-leaf) model, up-scaling of **leaf stomatal resistances** to the entire canopy is usually done by normalization with the leaf area index of the vegetation, *LAI* (defined as the projected canopy surface area per unit area of ground surface), according to:

$$r_s = \frac{r_{sto}}{LAI}$$

Leaf stomatal resistance can be measured using a porometer or photosynthesis measurement systems by placement of the leaf in a measurement chamber. Sunlit and shaded leaves are expected to behave differently. Models to describe the stomatal resistance range from simple mathematical expressions relating stomatal behaviour to climatic parameters such as radiation, temperature and vapour pressure deficit, to elaborate plant physiological models that combine a mechanistic model for photosynthesis with a leaf stomatal conductance sub-model. The leaf boundary-layer resistance is modeled using leaf dimensions and local wind speed.

In view of the high species diversity of tropical montane forests, up-scaling of leaf-based measurements of stomatal resistances (if available at all) to derive an estimate of surface resistance r_s is not an easy matter. The only real option is to resort to a certain degree of empiricism, inferring r_s from independent measurements of evaporation. For example, Bowen ratio method-based estimates of λE can be used in an inverted application of the Penman-Monteith model to derive r_s for known climatic conditions according to:

$$r_s = r_a \left(\frac{\Delta(R_n - G)}{\gamma \lambda E} - \frac{\Delta}{\gamma} - 1 \right) + \frac{\rho c_p VPD}{\gamma \lambda E}$$

The availability of an appropriate and extensive climatic data set allows the derivation of an empirical expression for r_s in terms of measured environmental variables, for example:

$$r_s = f(R_s, VPD, T_a, ...)$$

where *f* is an empirical (e.g. multiple exponential regression) function of such variables as short-wave (or net) radiation, vapour pressure deficit, and temperature. Inserting the appropriate climatic data into such an equation then gives r_s values that may then be used in a direct application of the Penman-Monteith equation to compute the corresponding actual evaporation rates.

Figure III.8 illustrates the average diurnal pattern of r_s derived by inverse application of the Penman-Monteith equation for selected measured half-hourly evaporation rates for a tall windward cloud forest in northern Costa Rica as determined by the current project. A typical daytime value of 25 sec/m was found.

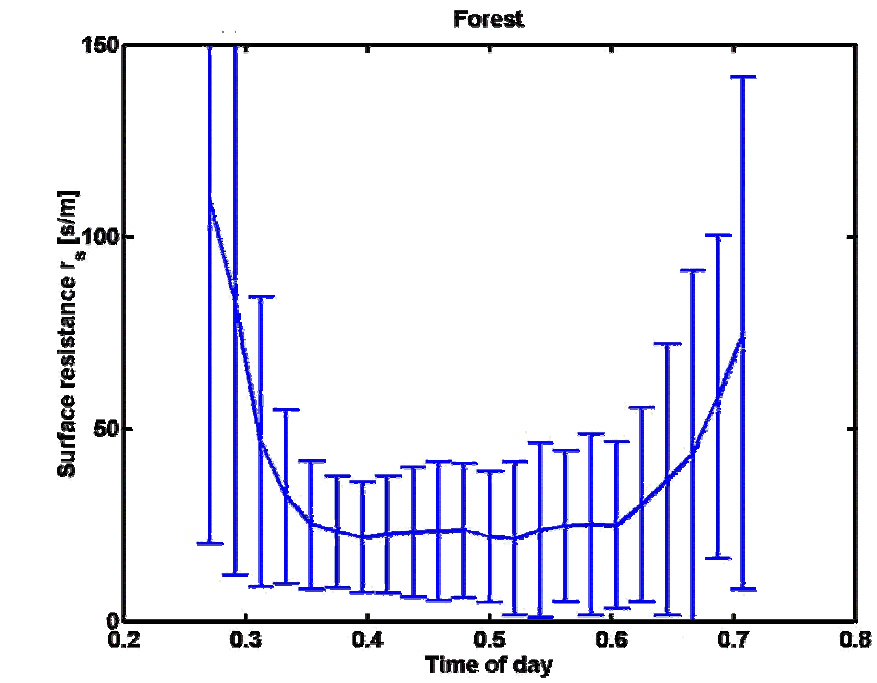

Figure III.8. *Mean diurnal pattern of surface resistance for a windward cloud forest in northern Costa Rica.*

The **bulk aerodynamic resistance**, r_{aV}, can be written as an expression in terms of the bulk aerodynamic resistance for momentum, r_{aM}, and an extra resistance r_b to account for the additional resistance to the transfer of heat or water vapour in the direct vicinity of each leaf (Figure III.6). Ideally, correction functions for atmospheric stability conditions need to be used which differ for latent heat and momentum transport. The bulk aerodynamic resistance to vapour transport, r_{aV}, for neutral atmospheric conditions, when atmospheric buoyancy effects are not important, is given by:

$$r_{aV} = \frac{\ln\left[\left(z_u - d\right)/z_{om}\right]\ln\left[\left(z_e - d\right)/z_{ov}\right]}{k^2 U_z}$$

where z_u and z_e are the respective heights at which wind speed and humidity are measured, and U_z is the measured wind speed. The two terms z_{0m} and z_{0v} are so-called roughness lengths [m] that mark the effectiveness of the surface to generate turbulence when wind is passing. These differ for momentum and vapour but they are both related to vegetation height h_c according to:

$$z_{om} \cong 0.123 h_c \text{ and } z_{ov} \cong 0.25 h_c$$

The remaining terms k and d represent the Von Karman constant (0.41) and the so-called displacement length of the vegetation, respectively. The latter represents the vertical distance over which z_0 needs to be lifted. Thus, atmospheric exchange starts at a level ($z_0 + d$). Both parameters can be derived from measurements of turbulence or the vertical profile of the wind speed but more often d is approximated simply as $d = 0.67h_c$.

Estimates can now be made of r_{aV} for a vegetation of known height h_c. Because it is usually not feasible to take full account of atmospheric stability corrections, an empirical allowance for stability can be used which can be written in general form as:

$$r_{aV} = \frac{4.72 \ln\left[\left(z_u - d\right)/z_{om}\right] \ln\left[\left(z_e - d\right)/z_{ov}\right]}{1 + 0.536 U_z}$$

Application of this so-called Thom and Oliver expression for the bulk aerodynamic resistance enables r_a to be expressed as an inverse relation to wind speed U_z. Figure III.9 gives an example for the same Costa Rican cloud forest (plus a nearby pasture) for which the bulk stomatal resistance has been portrayed in Figure III.8. The much greater aerodynamic roughness of a forest canopy compared to the shorter grass of the pasture is reflected clearly in the much reduced resistances for the forest.

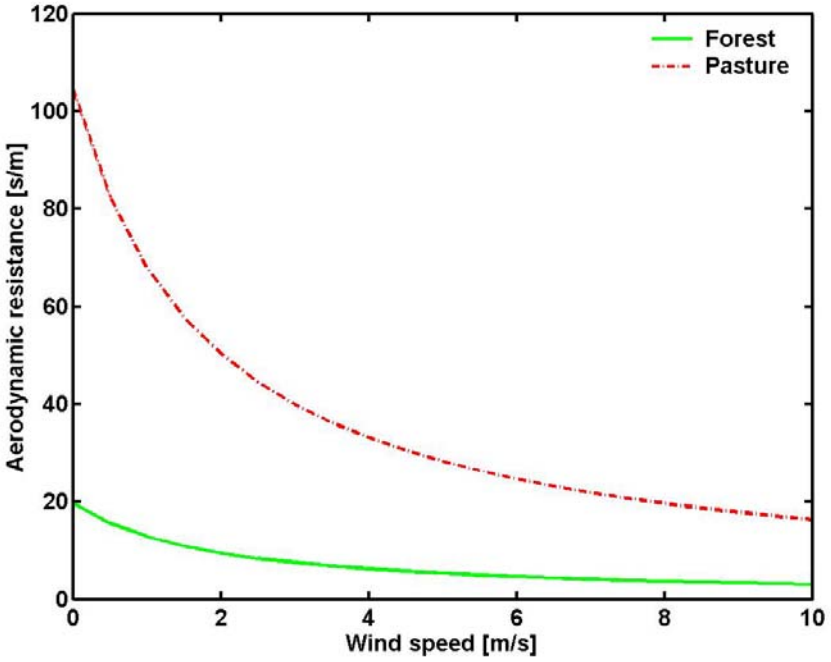

Figure III.9. *Aerodynamic resistances of cloud forest and pasture vs. wind speed.*

Once the bulk aerodynamic and surface resistances for a vegetation type are known, actual evaporation rates can be computed using the Penman-Monteith equations for dry and wet canopy conditions and summing the respective totals to give total actual evaporation. However, this requires some criterion to distinguish between wet and dry canopy conditions, i.e. interception evaporation and transpiration. The choice of the length of time required to dry a canopy rather affects the computed evaporation total as a longer drying time tends to boost the contribution by wet canopy evaporation at the cost of dry canopy evaporation and *vice versa*. Naturally, this effect is caused by the potentially large contrasts in wet and dry canopy evaporation rates under otherwise comparable ambient conditions, especially for forest vegetation (Figure III.7).

As an illustration, an annual evaporation total of 725 mm was computed for the Costa Rican cloud forest studied by the present project using the Penman-Monteith model in a ‘stop-go mode’ with zero canopy drying time. Increasing the drying time to 2 hours increased the total to 795 mm, mostly because of a strong increase in computed interception evaporation, whereas a further increase to 820 mm was found for a drying time of 3 hours. Canopy drying times may be estimated from detailed rainfall records in combination with so-called leaf wetness sensors. Interestingly, the effect of variable drying times was much less pronounced for a nearby pasture where the introduction of a two-hour drying time only produced an increase in evaporation of 10 mm. Again, this can be explained by the much smaller contrast between wet- and dry-surface evaporation rates observed for grassland as a result of the greater aerodynamic resistance of pasture compared to pasture (Figures III.7 and III.9).

III.3 **Instrumentation used in the determination of the radiation budget and evaporation**

Fluxes of sensible and latent heat are normally determined from 30-minute or hourly values of measurable parameters such as net radiation, wind speed, air temperature and humidity. The mean values are typically calculated from 60 to 240 instantaneous measurements of radiation, temperature and humidity and a count of rotations for wind speed. In addition, averages and standard deviations are preferably calculated for each 5-minute interval. Removing any trends in the data in this way does not influence the mean values but does give a better estimate of short-term variations because the diurnal trend is removed. In the following sections the most widely used types of instrumentation is discussed for the measurement of radiation components, wind speed, temperature and humidity as well as rapid variations therein, and the soil heat flux.

III.3.1 *Radiation balance*

III.3.1.1 Short-wave radiation

The solar radiation received by the Earth has relative short wave lengths, mostly 0.3 up to 3µm, hence the name short-wave radiation. The short-wave radiation that reaches the surface consists of direct and diffuse short-wave radiation. Diffuse short-wave radiation is multi-directional due to scattering of direct short-wave radiation by air molecules and dust particles present. During overcast conditions (full cloud cover) all short-wave radiation is diffuse. Normally, the short-wave radiation received at the surface is smaller than the solar constant, the amount received at the outer atmosphere (1367 W/m^2), due to absorption and reflection. During partly cloudy weather the incoming short-wave radiation at the surface can be larger than the solar constant during short periods due to additional reflected short-wave radiation by clouds. Part of the short-wave radiation received is reflected back into space. The reflection coefficient of the surface is called the albedo and depends on the direction of the solar beam, the proportion of diffuse radiation and the type of surface cover. Tall vegetation reflects less radiation than short vegetation, i.e. it has a lower albedo. Most tropical forests, including cloud forests, have an albedo of 0.12-0.14.

Measurement of short-wave radiation

Short-wave radiation is usually measured with a **pyranometer**, which measures the sum total of the diffuse and direct parts of the radiation. The most commonly used pyranometer is that produced by Kipp & Zonen (www.kippzonen.com). The pyranometer consists of a blackened disc topped by two concentric glass hemispheres with diameters of typically 30 and 50 mm, respectively (Figure III.10). The glass of both hemispheres is such that only radiation of wave lengths between about 300 μm and 3000 μm are transmitted, thereby preventing long-wave radiation from reaching the sensor. Usually, the pyranometer is mounted on a white plate which confines the radiation measurement to radiation coming from one hemisphere only. The diffuse radiation can be measured by applying a 'shadow band' shielding the instrument from direct radiation. The direct radiation then follows from the total radiation minus diffuse radiation.

The reflected radiation can be measured by hanging the instrument simply upside-down. More commonly, an **albedometer** is used which consists of two pyranometers, one measuring incoming short-wave radiation and the other (placed upside-down) measuring reflected short-wave radiation (Figure III.10). For a pyranometer, incoming short-wave radiation is related to the temperature difference between a disc that is exposed to the sun and a disc that is not heated by the solar beams. This results in the following linear relationship: $R_{s\downarrow}=C_{pyr}\Delta T$, where C_{pyr} is an instrumental constant and ΔT the temperature difference between the two discs. The instrumental constant is usually specified by the manufacturer. Intercalibration between pyranometer sensors used in a project ensures measurements that are directly comparable although external calibration by the manufacturer is advisable after prolonged field use. The typical accuracy of a pyranometer is ca. 5%. Night-time values can be used to derive a sensor offset. Although most of the reflected radiation received by the sensor originates directly underneath the sensor, it should be placed above a representative part of the vegetation and not too close to the mounting mast or tower, because the field of view of the instrument is about 180°. Careful horizontal positioning is also important.

Naturally, surrounding obstacles should not be allowed to cast a shadow on the sensor. Representative short-wave radiation values can be obtained from pyranometer measurements made each 15 or 30 seconds and taking the average for a 30-minute period.

Figure III.10. *Pyranometer (left) and Albedometer (right).*

Estimation of short-wave radiation

On many locations, daily averages of incoming short-wave radiation are still derived from daily records of sunshine duration. The latter are measured using a Campbell-Stokes Pattern Sunshine Recorder, which employs a glass sphere to focus the sun's rays to an intense spot. This will char a mark on a curved chart mounted concentrically with the sphere. The position of the spot moves across the chart due to the (apparent) movement of the sun. When the sun is obscured, the trace is interrupted. At the end of the day the total length of the trace, minus gaps, is proportional to the duration of sunshine. The daily incoming short-wave radiation ($S_{\downarrow}$) can be derived from the sunshine duration and the incoming short-wave radiation at the top of the atmosphere using the following empirical formula:

$$S_t = (a_s + b_s \frac{n}{N}) S_0 \qquad [MJ\ m^{-2} \quad day^{-1}]$$

where S_0 is the daily extraterrestrial radiation, a_s the fraction of S_0 on overcast days (n=0), a_s+b_s represents the fraction of S_0 on clear days, n/N is the relative cloudiness, n the number of bright sunshine hours per day and N the total day length. Available local measurements of daily incoming short-wave radiation (using a pyranometer) allow derivation of locally applicable values for the so-called Ångström coefficients a_s and b_s. Average values for a_s and b_s are 0.25 and 0.5 respectively.

III.3.1.2 Long-wave radiation

Between the earth's surface and the atmosphere a significant exchange of energy takes place in the form of long-wave radiation (wave lengths of 3-100µm). Both the ground and the atmosphere emit radiation with a spectrum that is characteristic of their temperature. Since the surface is on average warmer than the atmosphere, there is usually a net loss of energy as thermal radiation from the ground. Although most surfaces do not emit at black-body temperature, the emissivity ε_s is nearly 100% for most natural surfaces. The outgoing long-wave radiation from a surface consists of emitted radiation due to the surface temperature, and incoming long-wave radiation that is reflected at the surface according to:

$$R_{l\uparrow} = \varepsilon_s \sigma_b T_s^4 + (1 - \varepsilon_s) R_{l\downarrow} \qquad [W / m^2]$$

where ε_s is the surface emissivity, σ_b the Stefan-Bolzmann constant ($5.67*10^{-8}$ $Wm^{-2}K^{-4}$) and T_s the surface temperature.

Measurement of long-wave radiation

Long-wave radiation can be measured with a **pyrgeometer**. The most common pyrgeometers are the precision infrared radiometers (PIR) produced by Eppley Laboratory, Inc. (www.eppleylab.com; Figure III.11). Their Precision Infrared Radiometer is intended for unidirectional operation in the separate measurement of incoming or outgoing terrestrial radiation as distinct from the net long-wave flux. Representative long-wave radiation values can be found by making pyrgeometer measurements each 15 or 30 seconds and taking the average for a 30-minute period.

Figure III.11. *Pyrgeometer (Eppley-PIR, left) and two net radiometers (CNR1, middle) and (Q7, right).*

Estimation of long-wave radiation

The daily exchange of long-wave radiation between vegetation and soil ('outgoing') and atmosphere and clouds ('incoming') can be represented by the following radiation law:

$$R_{ln} = -f\varepsilon'\sigma_{bd}(T+273.2)^4 \quad [MJm^{-2}day^{-1}]$$

where R_{ln} is the net long-wave radiation, f an adjustment factor for cloud cover, ε' the net emissivity between the atmosphere and the ground, σ_{bd} the daily value of the Stefan-Bolzman constant ($4.903*10^{-9}$ MJ m^{-2} $^oC^{-4}$ day^{-1}) and T the mean air temperature (^oC). The net emissivity ε' can be estimated from:

$$\varepsilon' = a_e + b_e\sqrt{e_d}$$

where e_d is ambient vapour pressure [kPa] and a_e and b_e are coefficients that are ca. 0.34 and -0.14 respectively. If humidity measurements are not available, the net emissivity can be estimated from the average temperature according to:

$$\varepsilon' = -0.02 + 0.261\exp(-7.77*10^{-4}T^2)$$

The cloudiness factor f can be estimated using solar radiation data from:

$$f = a_c\frac{S_t}{S_{top}} + b_c$$

where S_t is measured solar radiation, S_{top} the solar radiation from clear skies, and a_c and b_c are calibration parameters that are about 1.35 and -0.35 respectively for arid areas and 1.0 and 0 for humid areas. If sunshine hours are available, and using the average Ångström values plus the parameter values for arid areas for a_c and b_c then the cloudiness factor becomes:

$$f = 0.9\frac{n}{N} + 0.1$$

III.3.1.3 Net radiation

Net radiation is the net input of radiation at the surface, i.e. the difference between the total incoming and outgoing short- and long-wave radiation components.

Measurement of net radiation

It is generally preferable to calculate the net radiation by adding up the independently measured components of the short- and long-wave radiation. The net radiation can be measured directly using a **net radiometer** as well. Examples include the Q7 manufactured by Radiation and Energy Balance Systems, Inc. (Seattle,USA, www.campbellsci.com) and the CNR1 (Kipp & Zonen) (Figure III.11). The CNR1 model measures the four radiation components separately: the two CM3 pyranometers measure the short-wave radiant flux from 0.3 to 3.0 mm and the two CG3 pyrgeometers measure the Far Infra Red radiant flux between 5 and 50 mm wave lengths. The wave-length gap between the two instruments produces negligible errors. The CNR1 is robust, virtually maintenance-free and calibration is relatively straightforward.

Most other net radiometers, including the Q7 measure the short- and long-wave radiation components combined. These instruments consist of two black plates facing up and down which are separated by an insulator. The difference in incoming and outgoing short- and long-wave radiation leads to a differential heating of the two plates which can be recorded. The net radiation can then be measured in a similar manner as the short- and long-wave radiation in a pyranometer and a pyrgeometer. The plates are protected by hemispherical domes that are either made of polyethylene or glass, depending on the type. The accuracy of combined net radiometers is usually not very high.

Estimation of net radiation

If only sunshine, temperature and humidity data are available, the daily net radiation can also be estimated for general purposes with the following equation:

$$R_n = \left(0.25 + 0.5\frac{n}{N}\right)S_0 - \left(0.9\frac{n}{N} + 1\right)\left(0.34 - 0.14\sqrt{e_d}\right)\sigma_{bd}T^4 \quad [MJm^{-2}day^{-1}]$$

where all the terms are as defined previously and e_d is ambient vapour pressure [kPa].

III.3.2 *Mean wind speed, temperature and humidity*

III.3.2.1 Wind speed

Wind speed is used in most of the methods to determine evaporation described in section III.2. Wind speed is measured mainly by relatively cheap **cup anemometers**. These instruments typically consist of three or more semi-conical cups that rotate horizontally (Figure III.12). The wind speed follows as a function of the number of rotations within a certain time period. The functional dependence between wind speed and rotation speed is derived by calibration in a wind tunnel as specified by the manufacturer. The accuracy of cup anemometers is usually about 1 m/s, though an accuracy of about 0.5 m/s may be obtained by using cup anemometers that have been designed specifically for use at low wind speeds. The limited accuracy of cup anemometers is caused by the fluctuating nature of wind speed. Cup anemometers tend to accelerate faster than they decelerate, and this over-speeding leads to a general overestimation of wind speed. In addition, cup anemometers do not record wind speeds below the instrument's stalling speeds (often around 0.3 m/s) and as such they underestimate wind speed.

Examples of cup anemometers include the A100R (Vector Instruments, www.windspeed.co.uk) or the PAH-LT (Wittich & Visser, www.wittich.nl). Various other wind sensors can be found at the Campell Science Inc. website: www.campbellsci.com. Cup anemometers are mounted on booms towards the main wind direction to prevent obstruction by the mast. A standard measurement height of 2m is used for use in the Penman-open water and Penman-Monteith methods (section III.2.3).

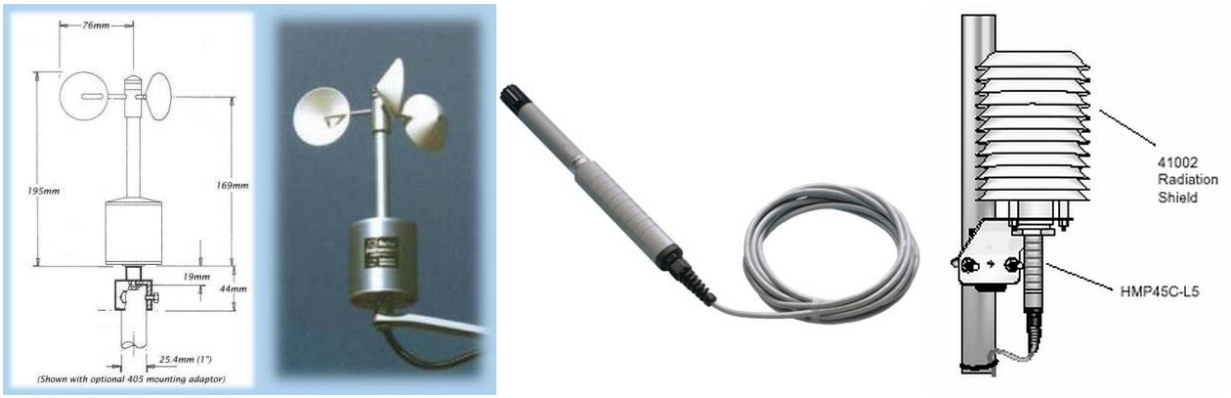

Figure III.12. Cup anemometer (Vector Instruments, left), Vaisala temperature and humidity sensor (HMP45, middle) and radiation shield housing Vaisala temperature and humidity sensor (right).

III.3.2.2 Temperature

The most well-known sensor for **temperature** measurement is the common **mercury thermometer**. This type of thermometer makes use of the fact that glass and mercury respond differently to changes in temperature. However, mercury thermometers cannot be used to register the temperature automatically. Therefore, temperature measurements are made either using (expensive) sonic anemometers (Figure III.4), or electrical thermometers. An electrical thermometer is a thermometer which uses electrical properties that are a function of its thermal state. Common examples include resistance thermometers whose electrical resistance changes with temperature (so-called RTD's and thermistors). A **thermistor** is a device that possesses a negative temperature coefficient, i.e. the resistance decreases with increase in temperature. An example is the P-107 (www.campbellsci.com) but it can also be produced cheaply by any electronics department. The thermistor is encapsulated for protection and can easily be installed in air, soil or water. An **RTD,** or more specifically a **PRT** is a **p**latinum **r**esistance **t**emperature detector which measures the resistance of a platinum element. The relationship between temperature and resistance is approximately linear over a small temperature range. PRT sensors having four wires are the preferred type for precision work as they offer excellent accuracy over a wide temperature range. Unlike thermo-couples (see below), it is not necessary to use special cables to connect resistance thermometers to a data logger.

A **thermo-couple** consists of a circuit of two wires made of different material that are coupled at two locations (denoted by T1 and T2 in Figure III.13). If the two connections are heated differentially, an electrical voltage difference develops between the two contact points. This voltage difference can be measured using a voltage meter. During operation, the temperature at contact point T2 is held constant, whereas the other contact point is allowed to take on the temperature of the environment (T1). The measured difference in electrical voltage gives the difference in temperature between contact points T1 and T2. As the temperature of T2 is known, the ambient temperature is obtained. The thermo-couple contact point T1 representing ambient temperature (Figure III.13 centre) can be several metres away from contact point T2 at the location of the data-logger (a device programmed, *inter alia*, to measure voltages at prescribed time steps (cf. Figures II.4 and II.5). It is necessary to connect points T1 and T2 with a special thermo-couple cable made up of the same metals as used at contact point T1. A typical combination of materials used in many thermo-couples is chromel and constantan with a diameter of the contact point of about 0.1-0.2 mm. For a wet-bulb thermo-couple that is equipped with a wick for the measurement of humidity (see next section) the typical contact point diameter is about 0.5 mm (Figure III.13 right-hand panel). The small time constant afforded by these small diameters allows measurement of rapid fluctuations in temperature apart from mean temperatures. A disadvantage of the thin wires of thermo-couples is their limited robustness and the need for frequent maintenance.

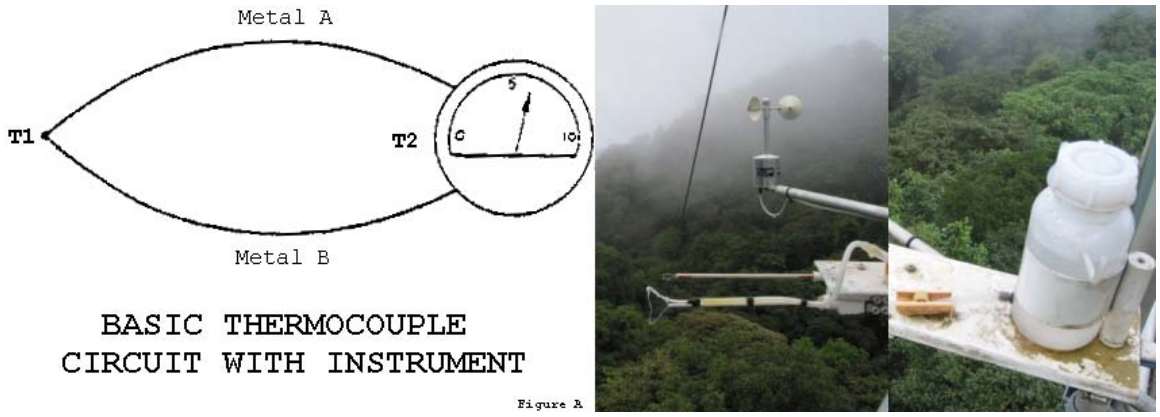

Figure III.13. *Thermo-couple temperature sensor principle (left), chromel-constantan thin-wire thermo-couple set (centre) and water supply for a wet-bulb thermo-couple (right).*

Generally, electrical temperature sensors like the ones described above need to be placed inside a radiation shield (Figure III.12) to prevent errors caused by direct insolation. Good ventilation of the shield is required, however, either naturally or artificially. At relatively windy sites natural ventilation is usually sufficient. In cloud forest environments errors due to insolation can be expected to be relatively small due to the prevailing wind speeds and modest radiation intensities for much of the time (frequent fog and low cloud). However, radiation shields tend to become soaked during fog events and take a long time to dry after the event (often several hours). Temperature sensors placed inside a shield are then effectively functioning as wet-bulb temperature sensors during the drying period. Non-protected thermo-couples for the measurement of rapid temperature fluctuations, on the other hand, dry up within minutes after wetting and are the preferred alternative in cloud forests. Mean air temperatures for 30- minute or hourly periods can be derived from measurements made each 15 to 30 seconds, depending on the time response of the sensor. Thermo-couple readings are typically taken each second, i.e. at a frequency of 1 Hz.

III.3.2.3 Humidity

Generally, **atmospheric humidity** is some measure of the water vapour content of the air. Mixing ratio, specific humidity, absolute humidity, vapour pressure, relative humidity and dew point are all measures of atmospheric humidity. The multitude of humidity measures is partly due to the many different methods of measurement. In the context of this manual, vapour pressure, specific humidity and relative humidity are briefly explained before describing the various sensor types.

The **saturation vapour pressure**, (e_{sat}), is the vapour pressure at the given temperature for which the water vapour is in equilibrium with a plane surface of water (i.e. the evaporation rate is equal to the condensation rate, cf. Figure III.1). The air is then said to be saturated with water vapour. The saturation vapour pressure appears to be a function of temperature T_a [°C] only, according to:

$$e_{sat}(T_a) = 6.1078e^{\frac{17.269T_a}{(T_a+237.3)}} \qquad [mb]$$

The **actual vapour pressure** of the air (e_a) is the partial pressure exerted by the water vapour molecules. The vapour pressure can be derived from the psychrometric formula:

$$e_a(T_a) = 6.1078e^{\frac{17.269T_w}{(Tw+237.3)}} - \gamma(T_a - T_w) \qquad [mb]$$

where T_a is the air temperature (dry-bulb temperature) and T_w the wet-bulb temperature (see below).

The **relative humidity** (*RH*) then is the ratio between actual and saturation vapour pressures:

$$RH = \frac{e_a}{e_{sat}} * 100 \qquad [\%]$$

The **specific humidity** (*q)* is the ratio of the mass of water vapour in the air to the total mass of air. It is related to the actual vapour pressure e_a according to:

$$q = \frac{e_a c_p}{\gamma \lambda} \quad [kg / kg]$$

where γ is the so-called psychrometric constant, λ the latent heat of vaporization and c_p the specific heat of air at constant pressure which is about 1005 J/(kg ^{o}C).

The psychrometric constant (γ) is given, in turn, by:

$$\gamma = \frac{c_p P}{0.622 \lambda} \qquad [mb /^0 C]$$

where *P* is the air pressure [mb].

The latent heat of vaporization (λ) is given by:

$$\lambda = (2.501 - 0.00237 T_a) 10^6 \qquad [J / kg]$$

where T_a is the air temperature in °C.

Finally, the slope of the saturation vapour pressure curve (Δ) can be estimated from:

$$\Delta = \frac{e_{sat}(T_a) * 17.269 * 237.3}{(T_a + 237.3)^2} \qquad [mb /^0 C]$$

Humidity sensors

A **hygrometer** is an instrument that measures the water vapour content of the air. There are six different types of hygrometers of which two groups are briefly described below. The first group consists of **psychrometers**, which utilize the thermodynamic principle. The second group is formed by a class of instruments that depend on the change of electrical properties brought about by the absorption of moisture (**electrical hygrometer** or **capacitance sensors**).

A **psychrometer** consists of two thermometers that are used side by side, one of which is the ordinary thermometer (‘dry bulb’), while the other (the ‘wet bulb’) has its sensor covered with a cotton jacket (‘wick’) that is kept saturated with distilled water. The temperature measured by the wet-bulb thermometer is generally lower (due to evaporation) than that measured by the dry bulb. The difference in temperature is a measure of the humidity of the air, a lower humidity enhances the rate of evaporation and hence the cooling of the wet bulb. The magnitude of this ‘wet-bulb depression’ is related to ambient humidity by the psychrometric formula given above. This equation is used to calculate the actual vapour pressure from dry-bulb (T_a) and wet-bulb (T_w) measurements of the air. All the types of temperature sensors described in section III.3.2.2 are used in psychrometers. Most psychrometers are equipped with a radiation shield such as used for air temperature measurement (cf. Figure III.12). Free evaporation from the wet-bulb sensor requires sufficient ventilation. An artificial ventilation rate of 4 m/s is often applied although the application of ventilation can be limited when measurements are made at a remote site due to restrictions in power supply. At relatively windy sites, shielded instruments can be assumed to have sufficient natural ventilation. However, the tendency of radiation shields to saturate in foggy environments already commented upon needs to be borne in mind. Furthermore, measurements of *RH* tend to be unreliable under near-saturated (fog) conditions.

Thin-wire thermo-couples have a rapid response time but are also more liable to breakdown than thermistors or PT100 sensors. Low-cost, sturdy thermo-couples can be custom-made using special thermo-couple wire to connect the two metals via a small welding (diameter, 1-2mm). Maintenance of a thermo-couple psychrometer is important in order to ensure the proper water supply to the wet-bulb sensor. The supply bottle (Figure III.12) needs to be replenished regularly and feeder tubes checked for blockages.

Capacitance sensors (electrical hygrometers) are used most often for climatic stations due to their low maintenance requirements and overall stability in performance. Examples include the combined temperature and relative humidity sensors produced by Vaisala, such as the HMP45c (www.campbelsci.com). The sensor is again placed within a radiation shield. The main disadvantage is the rather slow response time of the instrument, and humidity absorption at the permeable measurement heads of the sensor. In cloud forest situations, the frequent occurrence of fog both wets the internal radiation shield and the permeable measurement heads which both dry slowly. As a result, the measurement of relative humidity during short fog-free periods is mostly overestimated by this type of set-up. As mentioned earlier, taking precise measurements of *RH* under the near-saturated atmospheric conditions prevailing for much of the time in many cloud forests remains difficult and the use of wet- and dry thermo-couples is to be preferred (cf. discussion in section III.3.2.2).

III.3.3 *Soil heat flux*

The **soil heat flux** (*G*) is often ignored in energy balance studies because its magnitude is often small and the seasonal average is almost zero. However, in situations with semi-open canopies (e.g. elfin cloud forests) or where forest has been cleared to make way for pasture or crops, radiation levels reaching the soil surface can be large enough to affect the amount of energy going into the soil.

The soil heat flux at the surface itself is difficult to measure directly, but it can be estimated by measuring the heat flux at some depth below the surface using **soil heat flux plates** and knowledge of certain soil characteristics (see below). In addition, soil heat flux can be calculated using measured soil temperature profiles (cf. section IV.4.1). Two widely applied methods for the calculation of the soil heat flux are the so-called **integration method** and the **gradient method**. Both are discussed briefly below.

The magnitude of the soil heat flux depends on the thermal properties of the soil, such as its heat capacity, thermal diffusivity and thermal conductivity. In turn, these parameters depend on the composition of the soil material (mineral and organic matter contents). In addition, soil moisture status is also very important and the thermal properties of the soil have to be estimated from observations of soil temperature and soil moisture alike. The volumetric heat capacity of the soil C_s is approximated by:

$$C_s = x_{q,c}\rho_{q,c}c_{q,c} + x_w\rho_w c_w$$

where *x* denotes a volume fraction, ρ bulk density and c the specific heat capacity of the solid fraction (subscript *q,c*) or water (*w*). The solid fraction is 1.0 minus the soil porosity value (cf. section IV.3.3). The determination of a range of static and dynamic soil parameters is discussed in Part IV of this document.

Soil heat flux plates

The soil heat flux [W/m^2] can be determined according to:

$$G_0 = G_z - C_s\Delta z\left(\Delta T / \Delta t\right)$$

where G_0 and G_z are the surface soil heat flux and that through the flux plates respectively. Δz and ($\Delta T/\Delta t$) are the depth of soil [m] above the plates (typically ca. 0.02 m) and the change in mean temperature of this layer per unit time [K/s], whereas C_s is the volumetric heat capacity [$Jm^{-3}K^{-1}$].

The magnitude of G_z is measured by the heat flux plate. It should be noted that a heat flux plate measures the heat conductance through the plate rather than through the surrounding soil. The two may differ, especially when the soil is wet. The thermal conductivity of a wet soil is larger and the soil heat flux as measured by the plate is underestimated. An example of a widely used heat flux plate is that produced by Middleton & Co. Pty. (http://www/middletonsolar.com/products/product19.htm). The accuracy of this plate is stated to be ca. 5%.

Integration method

Using measured soil temperature profiles the soil heat flux can be calculated from the amount of heat stored in the soil profile during a certain time interval. The method needs the volumetric heat capacity and temperature measurements down to a depth where the temperature can be considered constant during the period under consideration. The flux is calculated from:

$$G_0 = \frac{C_s}{\Delta t} \sum_{i=1}^{n} \Delta z_i \Delta T_i$$

where n denotes the number of soil layers used. Each soil layer is characterized by its depth, Δz [m] and ΔT is the change in mean soil temperature [^{o}C] during a time interval Δt [s]. The volumetric heat capacity, C_s [$Jm^{-3}K^{-1}$] is considered uniform in the soil in this example but may be specified separately for each layer n with depth Δz using information on soil composition and moisture status. As changes in temperature near the surface tend to be the most pronounced, measurements near the surface are important. The integration method is not very sensitive to exact sensor positioning or differences between sensors.

Gradient method

This method uses the vertical temperature gradient and soil thermal conductivity k_s, to calculate the soil heat flux at a depth z:

$$G_z = -k_s \frac{T_{z_1} - T_{z_2}}{z_1 - z_2}$$

This method requires only two temperature (T) measurement depths (z_1 and z_2) instead of a profile measurement. However, the surface soil heat flux is larger than that measured at a certain depth z (≈ average of z_1 and z_2). Therefore, an estimate of the reduction in flux with depth, the so-called damping depth D_d, is needed. D_d is defined as the depth at which the amplitude of the temperature wave at the surface is reduced by a factor 1/e. The damping depth is a crude approximation which also neglects the phase shift in temperature with depth. In addition, the method is sensitive to sensor positioning, sensor differences as well as to the magnitude of soil thermal conductivity and estimated damping depth.

The soil temperature is most often measured with the thermistor-type temperature sensors described in section III.3.2.2. The absolute values of measured temperatures as used for the determination of temperature gradients are always less accurate than differential values such as the change in temperature of the same sensor during a time period. Therefore, the profile integration method is the preferred option.

Part IV: Characterization of soil water dynamics and soil physical properties in cloud forest areas, with special reference to volcanic soils

IV.1 Introductory remarks

Soil physics has developed strongly as a discipline since 1907, when Buckingham proposed the matric potential theory, and later in 1942 when reliable tensiometers for the measurement of matric potential were first constructed. During these early years, theory and experimental methods developed hand in hand. This was partly because of the necessity for many measurements to be carried out in the field but it also reflects the increasing importance attached to soil physical information in the context of soil management, crop production, and soil erosion. Many soil physical methods have been standardized, and their limitations, reliability, and areas of application are now well established. There are many books and technical notes that provide clear descriptions of soil physical methods. Nevertheless, specific cases of study require application of those techniques that are most suitable to that particular case or condition. Volcanic soils and the highly organic soils found in many cloud forest areas provide a case in point. Here, a protocol for the evaluation of physical and hydraulic properties of volcanic soils, more specifically volcanic soils with a coarse sandy to gravelly layer, is offered.

The magnitude of several physical properties of volcanic and cloud forest soils differs considerably from those for other soil classes. This can be attributed to the distinct properties of the volcanic parent material, including the presence of non-crystalline material and accumulation of soil organic matter under the cool and wet conditions prevailing in many cloud forest areas. Examples include the low bulk density, poor clay dispersion (altering textural analytical results) and high water holding capacity. Therefore, the following protocol for the identification of soil properties pertains specifically to the soil class of the Andisols.

IV.2 Selection of sampling areas

Physical and hydraulic properties of forest soils are very variable in space (and in time if land use changes are introduced). Therefore, soil sampling and *in-situ* measurements require *a priori* knowledge of soil distribution, the geomorphological features of the area, as well as the topographical position of specific sites within the landscape. Needless to say, the sampling sites should be typical of the soils that the samples are meant to represent. For this purpose, several samples for determining soil properties should be taken from each soil class at the selected sites and from each soil horizon, after completing the soil description and characterization protocol[8]. The sampling site should be away from roads, fences, houses, trees and other features that may have caused soil disturbance prior to the sampling. The characterization of some physical properties of soil, such as bulk density, porosity, water retention characteristics and hydraulic conductivity, requires undisturbed samples that are representative of the horizon being sampled. Different applications require differently sized sample rings (Figure IV.1). Other attributes (e.g. pH, organic matter content, or texture) may be determined on non-volumetric samples that can be obtained using a knife or trowel.

IV.3 Soil physical determinations

IV.3.1 *Soil texture*

Usually soil texture is determined in the field by taking a moistened soil sample and pressing it between the fingers. This empirical method provides an indication of the texture but a more accurate determination is obtained in the laboratory through soil particle analysis. Moreover, Andisols typically exhibit large differences in field- and laboratory-based textures. Soil particles are cemented together by non-crystalline materials, which react with the excess amount of sodium hexametaphosphate used

[8] See e.g. FAP (1977). Guidelines for soil profile description. FAO, Rome.

for clay dispersion in the laboratory. Moreover, the inorganic colloids present in these soils possess a different point for zero net charge, which makes their complete dispersion almost impossible. Therefore, more representative soil textural results are obtained with a modification of the widely used hydrometer method (Day, 1953). These modifications include the use of a longer time period for the settling of particles <2 μm (12 - 18 hours instead of the usual 2), and of Calgon for clay dispersion (5 g L^{-1} of sodium metaphosphate and sodium carbonate at pH = 8.3).

Figure IV.1. *Attributes used for the volumetric sampling of soil.*

Analytical procedure: take soil samples of approximately 100 g from the site of interest (at least three per site or horizon). Use the standard hydrometer (type ASTM-152H). For soils with high organic matter content or salts a pre-treatment is required as outlined below.

Procedure to separate the organic material from samples:

- Use 40 g of soil sample and put it into an electrolyte flask, add 1 cm of distilled water and 5 ml of H_2O_2 (30%). Mix and keep the flask covered during the reaction (effervescence) until this is finished. Repeat this treatment with H_2O_2 until the effervescence is over.
- Move the flask to an oven set at 60°C and add 5 ml of H_2O_2 and leave it covered for 8 hours.
- Filter the soil and repeatedly wash it with distilled water to remove the volatile elements.
- Dry the soil sample in an oven at 105°C during 24 hours and weigh it.
- Determine the loss of weight, which corresponds with the loss of organic matter and salts.

Procedure for soil particle size distribution: Steps

- Prepare the dispersion solution by mixing 50 ml of Calgon (10%) and fill it up to 500 cm^3 with distilled water.
- After drying and sieving the soil samples, use a rolling pin or mortar and pestle to break up any large particles that might still be present.
- Before transferring the sample to the suspension cylinder, separate the soil fraction with diameter > 100 μm (use sieving No. 140). Use a wetted filter of about 8 cm diameter in a clean funnel and place it on the cylinder. Move the suspension in the filter and leave it for

about 30 minutes to allow the fine particles to pass through the filter. Add more water and agitate the suspension until all particles have passed through the filter. Adjust the volume of the cylinder (1000 ml) with distilled water. Wash the residual material in the filter (particles >100 μ), transfer to a glass and dry during 24 hours at 105°C and weigh.

- Weigh 40 g of soil sample and put it into a 600 cm^3 (or larger) beaker. Pour the dispersion solution into the beaker, stir vigorously with a spoon or stirring rod to the bottom of the beaker. Avoid spilling any fraction of the soil suspension.
- When the soil and dispersing solution are thoroughly mixed, rinse any soil left on the stirrer into the beaker with the rest of the mixture. Set the beaker aside in a safe place and allow it to sit for about 24 hours.
- After the 24 hours, stir the suspension in the beaker again and pour it into a 1000 ml cylinder. Using a squirt bottle, rinse out the beaker with distilled water, and add this to the soil mixture in the cylinder. Add enough distilled water to fill the cylinder to the 1000 ml mark.
- Securely cover the top of the cylinder using a plastic wrap or another secure cover.
- Mix vigorously by rotating the covered cylinder hand-over-hand at least 10 times. Be sure the soil is thoroughly mixed in the solution and does not stick to the bottom of the cylinder. Also, try not to let any of the soil suspension leak out of the top.
- Gently put the cylinder down on a table, take out the embolus and immediately begin timing (sedimentation time) with a stopwatch. In case of foam add a drop of alcohol to the suspension.
- Record the time that the cylinder was put down to the second.
- After ½ and 1 minute carefully lower (do not drop) the hydrometer into the cylinder and allow it to float in the soil suspension. Steady the hydrometer to suppress its bobbing up and down. Read the lines in the hydrometer at these times that are closest to the surface of the soil suspension and record times and readings.
- Remove the hydrometer, rinse it, dry it, and gently put it down in a safe place.
- Suspend the thermometer in the soil suspension in the cylinder for about 1 minute.
- At the end of 1 minute, remove the thermometer from the suspension, read the temperature and record the reading. Rinse the thermometer and dry it.
- Allow the cylinder to sit safely without being disturbed.
- Take other hydrometer measurements in the undisturbed cylinder at 10, 30 and 90 minutes. Place the hydrometer carefully in the suspension about 30 seconds before taking the reading to allow it to settle. Take out the hydrometer and dry it.
- Take and record another temperature reading for the suspension at each time.
- Rinse the hydrometer and thermometer when they have been removed from the suspension and dry them at each measurement. Record the results and time for each measurement.
- Leave the cylinder undisturbed for exactly 4 hours and take another hydrometer and temperature reading.
- Leave again the cylinder undisturbed for exactly 18 hours. This time period is critical and should not be significantly longer than 18 hours. Take another hydrometer and temperature reading and record the measurements.
- Discard the soil suspension by pouring it into a special pail, and spill the contents outside in a place for discarding soil materials.
- Carefully rinse and dry the hydrometer, thermometer, beakers, and cylinders, and repeat the above steps at least 2 more times for the same horizon so that you have a total of 3 sets of results for each soil horizon.

This measurement involves considerable waiting time and should be done for at least three samples from each horizon in the soil profile. Thus, having multiple 1000 ml cylinders would allow you to accelerate the process for several samples, and one hydrometer should be adequate for use with at least three cylinders if the starting times of the settling are staggered by about three minutes. After a sample is mixed with dispersing solution and water initially, it should stand for a day before proceeding to do the measurement.

Particle size data analysis:

The weight (M) of the oven-dry sample can be determined by weighing the sample and the percentage of humidity *H* from paired samples:

$$M_s = M\left(1 + \frac{H}{100}\right)$$

The hydrometer gives the suspended grams of solids per litre of suspension at 20°C and taking 2.65 g cm^{-3} for the density of the soil particles. As the suspension is affected by temperature variations, hydrometer readings (*R*) need to be corrected for temperature (R_L). The concentration of solids in the suspension (*c*, in g L^{-1}) can be calculated from:

$c = R - R_L$

Now,

$R_L = R_L$ (calibration value) + R_L (correction value)

cf = c (corrected) x f (derived from a table), for particle densities different from 2.65.

The cumulative percentage of sediment material (Z_t) is:

$$Z_t = \frac{c(corrected)}{c_o}.100 = \frac{R - R_L}{M/V}.100$$

Where c_o is the initial concentration in the suspension (g/L) *M* (in grams) is the mass of soil needed to complete the cylinder volume *V* (in litres, usually 1000-1150 ml depending on cylinder type).

$$\Theta = 1000\sqrt{\frac{30\eta s}{g(\rho_b - \rho_L}} = 12.182\sqrt{s}$$

Where Θ is a parameter to calculate the diameter of the particle corresponding with each *R*-value, *g* = 980.7 cm/sec^2; density of particles ρ_b = 2.65 g/ml; density of water ρ_L = 0.99949 g/ml; viscosity η = 8.007 x 10^{-3} poise and *s* = the effective depth of the hydrometer.

Values for the correction of R_L for temperature (b) can be deduced from tables in the hydrometer manual; however it can also be deduced from the sedimentation temperature and particle density:

$$b = \frac{1000}{12.182}.\sqrt{\frac{30.viscosity}{980.8(particledensity - waterdensity)}}$$

By using the temperature-corrected value of Θ (i.e. Θb) the diameter of the particles (*d*, in μm) corresponding to the time of sedimentation *t* (in minutes) can be calculated from:

$$d = \frac{\Theta b}{\sqrt{t}}$$

IV.3.2 *Soil bulk density, ρ_b*

Andisols generally have a low bulk density which is attributed to their highly porous soil structure and presence of non-crystalline (amorphous) materials.

Procedure:

The following instruments are required: a stainless steel ring of 5x5 cm (100 cm^3 in volume), sharpened on one of the sides to improve its penetration into the soil, a hammer and a piece of wood to push the ring into the soil.

- For each soil class, choose at least three locations close to where you performed your soil description and remove vegetation and other litter material from the soil surface.
- At each location collect al least three samples (more are preferred), by pushing the ring into the surface of the soil horizon to be sampled. Collecting samples should preferably be conducted after the start of the wet season or after a rainfall event; if necessary, wet the soil to facilitate entering the ring. Stop when the first soil material pokes through the small hole in the bottom of the ring.
- If it is difficult to push the ring into the soil, place a piece of wood over the ring and carefully hit the wood with the hammer to spread the force of the blow equally over the surface. Be aware not to push the wood further when the soil sample fills the ring entirely, this is to avoid sample compaction.
- Using a trowel or shovel, remove the ring and the soil surrounding it. Trim any soil sticking out of the ring using a knife.
- Label the ring and cover top and bottom with a tight-fitting lid or other material.
- Repeat this procedure so that you have at least three bulk density samples for each soil horizon.
- Weigh the soil samples (wet weight) using a portable balance or take the samples to the laboratory and weigh them (Figure IV.2a).
- Dry the samples in an oven adjusted at 105 degrees, during 48 hours (Figure IV.2b). Let them cool down and reweigh them (dry weight).
- Apply the following equation to determine the dry bulk density of soil sample:

$$\rho_b = \frac{M_s}{V_t}$$

Where M_s is the dry mass of soil and V_t the total volume of the sample.

Figure 2. *Determining soil bulk density.*

IV.3.3 *Soil porosity (f)*

Soil porosity is the relative volume of the soil pores expressed as a fraction or percentage of the bulk volume of the soil. It can be determined indirectly from the ratio between the volume of empty (air-filled) spaces in the soil sample (V_f) and the total volume of the soil sample (V_t), as follows:

$$f = \frac{V_f}{V_t} = \frac{V_a + V_w}{V_s + V_w + V_a}$$

Where the subscripts *s, w* and *a* stand for solids, water and air, respectively. With the exception of the water-filled pore volume V_w (which equals volumetric moisture content θ, see section IV.3.9.2), there are no direct methods to determine the magnitude of these individual parameters. Therefore, the total soil porosity is deduced from the relationship between the dry bulk density of the soil (ρ_b) and the mean soil particle density (ρ_s) which is taken as 2600 kg/m^3 for volcanic soils:

$f = (1 - \rho_b / \rho_s)$.

Alternatively, by weighing a saturated soil sample, and reweighing after over-drying it for 48 h, the saturated moisture content is obtained which equals the total porosity of the sample (cf. section IV.3.9.2).

IV.3.4 *Soil water retention curves – (pF-curves)*

Andisols are capable of retaining large amounts of water. This is partly due to their large volume of mesopores and micropores, the formation of which is enhanced by the presence of non-crystalline material and soil organic matter. However, some young Andisols under primary forest have large numbers of macropores increasing their water holding capacity, but losing this extra water already at low suctions. According to Saigusa et al. (1987), about 60% of the water held at field capacity (-33 kPa tension) is available to plants, suggesting that taking -33 kPa as the field capacity value may not be a proper threshold to evaluate water availability in these soils, which should rather be somewhere close to -10 kPa instead.

The functional relationship between the matric potential (soil water tension) and the volumetric soil water content is called the soil water characteristic function or water retention curve. This function is often evaluated by measuring matric potential and water content simultaneously at a certain soil depth or in undisturbed soil samples. In the field this is achieved by using tensiometers for measuring matric potential (section IV.4.1) and some field technique for the water content (IV.4.2). In the laboratory use is made of undisturbed soil samples (preferably paired or more) and applying the desaturation technique, with sand boxes for low suctions (applying the principle of hanging water column) and pressure plates for pressures above 1 bar. Because of the wide range of matric tensions encountered, often their (negative) logarithmic values are taken (pF), hence the frequently used alternative name for the soil water retention curve: pF-curve.

Procedure:

Sample collection and preparation: stainless steel rings of 5 cm diameter and 1 cm height are used to collect undisturbed samples for the proper determination of soil water retention curves. For a better description of the water holding capacity and water availability of soils, including their spatial variability, at least 3 samples need to be collected from each site and each soil horizon. Sites need to be determined according to the requirements of the study or based on the prevailing spatial soil class distribution. Samples need to be carefully collected by hand, pushing the sampling ring into the soil surface (for each horizon) until filling the ring up to about 1 cm below the edge, which will avoid sample compaction. Following the main direction of the pores, samples should be collected vertically

from each soil horizon. Furthermore, a similar ring is placed on top of the first sampling ring and pushed down gently until the sample fills the lower ring completely.

The rings containing the samples should be properly marked with a number that identifies the specific date and site (including depth interval) from which they were collected. They are then wrapped in aluminium paper and carefully packed to be transported to the laboratory avoiding disturbance and keeping them moist. In the laboratory the sample is prepared for analysis by removing all excess material outside of the ring's bottom and top, using a small saw to avoid closing of the pores. Once the sample is thus prepared, a nylon membrane is added to the bottom of the sample with a rubber band to keep it in place. The sample is left on a saturated sand box until complete saturation (reached when repeated weighings of the sample indicate constant weight). Upon saturation the sample is placed on the porous ceramic plate in the hanging water column device, to start the desaturation process.

*Hanging Water Column technique (for the tension range of -200 cm < **h** < 0)*:

The hanging water column device consists of a water-saturated, highly permeable porous ceramic plate connected via a capillary tube to a water column terminating in a reservoir open to the atmosphere. Water-saturated samples of soil held in rings are placed in contact with the flat plate when the water reservoir height is adjusted so as to be even with the top of the plate at the first measurement. By the equilibrium principle, water will flow from the soil sample through the ceramic plate and the tube to the reservoir overflow until the total water potential of the system is constant or in equilibrium. At this time the total potential *H* of the free water reservoir may be set equal to zero (no flow) and at the height *z* of the soil sample (*z* = 0, *P* = *Patm*) we may write:
$H = 0 = h + z$ and thus *h* = -*z* (in cm).

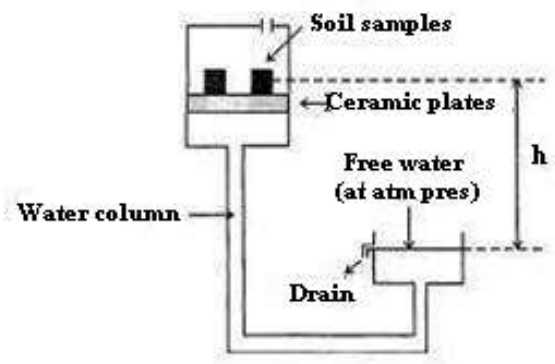

Figure IV.3. *Water retention measurement using the hanging water column device..*

After weighing the sample to determine its gross weight at saturation, the reservoir may be lowered to a new position and new measurements can be performed at the new selected depth *z* (e.g. -10 cm or pF = 1). Upon equilibration the sample is reweighed. The range of the measurements is limited chiefly by the space available for lowering the water column, until 2 m.

Before starting the measurements the ceramic plate of 1 bar should be left for 24 hours in water to ensure complete saturation of the pores in the plate. Afterwards, samples are placed on top of the plate to begin the desorption experiment. Measurements can be made at -10, -50, -100 and -200 cm and samples, depending on the texture, can be left on top of the ceramic plate for 24 hours, or until equilibrium is reached. For volcanic soils, a preliminary experiment showed that 24 hours is enough for samples of 1 cm height and 5 cm diameter to reach equilibrium. When there is good contact between the soil sample and the ceramic plate, equilibrium is reached rapidly (i.e. after several hours) since the samples are quite moist. However, clay soil needs a longer time, ranging from 36 to 48 hours.

*Pressure Plates (tension range between – 15,000 cm < **h** < - 300 cm)*:

The pressure plate now consists of an air-tight chamber enclosing a water-saturated, porous ceramic plate connected on its underside to a tube that extends through the chamber to the open air (Figure IV.4). To obtain a complete water retention curve, samples from the hanging water column, after having reached a water potential of -200 cm, are placed on top of the ceramic plate, assuring good contact between the sample and the plate. The chamber is then pressurized, by using air, which squeezes water out of the soil pores, through the ceramic plate, and out the tube. At equilibrium, flow through the tube will cease.

When equilibrium is reached, the chamber may be depressurized and the water content of the samples is measured, by weighing, drying (oven at 105 ^{o}C for 24 h) and reweighing the samples (cf. section IV.9.2). The pressure plate method is typically used up to air gauge pressures of about 15 bars (0.3, 1, 3, 5, 10 and 15 bars). The corresponding ceramic plates have a very high flow resistance; therefore it requires a substantial amount of time to remove the last small amount of water from the soil samples. For the volcanic soils of the study area equilibrium was established within ca. 48 hours at each pressure. Thus, samples were left in the chamber for 48 hours and then a new (higher) pressure was applied until completing the desorption curve (15 bars). After exposing the samples to the first pressure (0.3 bars), one should purge the air from the sample and the tube, by applying a small pressure before applying the desired pressure to begin the experiment. The air flows out through a tube which should be submerged under water to avoid return of the air to the sample or to the plate.

At the end of the experiment the weight of the dry soil sample is determined by oven-drying at 105°C for 24 hours. Finally the relationship between the respective soil pressures (or tensions, expressed as the logarithm of *–h*, matric potential head in cm) and volumetric water content (θ) represents the pF-curve.

Figure IV.4. *Pressure plates for determination of water retention characteristics at high tension values.*

IV.3.5 *Saturated hydraulic conductivity (Ks)*

The hydraulic conductivity of a soil determines the rate of movement of water through the soil. Its value depends on the wetness of the soil and on the size distribution of the soil pores. Measurements of hydraulic conductivity can be made in the laboratory or in the field using a variety of techniques and sample sizes.

IV.3.5.1 Laboratory determination of Ks: the constant-head method

In the laboratory the determination of the saturated hydraulic conductivity *Ks* is often achieved using the so-called constant-head method, which is briefly described below.

Taking undisturbed soil samples:

The procedure for collecting undisturbed soil samples for saturated hydraulic conductivity (*Ks*) is essentially the same as that for soil bulk density. However more accurate *Ks* values are obtained when using larger rings of 7.5x7.5 cm (believed to be more representative of micro-scale variability) and avoiding the use of hammering as this produces small fractures in the sample that may affect the measurement. Transport, preparation and saturation of the samples are as described previously for the pF-curve (IV.3.4). Once the sample is ready, another ring of the same dimensions is placed on top of the sampled ring using sticky tape to avoid water losses at the connection point. After saturation, the sample is placed on the saturation table with constant head (Figure IV.5). The table is equipped with a water tank having a constant water level, and siphons connecting the tank with each sample in such a way as to maintain a constant pressure at the top of the sample (constant 'head') (Figure IV.5).

Fill the top ring with water, avoiding sample disturbance and ensure that the level of the water in the reservoir is the same as that above the sample. Keep the water level in the reservoir constant by connecting the tank to the water supply through a balloon water valve. Place an Erlenmeyer flask underneath each soil sample, so that the amount of water flowing through each sample can be collected and measured (Figure IV.5).

Figure IV.5. *Table siphon system to determine saturated soil hydraulic conductivity through the constant-head method.*

Collection of the outflowing water is terminated when the rate of flow becomes steady (last three measurements should be equal or similar). Saturated hydraulic conductivity *Ks* of the sample can then be calculated from the Darcy flow equation:

$$v = \frac{Q}{At} = -Ks\frac{\Delta H}{l}$$

Where *v* is the velocity at which the water passes through the soil sample, *Q* the volume of the water flowing down per time interval (cm^3 $hour^{-1}$), *A* the cross-sectional area of the sample cylinder or ring (cm^2), *Ks* the saturated hydraulic conductivity (cm $hour^{-1}$), ΔH the (constant) difference in hydraulic head maintained between the top and bottom of the sample (cm), and l the length of the soil column (cm).

IV.3.5.2 Field determination of Ks: Guelph permeameter

In the field *Ks* was determined with the so-called Guelph Permeameter (Figure IV.6). This method provides simultaneous measurements of saturated (field) hydraulic conductivity (K_{fs}), sorptivity (*S*), and the hydraulic conductivity - pressure head relationship, *K(h)* (see also section IV.3.7). The Guelph permeameter is a constant-head device operating under a Mariotte siphon principle (Figure IV.6). It is based on the measurement of steady-state flow of water into the soil (*Q*, m^3 s^{-1}), from a cylinder of radius *a*, in which the depth of water (*H*, in m) is kept constant. The Mariotte bottle is used to both maintain *H* and to measure *Q*. At least two data-pairs of *Q*-*H* are needed to obtain K_{fs} and the other soil properties.

Figure IV.6. *Field determination of saturated hydraulic conductivity using the Guelph Permeameter.*

Before taking a measurement in the field the instrument is assembled following the instructions of the instrument's manual. The procedure is as follows:

Use the auger coming with the instrument and dig a bore-hole down to the desired depth. The instrument is designed to work properly in uncased wells down to 1.0 m deep. To avoid smearing of the walls of the bore-hole, use a brush of 6 cm diameter, lower it all the way down to the bottom and pull the brush back up while rotating it to remove any smear left by the augering. Do this once or twice but avoid enlarging the well-hole diameter.

Place the water-filled and assembled permeameter into the well hole using the tripod to keep it in place. Centre the tripod over the well hole and lower the permeameter in such a way that the support tube enters the well hole (Figure IV.6). Check for appropriate connections between the inner and outer reservoirs (see manual for assembly). For more representative *Ks* determinations, measurements of the falling rate of the water should be made at two well-head heights. Establish the well-head height (H1) as 5 cm, from the air inlet tip. Depending on the rate of water flow into the soil, determine the use of the inner or the combined reservoir to provide water to the hole. For highly permeable soils, both reservoirs are to be opened, whereas for soils ofd low permeability only the inner reservoir is used.

Once the appropriate reservoir is selected, measurement can start by continuous readings of the level of water in the reservoir. These measurements should be made on a regular basis, the time depending on the falling rate (R), which equals the difference between readings at consecutive intervals divided by the time intervals. Keep monitoring the rate of fall of water in the reservoir until the rate of fall does not change significantly in three consecutive readings (quasi stationary flow).

Establish the well head height as 10 cm, by slowly raising the air inlet tip, through grasping the upper air tube. Re-start monitoring the rate of fall of water in the tube until steady state rates of fall are obtained. Calculate the field-saturated hydraulic conductivity (K_{fs}) and the matric flux potential (φ_m), by applying the following equations:

When using the inner reservoir:

$$K_{fs} = \left(0.0041.Y.\overline{R_2}\right) - \left(0.0054.Y.\overline{R_1}\right)$$

and

$$\phi_m = \left(0.0572.Y.\overline{R_1}\right) - \left(0.0237.Y.\overline{R_2}\right)$$

When using the combined reservoir:

$$K_{fs} = \left(0.0041.X.\overline{R_2}\right) - \left(0.0054.X.\overline{R_1}\right)$$

and

$$\phi_m = \left(0.0572.X.\overline{R_1}\right) - \left(0.0237.X.\overline{R_2}\right)$$

Where X and Y are constants for use with the inner and combined reservoirs respectively, as provided by the Guelph Permeameter manufacturer.

IV.3.6 *Soil infiltration capacity (double-ring method)*

The term infiltration signifies the entry of water into the soil through its surface. The amount of water entering the soil surface is frequently measured using a so-called double-ring infiltrometer (Figure IV.7). The infiltration rate is measured by observing the decrease in water level within the inner ring, or by measuring the inflow provided from a Mariotte tube to the ring in order to keep a constant water level (Figure IV.8). The outer ring serves as a hydraulic buffer zone to minimize lateral flow below the inner ring into the drier surrounding soil. As a result, flow paths below the inner ring are nearly vertical.

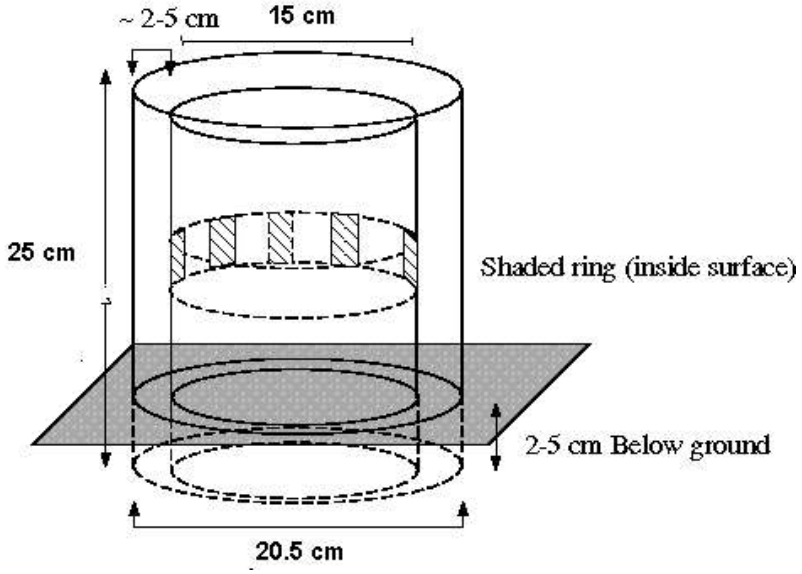

Figure IV.7. *Principle of the double-ring infiltrometer.*

However, when distinct soil layers exist in a profile, as in many volcanic soils, a strong divergence of flow paths may occurs and the assumption regarding one-dimensionality of the experiment is violated. Hence, the measured data can be evaluated only for the period up to the time when the wetting front reaches the top boundary of the less permeable layer (the Bw-horizon in the volcanic soils of the present study). This is theoretically reached at the first moment of quasi steady-state flow.

Basically, the instrument consists of two concentric rings, and a driving plate, with handles, for the inner and outer rings. The outer ring has a diameter of 20.5 cm vs. 15 cm for the inner ring (Figure IV.7). The two rings are driven into the ground and partially filled with water (ponding). The water level is maintained for a specific period of time, using a Mariotte tube (Figure IV.8). The volume of water needed to maintain a specified level and the time are recorded. This information is converted into a specific infiltration rate using the data sheet provided with the kit (see below).

The rate of infiltration is determined as the amount of water that penetrates the soil per surface area and time unit. This rate can be calculated on the basis of the measuring results and the Law of Darcy. To achieve good measuring results it is important to take into account several factors that may influence the measurement, such as the surface vegetation, soil compaction, moisture content and the presence of soil layers. Best results are obtained when the soil has a humidity level close to field capacity. Infiltration rate is determined by measuring the time it takes the level of water in the tube to drop a fixed distance. This rate changes with time as the soil pore space fills with water and reaches a steady rate, characteristic of water flow through a saturated soil. During unsaturated flow conditions the initial flow rate is high as the dry soil pores fill with water. Upon reaching saturation the flow rate becomes steady and water moves into the soil at a rate determined by soil texture and structure.

Measurement procedure:

Site preparation: Select a location within 5 m from the soil characterization / sampling site (or soil moisture profile measurement site). Be careful not to choose a location close to a tree trunk or to a house, road or pavement as the surface conditions will be too site-specific.

Figure IV.8. *Field application of the double-ring infiltrometer showing graduated feeding cylinder.*

Preparations before start of measurement: Measure and record the widths of the feeding bottle (to convert drops in water level to volume) and of the inner and outer rings (in cm). For timing use either a stopwatch or a watch with a second hand to time the water flow into the soil. When using a stopwatch, start it as water is first poured into the inner ring and read the elapsed time for each starting time and ending time.

Actual measurement:

1. Remove any vegetation at the ground surface or litter over an area just larger than the outer ring, without disturbing the soil.
2. Twist the rings 5 cm into the soil surface, by pushing with the hands or using a hammer in dry or hard soil surfaces. If a hammer is used a block of wood should be also used between the hammer and the top of the rings to distribute the force of the hammering. Do not use force indiscriminately as this may damage the rings.
3. Pour water into both rings, and maintain a level in the outer ring approximately equal to the level in the inner ring. Note that the water level in the outer ring tends to drop more quickly than that of the inner ring. Pour water into the inner ring, to just above the upper reference mark. The outer ring should not be leaking water to the surface around its rim. If it is, start again at another location; push the outer ring deeper into the soil or pack mud around its base if needed.
4. Install the filled water Mariotte tube on top of the rings.
5. Start the stopwatch or note the time to the second and record it on the Infiltration Data Work Sheet.
6. Record the elapsed time as your start time, at fixed intervals. During these intervals measure the level of the water in the Mariotte tube.
7. During the timing interval, keep the water level in the outer ring approximately equal to the level in the inner ring, but be careful not to pour water into the inner ring (using a funnel can help) or to let either ring go dry.

8. Keep measuring the level of the descending water in the Mariotte tube until reaching steady or quasi-steady state. This is reached when tree consecutive readings are equal. If the Mariotte tube reaches the lowest level of water content before reaching steady-state conditions, refill the tube and restart measurements again, until steady state conditions are reached.
9. Record the time at which you stopped your observations as the end time. Your infiltration measurement will consist of a single data interval.
10. Remove the rings and wait for about 5 minutes so the water on the surface can infiltrate into the first cm of soil.
11. Measure the near-surface (0 - 5 cm depth) soil moisture content from the spot where you just removed the rings. Follow the gravimetric soil moisture protocol given below (IV.3.7.2).
12. Take additional infiltration measurements within the area or land cover of interest, either on the same day or over several days to obtain an average infiltration estimate.

Data analysis and presentation

The infiltration rate is found from the distance that the water level decreased divided by the time used for this decrease. This is equal to the width of your reference band divided by the difference between the start and end times for each time interval. The flow rate observed for each timing interval is the average value during that interval. Infiltration should decrease with time and it is important to keep track of the cumulative time since water was first poured into the inner ring. Calculations can be made according to the following table:

Time intervals (min) 1	Time in hours 2	Volume (cm^3) in each interval 3	Accumulated volume (cm^3) 4	Infiltration(cm): (volume (4) / infiltration area) 5	Infiltration rate ($cm\ h^{-1}$) (5)/(2) 6
2	0.03	108	108	0.48	16
5	0.08	62	170	0.76	9.45

Diameter of the outer infiltrometer = 20.5 cm
Area of the infiltrometer (inner ring) = 225 cm^2
Initial volume for a 4 cm drop in water level = 4 cm * area of infiltrometer = 900 cm^3

IV.3.6 *Field determination of unsaturated hydraulic conductivity k(h)*

Unsaturated hydraulic conductivity *k(h)* can be measured in the field using a so-called tension-infiltrometer, which consists of a 20 cm diameter infiltrometer (ceramic plate) connected with a water tower (feeding reservoir) and a 'bubbling' tower (which controls the tension at the soil surface; Figure IV.9).

Soil surface preparation and field installation: In an area of about 22 cm diameter, remove the soil surface detritus (litter) under forest conditions or the grass in a pasture setting, avoiding smearing the soil surface. Press the metal ring gently into the soil and put the contact material (fine silica sand) in place as a layer of about 3 cm thickness and moisten it to establish optimum contact between the ceramic plate and the soil underneath (Figure IV.9).

Follow the manufacturer's instructions for connecting the ceramic disk to the water tower, and to fill the tower and the infiltrometer disk with water. Keep the disk in water until installation on the soil surface to avoid air entry into the pores and fill the system while the disk remains submerged in a bucket filled with water and follow the instructions for closing the valves. Use a 400 mesh nylon membrane to cover the infiltrometer disk.

Figure IV.9. *Tension-infiltrometer to derive unsaturated hydraulic conductivity k(h) in the field showing ceramic disk (left), water reservoir (centre) and bubble tower (right).*

Before starting the measurement ensure that the bottom of the bubble tower is at the same elevation as the bottom of the infiltrometer disk. First establish a tension of -5 cm in the bubble tower and open the clamp of the tubing between the water tower and the bubble tower. Also open the clamp of the air-entry tube on the bubble tower. Start taking regular readings of the water level in the water tower (reservoir), the time interval depending on the rate of falling of the water column. Keep monitoring the rate of fall of water in the reservoir until de rate of fall does not change significantly in three consecutive readings. Repeat this procedure, after refilling the tower with water and establish tensions of -10 and -15 cm, again until reaching steady state rates of fall. Calculate the unsaturated hydraulic conductivity *k(h)* using the following equation:

$$Q = \pi.r^2.k(h)\left[1 + \frac{4}{\pi.r.\alpha}\right] \qquad \text{(A)}$$

Where *Q* is the volume of water entering the soil through the infiltrometer disk per unit time ($cm^3\ hr^{-1}$), *k(h)* the hydraulic conductivity (cm hr^{-1}), *h* the matric tension applied (cm) and α a parameter linking saturated (K_s) and unsaturated (*k(h)*) hydraulic conductivities as follows:

$$k(h) = K_s \exp(\alpha h) \qquad \text{(B)}$$

In tension infiltrometry the volume of water (*Q*) entering the soil surface per unit of time is measured at two tensions, h_1 and h_2. Thus for unsaturated soils, by substituting *k(h)* in equation (A) by expression (B) one obtains:

$$Q(h_1) = \pi r^2 K_s \exp(\alpha h_1)\left(1 + \frac{4}{\pi r \alpha}\right) \quad \text{at tension } h_1 \qquad \text{(C)}$$

and

$$Q(h_2) = \pi r^2 K_s \exp(\alpha h_2)\left(1 + \frac{4}{\pi r \alpha}\right) \quad \text{at tension } h_2 \qquad \text{(D)}$$

Alpha (α) can be derived by dividing equation (D) by equation (C):

$$\alpha = \frac{\ln\left[Q(h_2)/Q(h_1)\right]}{h_2 - h_1} \qquad \text{(E)}$$

$Q(h_1)$ and $Q(h_2)$ are measured, whereas h_1 and h_2 are known, so that α can be calculated from (E). For known α, K_s can be calculated from equation (C) or (D) thereby giving the relationship between hydraulic conductivity *k* and tension *h* for the soil under consideration, i.e. equation (B).

IV.4 Determining dynamic soil variables

IV.4.1 *Soil temperatures*

To detect diurnal changes in soil temperature for use in surface energy balance computations (section III), and for calibration calculations of volumetric soil water content using TDR probes (section IV.4.2.2), measurements of soil temperature are needed. Ideally, soil temperatures are to be measured for the same depths and time intervals at which soil water content is being measured. Measurements can be made using thermograph probes connected to a data-logger for a continuous record, or manually at the soil surface, within the first 5 cm. Below, the procedure is outlined for automatic measurement using thermo-sensors connected to a Campbell CR23X data-logger at 5-minute intervals.

Site selection and timing: measurements should be made adjacent to soil moisture measurement sites, and at the same depths. The following points should be adhered to:

- Select representative sites within an area having similar topographic characteristics, for each soil class or vegetation type under consideration.
- Open a soil profile ('pit face'; cf. Figure IV.12) and install the probes horizontally within the respective soil horizons, by pushing the probes 7 to 12 cm into the ground, without compacting the adjacent soil material.
- Make sure there is good contact between the probe and the surrounding soil.
- Connect the probe to the data-logger and program it to read the probes at the desired time interval.

The temperature data can be used directly to determine soil heat fluxes (section III.3.3) and for the calibration of soil water probes (IV.4.2.2).

IV.4.2 *Soil water matric potential and soil water content*

Soil water is classified according to how tightly it is being held in the soil. Free water or gravitational water will drain from a soil until the soil water potential (or matric potential, *h*) reaches -1/3 bar or 'field capacity', i.e. the remaining water is retained by the soil matrix. The free-draining water is not really available for plants because it remains in the soil for a short time only. Also, under nearly saturated conditions levels of oxygen tend to be reduced, which impedes the plants' capacity to absorb water. As the water that is held at increasingly more negative matric potentials (i.e. < -1/3 bar) as the soil dries out, the plants will need to invest increasing amounts of energy to take up the remaining water. The point at which the plant roots can no longer remove water is called the permanent wilting point and this occurs at -15.8 bars water potential for most plants (pF 4.2). Water held at matric potentials between -1/3 and -15.8 bars is called the plant-available water (pF range 2.5-4.2).

IV.4.2.1 Tools for measuring soil water potential in the field

Measuring soil water potential in the field (*h*) can be done with a vacuum gauge tension meter (tensiometer). In its basic form a tensiometer consists of a porous ceramic cup connected to a manometer via a tube filled with de-aerated water (Figure IV.10a). The matric potential in the soil around the ceramic cup is in equilibrium with that of the water in the cup. Manometer readings need to be corrected for the length of the water column in the tube between the manometer and the centre of the cup, to give h at the level of the ceramic cup (Figure IV.10a). More sophisticated, recording types of tensiometer are equipped with a pressure transducer (Figure IV.10b).

Tensiometer readings of soil water potential *h* need to be combined with the corresponding gravity potential value (*z*) to give total hydraulic potential *H* in that point. Unsaturated flow is driven by the gradient in hydraulic potential within a soil or slope. Therefore, tensiometers are indispensable in hillslope hydrological studies of flow pathways during and in between rain storms.

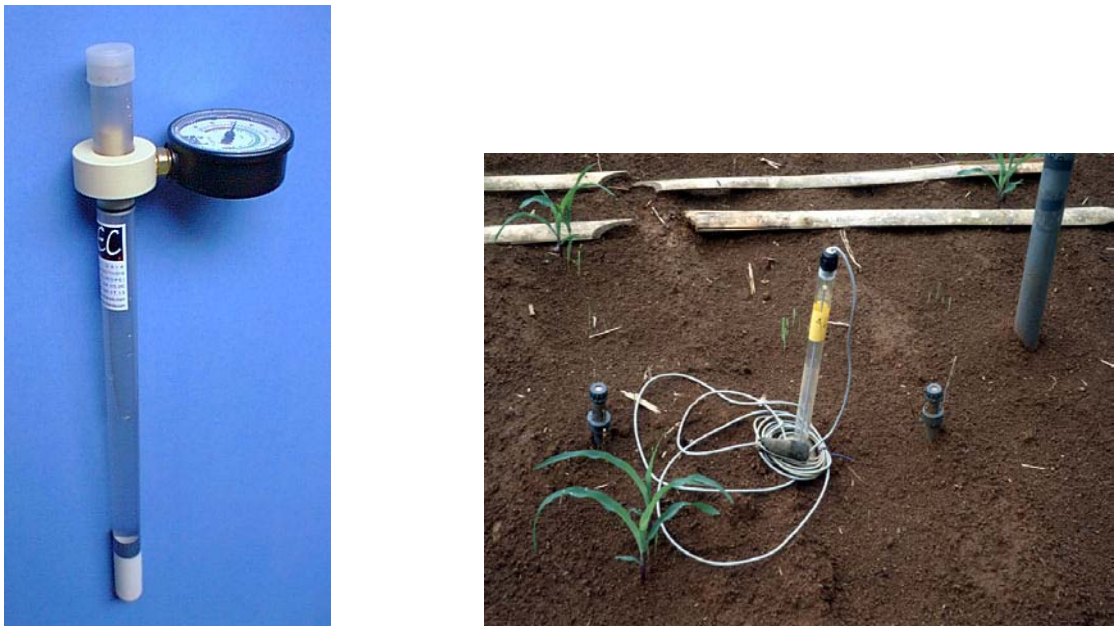

Figure IV.10. *(a) Vacuum-guage tensiometer showing ceramic cup, manometer and connecting tube. (b) Recording tensiometer with its connection cable to the data-logger disconnected. Several manually-read 'septum-type' tensiometers are shown as well.*

The instrument only works in the tension range down to -800 cm, beyond which the air entry value of the pores of the ceramic cup is exceeded and water will be sucked from the device into the soil. Volcanic soils under undisturbed cloud forest conditions typically remain wetter than field capacity or close to saturation. Therefore, tensiometers are appropriate tools to measure soil water tension under such conditions. Because the soil water retention curve (section IV.3.4) links soil water content θ to soil water tension h, tensiometer readings can also be used for the determination of soil water content.

Often, volcanic soils exhibit at a certain depth a coarse, sandy to gravelly layer marking the first material to be deposited during a volcanic event (cf. Figure IV.12 below). Such a layer is often almost free of organic matter and has a very low root density, mostly because the water movement through the coarse material is very rapid. Because of the typically very loose structure of such horizons, it is difficult to establish close contact between the tensiometer cup and the soil. Therefore, readings made with tensiometers installed in these layers are prone to error and should be viewed with caution.

It is best to make manual or automatic measurements of soil water potential at locations where other hydrological measurements are performed as well (notably soil water content). This allows for the derivation of field pF-curves which may be more realistic than the desaturation curves obtained in the laboratory (section IV.3.4). Manual or recording tensiometers can be installed at different depths to evaluate changes in soil water tension over time with depth. For the specific case of the presently studied cloud forest in the layered volcanic soils of northern Costa Rica, tensiometers were installed at eight depths (10, 15, 25, 35, 50, 80, 100 and 150 cm). Manual measurements were carried out daily at the same time when manual soil water content readings were taken (see below) whereas the recording tensiometers were read each 5 minutes.

IV.4.2.2 Soil water content (in-situ)

The capacity of a soil to retain water is a property of major importance, as it determines the amount of water available to plants. Direct and indirect methods are often used to measure soil water content, and results are expressed in terms of either mass or volume ratios, percentages or fractions.

Gravimetric water content:

Soil samples for thermo-gravimetric water content determinations are usually collected by means of 5x5 cm stainless steel rings (destructive sampling). In contrast to sampling for the determination of some other soil properties, samples for soil water content can be collected throughout the year to cover wet and dry periods and any transitions between these.

Procedure:

- Specific sites, soil depths and timing of sampling should be determined beforehand and depend on a project's objectives. Special attention should be paid to the sampling of soil moisture during representative periods for the studied region.
- Remove the surface or ground vegetation or other litter material.
- Collect al least three samples (more samples may be needed for topsoils in forest), by hand-pushing the sampling ring into the surface of the soil horizon to be sampled. Stop when you can see some soil emerging through the small hole in the bottom of the ring.
- If it is difficult to push the metal ring into the soil, place a piece of wood over the ring and carefully hit the wood with a hammer to equally distribute the force of the blow. Do not push the wood further when soil material has filled the ring entirely, to avoid sample compaction.
- Samples at different depths can also be collected by augering to the desired depth and then taking a sample using a ring attached to the auger or some other ring-holder.
- Once the ring is filled entirely, use a trowel or shovel to remove it from the soil. Trim any excess soil material sticking out of the ring.

- If the sample is merely to be used for soil water content determination, the soil material can be deposited in a plastic bag. Label the bag and close it properly to avoid any loss of material, or water by evaporation. Bring the samples to the laboratory.
- Weigh the moist soil samples either in the field (portable weighing scales) or in the laboratory before drying (wet weight; Figure IV.11).
- Dry the samples in an oven adjusted at 105°C for 48 hours. Let them cool down and weigh them (dry weight; Figure IV.11). Note: if the soil sample contains large amounts of organic matter it should be dried for 24 hours to avoid loss of organic matter via oxidation.

Expression of gravimetric and volumetric water contents:

The mass of water relative to the mass of oven-dry soil particles (θ_g), also called gravimetric water content, can be determined from:

$$\theta_g = \frac{M_m - M_s}{M_s} = \frac{M_w}{M_s}$$

where M_m is the moist soil mass, M_s the oven-dry soil mass (i.e. solids) and M_w the water mass in the sample. Soil water content can also be expressed as the volumetric fraction θ_v of the total volume of the sample (V_t):

$$\theta_v = \frac{V_w}{V_t} = \frac{V_w}{V_s + V_w + V_a}$$

where V_w is the volume of the water in the sample (in cm^3 and equal to the weight of water in grams). The total volume is the sum of the volumes occupied by solids (V_s), water (V_w) and air (V_a).

A sample's volumetric water content θ_v can be obtained from its gravimetric water content θ_g by multiplication times the sample's bulk density ρ_b (taking the density of water as 1 g cm^{-3}):

$$\theta_v = \frac{\theta_g \rho_b}{\rho_w} = \theta_g \rho_b$$

Application:

Soil water content is normally used to characterize soil water dynamics in space and time. It is also used for the calibration and validation of simulation models focusing on soil water fluxes and soil-vegetation-atmosphere transfer (SVAT) processes. Furthermore, the total amount of water present in a soil profile (L_t) or in a separate layer (L_i) can be calculated from data on the variation of soil water content (θ) with depth (z), using the following equations:

$$L_i = \theta_i . z$$

and

$$L_t = \sum_{i=1}^{n} L$$

By comparing summed values determined for different points in time the change in soil water storage over the corresponding period can be determined (e.g. in water budget computations; cf. section I.3).

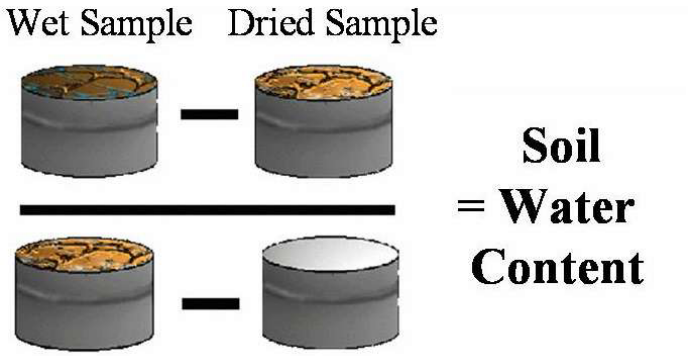

Figure V. 11. *Determination of soil water content through the thermo-gravimetric method.*

Indirect methods for Volumetric soil water content:

There are several methods for the non-destructive determination of soil water content and each has its advantages and limitations. One of the currently most widely used methods is the Time Domain Reflectometry (TDR) technique which makes use of the fact that the dielectric constant of a soil (ε) varies in a predictable way with its moisture content. Although use is often made of a 'universal' calibration equation linking θ to ε for all soil types, it is best to calibrate one's sensors in relation to the soil under study. This holds even more in the case of the often highly organic soils of cloud forest ecosystems and for volcanic soils in general.

For specific projects it is advisable to consider the purpose for which the soil water determinations are to be made and the features of each possible method, including the cost of equipment and operating and maintenance costs. It is also necessary to determine the depths at which measurements need to be taken in advance. One obvious criterion for deciding measurement depths is to distinguish the different soil layers until a given depth, usually the depth of fine root distribution. In view of the distinctly layered nature of volcanic soils, more sensors may need to be used under those circumstances than in soil types with less pronounced textural and other changes with depth (e.g. oxisols) (cf. Figure IV.12).

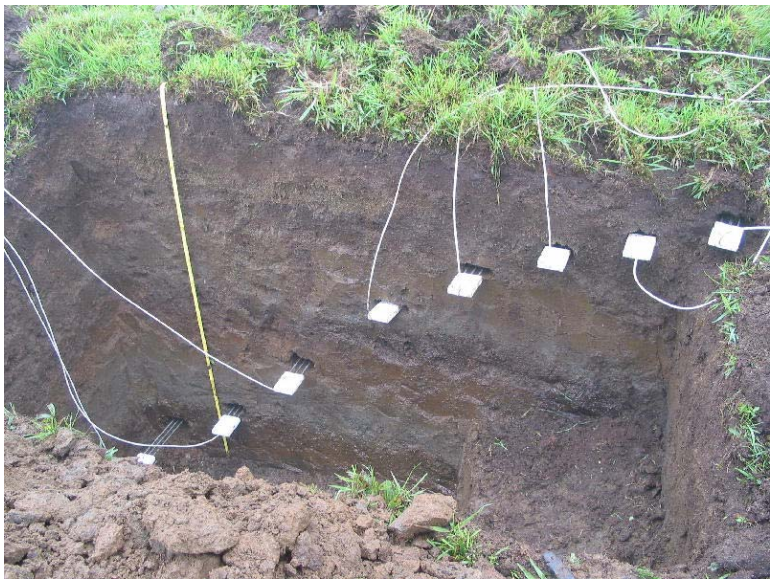

Figure 12. *TDR probes for recording volumetric soil water content in a layered volcanic soil.*

The number of TDR sensors and the time interval between measurements will depend on a project's objectives as well as instrument availability. It is advisable to consider at least one sensor per soil horizon (at each site) and daily measurements (in the case of manual measurements) or short time intervals (from 5 minutes to one hour depending on soil hydraulic conductivity) if automatic measurements are taken.

Procedure for TDR probe installation and measurement:

- Dig a soil profile of 1x1x0.8 m (or smaller or larger as required; cf. Figure IV.12).
- Clean the pit face in which the sensors are to be installed. On slopes the uppermost pit face is preferred to avoid any slope effect on the measurements.
- Install the TDR probes horizontally and in a diagonal line with respect to each other (from the upper towards the lowest part of the profile), starting with the shallowest one. Do not install a sensor exactly below another one, since soil disturbance above it may interfere with soil water movement (Figure IV.12).
- Dig a horizontal hole (of about 5 cm deep) at each selected soil depth (e.g. in the middle part of each soil layer). Carefully push the probe electrodes into the soil at the hole, so that the entire probe is within the soil and the top (head) of the probe positioned within the small hole (Figure IV.12).
- Fill the remaining openings in the hole with soil from the same site, to avoid any interference by water coming from above.
- Lead the labeled cables of the probes out of the soil pit and refill the pit using the original soil material.
- For automatic measurements, connect the terminals of the probes to the data-logger and program it to read them at the desired time interval.
- For manual measurements, cover the probe heads with plastic to avoid water from entering the sensors, or damage by animals.
- Use cable tester (Tektronix TDR 1502B) and computer to measure soil water content.
- Open a data worksheet for storing and processing of the data.

Sensors for manual measurements of soil water content in the layered volcanic soils of the present study area were installed at 8 different depths, according to the soil horizon distribution: viz. at 5, 10, 15, 25, 50, 80, 120 and 150 cm depth. These sensors were measured daily over 18 months at three locations (cloud forest, pasture and secondary forest). For automatic soil water measurement, one station was installed in each vegetation type, with a total of 5 sensors per site at the following depths: 10, 25, 50, 100, and 150 cm. These measurements were performed over 16 months on a half-hourly basis.

Calibration and de-installation of TDR probes

For accurate determination of soil water content, a calibration of the TDR probes is required at the end of the field campaign, before removing the probes. Calibration can be carried out by paired measurements of soil water content by TDR and the thermo-gravimetric method, through direct comparisons of paired volumetric water content data or by the determination of the so-called refraction index (n_a) and its relation to soil volumetric water content (Tobón, 1999). Here, paired measurements of volumetric water content by TDR and the thermo gravimetric method are used (Figure IV.13).

At the end of the field campaign and with the TDR sensors still in place, rectangular PVC boxes of 35x5x9.25 cm were pressed horizontally into the soil profile at each TDR sensor location (Figure IV.13 top). The molds containing the *in situ* soil and the sensor were carefully removed from the profile, wrapped and transported to the field laboratory. Next, the soil samples with the sensors were completely saturated and TDR measurements carried out each hour to record saturated until almost completely dry soil conditions.

Figure 13. *PVC molds for calibration of TDR sensors and set-up at field station..*

At the same time when a TDR measurement was carried out, the entire sample was weighed to determine the corresponding loss of weight. At the end of the measurements when the soil was almost completely dry, the sensors were removed and the entire soil sample was collected, weighed, dried at 105°C for 48 hours and reweighed (cf. Figures IV.13 bottom and IV.11). From this, the weight and bulk density of the dry soil were determined (knowing the volume of each mold). Weights of the sensor and the mold were also determined by difference.

The losses in weight (i.e. water loss) between measurement intervals were used to determine the volumetric water contents of the sample gravimetrically at each specific TDR measurement. Paired TDR-based measurements and gravimetrically determined volumetric water contents were compared and a linear relationship derived for each individual sensor (read: site and depth). These regressions were used to convert all TDR readings to calibrated volumetric water contents for each sensor.

Note: after the calibration procedure the probes should be properly cleaned and stored until future use. Dirty probes or oxidation of the electrodes by humidity can result in considerable damage.

IV.4.3 *Surface runoff (overland flow)*

Water that does not infiltrate into the soil and runs off along the surface is called surface runoff or (infiltration-excess) overland flow. Amounts of overland flow can be determined using so-called runoff plots (Figure IV.14). The size of a runoff plot may vary, depending on the land cover of interest, annual rainfall and slope. Standard runoff plots for the measurement of erosion from agricultural fields measure 2.5 x 22.1 m but often it is more practical to use much smaller plots (for example, on steep, complex slopes receiving high rainfall): e.g. 3x1 m or 3x2 m. The number of replicates depends on the project's objectives, budget and time availability. However, plots need to be large enough to ensure that natural hydrological processes can occur and be replicated in sufficient numbers to represent soil and vegetation conditions and their spatial variability. Thus, locations of runoff plots should be chosen on the basis of soil type, topography (landscape position and slope), and land use (Figure IV.15).

Figure IV.14. *Bounded plot for surface runoff measurements in a pasture formerly occupied by cloud forest. Note runoff collection tank at downslope end and sheet metal boundaries.*

Site selection may also involve the mapping of specific surface runoff-producing zones in a catchment. Typical situations include: (i) flat areas and wet footslopes adjacent to the stream channel (riparian zone); (ii) side slopes of variable gradient; and (iii) plataux and ridge tops of low relief.

In the presently studied pasture catchment three simple, non-replicated runoff plots were installed in the upper, middle and bottom parts of the catchment to obtain a first idea of variations in surface runoff production (Figures IV.14 and 16). Plot boundaries were defined by inserting sheet metal into the soil to prevent water from outside the plot from entering. A 120-L container was installed at the base of each plot to collect surface runoff. Special care was taken to minimize soil disturbance during installation of the plots and containers.

Surface runoff volumes can be collected manually once a day or after each precipitation event, or during events using a tipping bucket and logger system. Volumes need to be converted to depth (mm of water) using a conversion factor deduced from the total area of the plot.

In addition, rainfall (intensity) at the site needs to be measured to determine the amount of water input. Soil moisture at the surface and in the upper 20 cm may also be measured to determine the threshold moisture content value at which runoff is produced for a given rainfall.

Figure IV.15. *Complex topographical and land cover patterns require stratified sampling of rainfall inputs, soil water dynamics as well as soil physical properties and runoff production.*

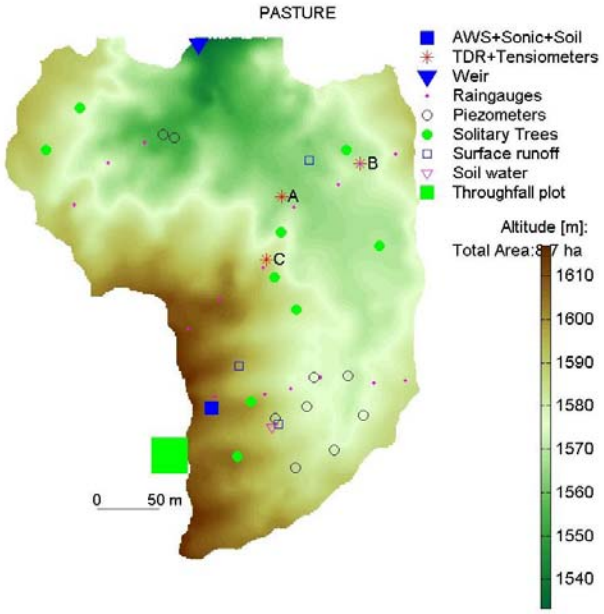

Figure IV.16. *Location of runoff plots (□) in relation to automatic weather station (AWS), rain gauges, soil water (TDR), and groundwater (piezometer) stations in a pasture micro-catchment.*

Data analysis

Field runoff data can be used to determine the proportion of precipitation that becomes runoff (excess precipitation) per event, season or year. Pearson's correlation procedure can be used to test the significance of relationships between runoff amounts and rainfall intensity, duration and amount, or soil moisture vs. runoff amounts, or land use vs. runoff. An analysis can also be made to see whether there are significant differences in surface runoff production and percent soil moisture between topographical zones, e.g. using a split-plot design analysis of variance and Duncan's multiple comparison procedure. Each runoff event is then treated as a block, with differences in surface runoff or soil moisture levels between zones tested using data from plots nested within specific zones. Furthermore, paired rainfall-runoff data can be used to quantify the average infiltration rate across a plot during given events. Such data are useful in the up-scaling of point measurements of infiltration as made for example with the double-ring or Guelph permeameter methods (sections IV.3.6 and 3.5).

Part V: Streamflow measurement

V.1 Introduction

This part of the measurement protocol gives an overview of streamflow measurement techniques as used in the FIESTA project. Additional details can be found in Annex 5 to the overall Final Technical Report (training course materials). An extended manual on streamflow measurement can be found online at: http://www.usbr.gov/pmts/hydraulics_lab/pubs/wmm/ and in the handbooks listed at the end.

Streamflow is defined as the instantaneous flow rate, or discharge, of water, expressed as volume per unit of time (e.g. L/s or m^3/s), along a defined natural channel. Streamflow at a particular point on a channel is made up of outflow from the area's groundwater aquifer ('baseflow') plus the quickflow that is contributed during and shortly after rainfall via various forms of overland flow and rapid subsurface flow through pipes and other macropores (cf. Figures I.1 and I.2). Depending on a catchment's rainfall patterns, surface status, geology, soils and topography, as well as size, the temporal variations in the streamflow record (or hydrograph) can be more or less peaked (Figure V.1). Clearly, the more variable the discharge in time, the greater the need for continuous registration of streamflow rates for a proper assessment of the total amounts of streamflow leaving an area.

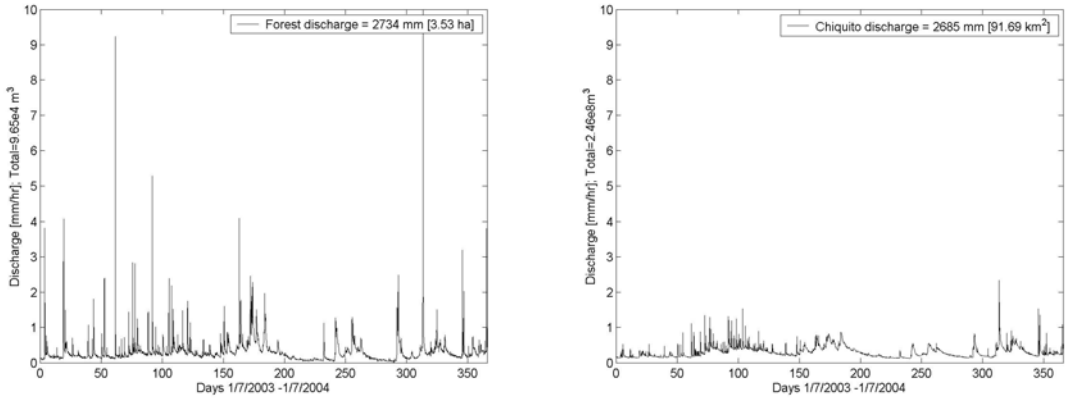

Figure V.1. *Streamflow patterns for a micro-catchment (3.5 ha) under cloud forest (left-hand panel) and a meso-scale catchment (92 km^2) with mixed (cloud) forest and pasture (right-hand panel), northern Costa Rica*

Generally, a station for streamflow measurement requires:

- A suitable measurement site that has either a natural or artificial (weir/flume) hydraulic control.
- A continuous water level (stage) measurement with reference datum.
- A well-defined relation between water level (stage) and streamflow (discharge), also called the stage-discharge or 'rating' curve, that is valid for the natural or artificial control in question.

In small streams an artificial hydraulic control (e.g. a sharp-crested V-notch weir; Figure V.2) can be used which has the advantage of possessing a predetermined rating curve (determined experimentally in a laboratory), although field calibration of the gauging structure by on-site discharge measurements remains advisable. As discussed further below, the use of an artificial hydraulic control allows streamflow to be determined directly from a stage height record. Detailed information on different types of gauging structures (weirs and flumes in general) can be found in chapter 7 of the online manual referred to earlier.

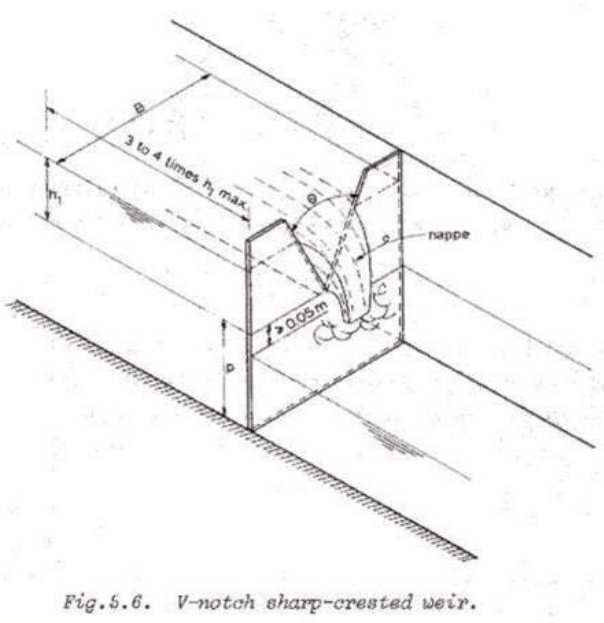

Fig.5.6. V-notch sharp-crested weir.

Figure V.2. *Example of a sharp-crested V-notch weir.*

For rivers too large for the use of a fixed measuring structure, a channel section should be selected where a stable rating curve can be derived for the observed range of flow conditions. A natural channel section often has more than one flow control depending on the flow level. An artificial constriction such as at a bridge where the width of the waterway is narrower than the natural channel is an example of a section channel control. The presence of the bridge also facilitates the measurements of discharge and river cross-sectional profile that are required for the establishment of a rating curve for the section. This type of gauging station can be called a velocity-area station.

Figure V.3. *Example of a natural channel section with a constriction afforded by a bridge (Lower Rio Chiquito, northern Costa Rica).*

Ideally, for both artificial and natural streamflow gauging sites no subsurface or groundwater flow should bypass the site and at all stages the total flow should be confined either to a single channel or the artificial structure used. In practice, many catchment areas lose water via ungauged subterranean flows (catchment leakage), particularly in volcanic or karstic terrain. Leakage losses may be minimized by selecting gauging sites where the stream has incised itself down to the local bedrock level.

In addition, the following site selection criteria should be taken into account (although keeping in mind that ideal sites are rare):

- The stream course is straight for about 100 m upstream and downstream of the gauge site.
- At all stages, the total flow is confined to a single channel.
- The streambed in the vicinity of the site is not subject to changes (scour, fill).
- The location is free of aquatic plants.
- The banks of the stream channel are permanent, free of bushes, and high enough to contain floods.
- The gauging site is removed far enough from the confluence with another stream (backwater effects) or from tidal effects to avoid possible impacts on the measurement of stream stage.
- Within the proximity of the gauge site, a reach for the measurement of discharge at all stages is available.
- A fixed element (e.g. a rock wall or bridge pillar) is present for the establishment of reference datum points to relate measured water levels to and for the repeated determination of river bed profiles.
- The location is always accessible for installation, operation and maintenance purposes.

The two types of measurement stations (i.e. artificial structure and velocity-area station) are discussed more fully in the next section. This is followed by a description of the equipment used for the measurement of water stage and discharge as applicable for the two types of measurement stations with examples taken from the current project.

V.2 Approaches to streamflow measurement

V.2.1 *Sharp-crested V-notch weir*

Generally, weirs and flumes are designed in such a way that the downstream water level does not affect upstream head (water level). The structure provides a unique relation between head *H* and discharge *Q* by forcing a transition from sub-critical to super-critical flow over the structure (Figure V.2). A stage measured upstream of the structure together with the pre-calibrated formula relating *Q* to *H* yields the streamflow at the station. Different structure designs are possible and range in size from several cm to 15 m. Weir structures provide accurate measurements for a whole range of flow rates as a small change in discharge provides a measurable change in water level. After construction they generally have low maintenance. However leakage may occur underneath the structure through scour and solid rock bedding is preferable. Also, V-notch weirs can easily be blocked by debris (leaves, branches) and weirs in general fill up easily for rivers with a high sediment yield. Where sediment loads are high, a flume-type structure with a constriction enabling sediment to be flushed through naturally is preferred. Construction and installation procedures of weirs and flumes can be found in the online manual and the handbooks listed at the end of this document.

In short, sharp-crested V-notch weirs are suitable for the measurement of flows from small catchment areas producing relatively little sediment only (Figure V.4). Any sediment accumulating behind the weir will have to be removed regularly.

The experimentally determined *Q*-*H* relation for a sharp-crested V-notch weir is given by:

$$Q=C_e\ 8/15\ (2g)^{0.5} \tan(\theta/2)\ h_e^{2.5}$$

Where Q is discharge (m^3/s), θ the angle of the V-notch (90º), C_e (0.577) represents the effective coefficient of the discharge and h_e is the so-called effective head (m). The effective head is the summation of the measured stage (section V.3) and a head correction factor (K_h) which represents the combined effects of fluid properties and is about 0.8 mm for a 90º V-notch. Note that the value given above for C_e is valid only in case of fully contracted flow as this parameter becomes a function of the approach channel if the flow is not fully contracted. If the riverbed and sides of the approach channel are sufficiently remote from the edges of the V-notch to allow for a sufficiently large approach velocity component parallel to the weir surface, contraction at the overflow is fully developed. Several rules have been derived to determine whether this situation occurs. A weir is fully contracted if the head is less then 40% of the depth of channel below the crest and if the depth of the channel is less than 20% of the width of the channel. Furthermore, the approach channel should be wider than 90cm and the depth below the crest more than 45cm, whereas the head should be larger than 5 cm and smaller than about 40 cm.

Figure V.4. *Sharp-crested V-notch weir as used to gauge the project's micro-catchments.*

The record of streamflow derived from the stage record and the theoretical stage-discharge relation for a weir should be calibrated with field measurements of discharge, e.g. using a volumetric or salt dilution technique (see chapter 12 in the online manual referred to earlier).

V.2.2 *Velocity-area stations*

Discharge is essentially a multiplication of the (average) velocity of the water times the cross-sectional channel area. In the case of the sharp-crested V-notch weir (section V.2.1) this multiplication is replaced by a unique expression of discharge Q in terms of stage H. The expression relating discharge to stage in general - the rating curve - allows the conversion of a continuous stage record into a discharge record. At a natural control site, e.g. a straight channel section as shown in Figure V.5 or the bridge in Figure V.3, a site-specific rating curve has to be derived from regular simultaneous stage and discharge measurements. Because discharge is often computed from streamflow velocity measurements made with a current-meter across the channel (see below), this type of gauging station is frequently called a velocity-area station (Figure V.5).

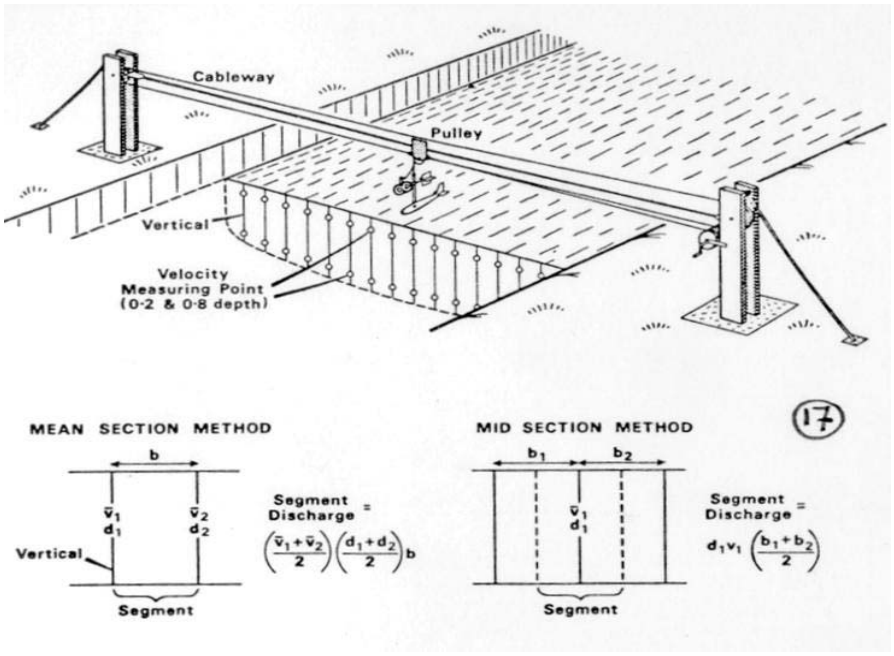

Figure V.5. *Typical set-up of a velocity-area gauging station showing a cableway installation for the measurement of streamflow velocities across the channel using a current-meter.*

V.2.2.1 Determination of stream velocity

Streamflow velocity is often measured using some sort of current-meter. A current-meter consists of a precisely calibrated propeller whose rotation rate is proportional to the water velocity (Figure V.6). The number of rotations for preset time periods (e.g. 30 or 60 seconds) is measured by a counter. Different types are in use for different flow conditions (see e.g. www.ott-hydrometry.de) and measurements can be done on the spot by an observer wading in the stream (Figure V.7) or by lowering the instrument from a cable way or bridge. In the latter case a sinker weight is often needed to stabilize the current-meter in the flow (Figures V.5 and V.6b).

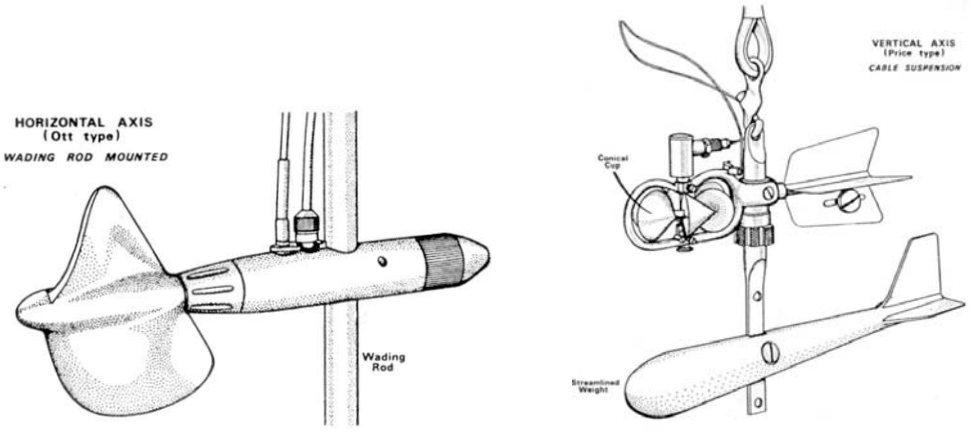

Figure V.6. *Examples of current-meters. (a) C20 OTT current-meter and (b) Price current-meter and sinker weight for use in larger rivers.*

Figure V.7. *Manual streamflow velocity measurement using a current-meter.*

V.2.2.2 Velocity-area method for the measurement of stream discharge

The velocity-area principle is used to compute discharge from velocity data that are usually obtained from current-meter data of streamflow velocity (Figures V.5-V.7). Total discharge is determined by summation of partial discharges. A partial discharge q_n is the product of an average point or vertical line velocity $\overline{V_n}$ and its associated partial area a_n, expressed as:

$$q_n = \overline{V}_n a_n$$

The total discharge for *n* partial surface areas is then:

$$Q = \sum_{1}^{n} \left(\overline{V}_n a_n \right)$$

The mean-section method (simple average for entire section) and the mid-section method (Figure V.5, bottom part) are two methods in which the channel is broken up into straight-line sections. They are summarized below.

The mean-section method makes use of two successive vertical depths, their mean velocity, and the distance between them and derives the associated discharge from:

$$q_n = b\left(\frac{\overline{v_1} + \overline{v_2}}{2} \right)\left(\frac{d_1 + d_2}{2} \right)$$

The two integers used as subscripts denote that the partial discharge, *q*, is for the area between two consecutive vertical measurement points as numbered, whereas *v* denotes the velocity and *d* the depth measured, and *b* the distance between consecutive profiles (Figure V.5).

The mid section method makes use of the depth and mean velocity measured for each of a number of verticals along the cross section. The depth at a vertical is multiplied by the width, which extends halfway to the preceding vertical and halfway to the following vertical, to develop a cross-sectional area. The product of this area and the mean velocity at the vertical gives the discharge for the partial section between the two halfway points (Figure V.5 bottom part). A summation of the partial discharges gives the total discharge. The formula for computing the partial discharge using the mid-section method is:

$$q_n = d_1 \overline{v}_1 \left(\frac{b_1 + b_2}{2} \right)$$

The subscript $n\pm$ denotes the partial discharge *q* for the area extending halfway back and halfway toward the two adjacent vertical measurement points (Figure V.5 bottom part).

For both the mean-section and mid-section methods, the verticals do not need to be equally spaced over the cross section (cf. Figure V.5), but the verticals should be chosen such that:

(1) The error of computing the area between two verticals does not exceed 3% when the bed is treated as a straight line between the verticals.

(2) Except near the banks, the difference between the mean velocities at two adjacent verticals does not exceed 20% (relative to the lower velocity of a pair of verticals).

The mean velocity for a vertical can be determined in several ways (see chapter 10 of the online manual for a full discussion), of which the following two are the most widely applied:

The two-point depth method consists of measuring the velocity using a current-meter at 0.2 and at 0.8 times the depth (measured from the water surface), and using the average of the two measurements. High accuracy can be obtained with this method and its use is recommended. However, the method should not be used where the depth is less than about 60 cm.

The six-tenths-depth method consists of measuring the velocity at 0.6 of the depth from the water surface and is generally used for shallow flows where the two-point method is not applicable. The method generally gives satisfactory results.

V.2.2.2 Determination of river bed profile

Natural control sites are liable to shifts in the stage-discharge relation due to changes in the physical features that control the station (e.g. the riverbed). Where scouring or deposition processes affect the stability of the river bed, regular measurement of the channel cross-sectional bed profile is needed to enable adjustment of the rating curve to the changed conditions (Figures V.8 and V.9a below). Such measurements should always be carried out with reference to a pre-determined fixed point. Having a fixed reference point also allows comparisons of flow records before and after a waterlevel recorder or staff gauge is washed away during a flood.

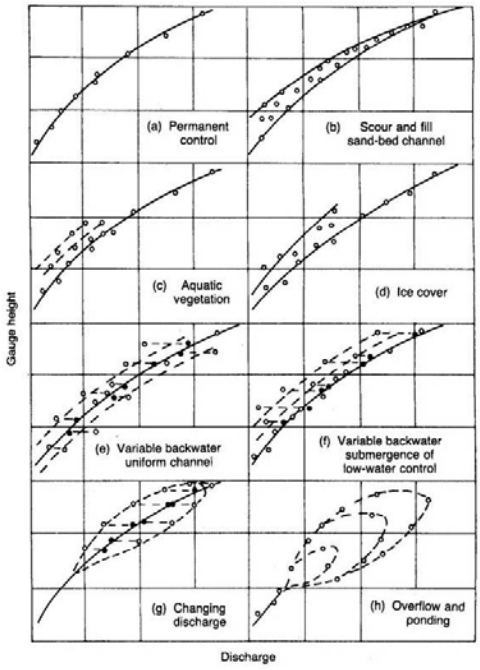

Fig. 4.4 Rating curves for different hydraulic conditions.

Figure V.8. *Possible causes of shifts in the Q-H relationship.*

V.2.3 *Stage-discharge relations (rating curves)*

A good stage-discharge relationship is a prerequisite for the conversion of measured stage records to reliable discharge records. For optimum results, the rating curve needs to be based on measured *Q-H* data pairs for a wide range of flow conditions and a stable section. It is important that a unique relation exists between stage and discharge at a gauging site, i.e. the mean velocity across a channel section should be the same for a given stage height. In practice, this is not always achieved for various reasons (Figure V.8).

Furthermore, discharge data are often collected during planned station visits that mainly take place during regular office hours. This tends to limit data collection to baseflow situations whereas the less frequently occurring high flow situations are easily missed. Prediction of high flows can then only be achieved if the rating curve is extrapolated beyond the range for which measurements are available. Clearly, the more data points used to develop the rating curve, the better.

Figure V.9ab illustrates these points for the Chiquito River in northern Costa Rica (gauged by the current project). Evidence of changes in the natural control in the form of different discharges for the same stage was found during the last month of observations (Figure V.9a). Several large storms had caused massive landsliding in the upper catchment. The sediment generated in this way was transported downstream and changed the riverbed.

Measured discharges for the Chiquito River were only available for stage heights up to ca. 0.77 m (corresponding with a discharge of ca. 22 m^3/sec; Figure V.9a) whereas the maximum observed water level was 1.3 m. Extrapolation of the rating curve was required, therefore. Conform to theoretical expectations (Figure V.10) the streamflow velocity in the Chiquito reached a maximum value at higher stages and this knowledge was used in combination with corresponding values of channel cross-sectional area to extrapolate the stage-discharge curve to the observed range of stages (Figure V.9b).

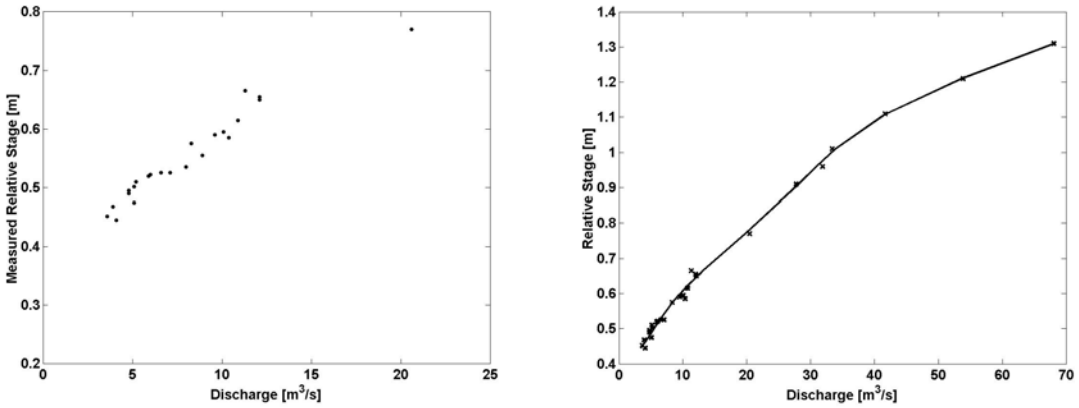

Figure V.9. *(a) Measured stage-discharge relation for the Rio Chiquito (northern Costa Rica) and (b) Extrapolated discharge data and fitted rating curve.*

Special problems may occur during conditions of rapidly changing discharge (e.g. during intense rain storms) because velocity and discharge are greater during the rising stage of the hydrograph than under steady flow conditions for the same stage. Large rivers with a low gradient are especially sensitive to this looping effect (Figure V.8g). Smaller streams with good section control have a negligible looping effect. Information on streamflow velocity during flood stages can be obtained using floats (see chapter 13.10 in the online manual).

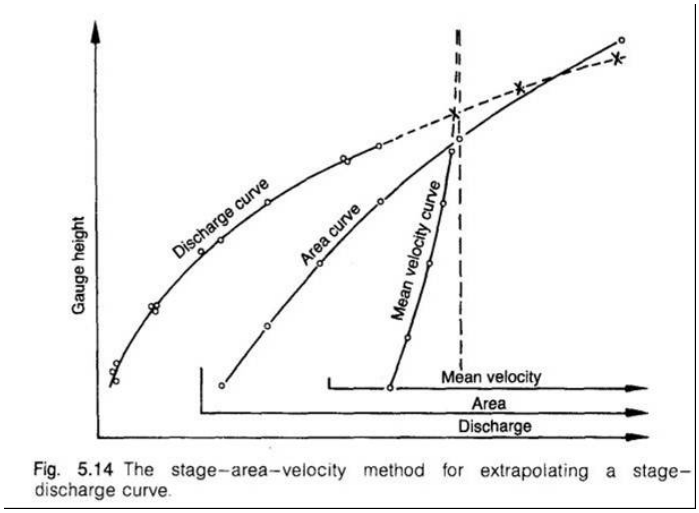

Figure V.10. *The stage-area-velocity method for extrapolating a rating curve / data quality control.*

V.3 **Measuring stage (water level)**

V.3.1 *Background considerations*

The stage, or gauge height, of a stream is usually expressed in cm or m above a predefined reference level. Stage records may be obtained from a series of systematic readings of non-recording gauges (e.g. a staff gauge) but preferably using automatic water-stage recorders of which there are various types available (see suggestions for further reading at the end of this document).

Thus, obtaining a stage record requires:

- Definition of a reference level (gauge datum).
- Installing a staff gauge for manual referencing.
- Automatic water level recording.

A convenient and meaningful elevation datum should be selected for the station. The datum should be permanent for the expected life of the station. For artificial structures the datum is usually set at the elevation of zero flow (e.g. the bottom of the 'V' in a V-notch; Figure V.4). For a natural control site (i.e. velocity-area station, Figure V.5) an arbitrary datum below the elevation of zero flow is usually chosen to avoid negative gauge heights (see also section V.2.2.2).

A staff gauge typically consists of a graded metal or wooden board, or a plastic tape attached to a board or pipe from which readings of stage (in cm) can be taken directly by measurement of the height of the water level above the predetermined reference height (Figure V.11). Staff gauges are often used in addition to an automatic water level recorder as a manual reference, for example in relation to data quality control. In the case of artificial structures in forested areas where blockage of the weir by floating organic debris tends to occur regularly, frequent manual readings (as well as cleaning of the weirs) are recommended.

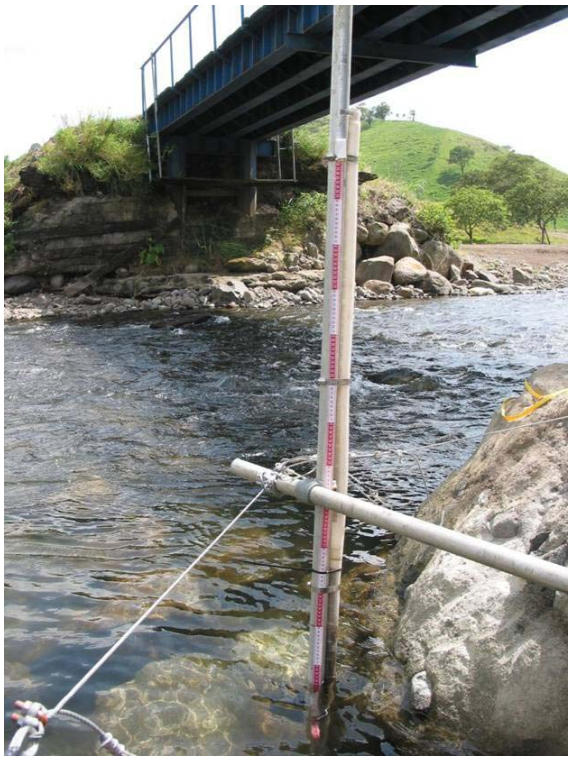

Figure V.11. *Tape measure used as a staff gauge for manual water level readings. Diver water-level recording device placed in vertical tube to the right of staff gauge.*

As the name implies, a water level recorder produces a record of water surface elevation over time. Instrument output may be analog (e.g. a trace on paper) or, more commonly of late, digital. The digital format allows for faster data processing. Regardless of recorder type used, it should be capable of covering the full range of water surface changes expected at a gauging site. Further important considerations upon installation of a water level recorder include the proper sizing and installation of a

'stilling' well in which the sensor is to be placed, and the establishment of a fixed reference datum level for the site. The gauge should be accessible at all times and of sufficiently robust construction to ensure instrumental security and reliability.

The required water-level recording frequency (in the case of electronic observations) depends on the size of a catchment. Small cloud forest headwater catchments that respond rapidly to rainfall typically require a recording every minute whereas a frequency of 5 minutes is sufficient for rivers draining catchments of intermediate size (e.g. 100 km^2). Data retrieval frequency should match the chosen data recording frequency, sensor storage capacity as well as consider logistical factors such as time constraints and travel distance. However, frequent data retrieval also permits more frequent control of instrumental malfunctioning (e.g. dead batteries) as well as overall station performance (e.g. blocking of flow by leaves or branches trapped behind a V-notch weir). Downloading of water level data onto a laptop computer on a weekly basis for small catchments (1-min recordings) and once every fortnight for more remote larger rivers (5-min recordings) worked well in the present case.

3.2 *Water-level recorder and installation*

Digital pressure transducer sensors are widely used nowadays to record the changes in water level through the measurement of the corresponding change in water pressure. Calibration of the instruments gives the water level expressed in cm. The current project employed a so-called Diver sensor produced by Van Essen Instruments, Delft, The Netherlands (Figure V.12). Detailed technical information on the Diver sensors can be found at the manufacturer's website (www.vanessen.com). The DI240 type was selected because of its large measuring range (4 m) and good resolution (0.1 cm). The DI240 consists of a combined sensor and data-logger capable of storing its own measured data (cf. Figure V.12). The sensor provides an absolute pressure reading which requires simultaneous atmospheric pressure readings using a so-called Baro-Diver (type DI250) manufactured by the same company.

Figure V.12. *Diver DI240 device for the automatic recording of water levels.*

The DI240 Diver sensor can easily be installed by lowering it inside a permeable access tube placed inside the stream (Figures V.11 and 13). The tube is typically placed at the side of the stream and attached to a metal pole that has been hammered thoroughly into the riverbed for greater stability. Additional support may be afforded by further constructions linking the metal pole to the river bank (as required). Both the permeable tube with the DI240-sensor and the staff gauge used for manual readings of water levels are attached to the metal pole (cf. Figure V.11). Regular checking of the position of the metal pole in the river bed against an independent absolute reference level is needed.

In the case of V-notch weirs it is convenient to equate the zero stage on the staff gauge or measuring tape with the bottom of the V in the notch (zero flow). However, the tip of the DI240 sensor itself should be placed below the bottom of the V-notch as the sensor is incapable of detecting the first few

cm's of water above its tip and as such does not give a zero stage at zero flow. Such an arrangement helps to keep the sensor submerged and so makes the reading less sensitive to temperature changes. Naturally, manual stage readings are required to determine the offset of (i) the water level sensor relative to the level of zero flow, (ii) between the water level sensor and the atmospheric pressure sensor (if any), and (iii) to detect for shifts in the calibration of the sensor.

Figure V.13. *Diver DI240 water level sensor (temporarily taken out of installation tube shown in background) and laptop computer placed on top of sharp-crested weir during downloading of stage data.*

The DI250 Baro-Diver measuring atmospheric pressure is to be placed in the air at a nearby location that should ideally be subject to similar temperatures as experienced by the DI240 in the water. Normally, pressure deviations due to differences in temperature between the two sensors become noticeable only if the Baro-Diver is heated substantially by direct sunlight. A shaded position for the sensor is advisable, therefore. Allowing for the offset between the level of zero flow and the tip of the sensor, the stage at a V-notch weir is now given by the difference between the Diver reading in the river (DI240) and the atmospheric pressure reading (DI250). The stage for a natural control site is derived in a similar way as for artificial structures although this time stage is expressed relative to a reference datum level as explained previously.

Disclaimer: This publication is an output from a research project funded by the United Kingdom Department for International Development (DFID) for the benefit of developing countries. The views expressed are not necessarily those of DFID (R7991, Forestry Research Programme).

Suggested reading and websites

Cloud forest hydrology

- Bruijnzeel, L.A. (2001). Hydrology of tropical montane cloud forests: A reassessment. *Land Use and Water Resources Research* **1**: 1.1-1.18. (http://www.luwrr.com)

- Bruijnzeel, L.A. and Proctor, J. (1995). Hydrology and biogeochemistry of tropical montane cloud forests: what do we really know? In Hamilton, L.S. et al. (Editors), *Tropical Montane Cloud Forests. Ecological Studies* **110**: 38-78.

- Zadroga F. 1981. The hydrological importance of a montane cloud forest area of Costa Rica. In *Tropical agricultural hydrology*, Lal R, Russell EW (eds). John Wiley & Sons, New York, USA, 59-73.

Precipitation

- Førland, E.J. et al. (1996). *Manual for operational correction of Nordic precipitation data*. Norwegian Meteorological Institute, Oslo, Norway.
- Nespor, V. and Sevruk, B. (1999). Estimation of wind-induced error of rainfall gauge measurements using a numerical simulation. *Journal of Atmospheric and Oceanic Technology* **16**: 450-464.
- Sevruk, B. and Zahlavova, L. (1994). Classification system of precipitation gauge site exposure: evaluation and application. *International Journal of Climatology* **14**: 681-689.
- Sharon, D. (1980). The distribution of hydrologically effective rainfall incident on sloping ground. *Journal of Hydrology* **46**: 165-188.
- Sharon, D. and Arazi, A. (1997). The distribution of wind-driven rainfall in a small valley: an empirical basis for numerical model verification. *Journal of Hydrology* **201**: 21-48.
- Smith, J.A. (1992). Precipitation. Pp. 3.1-3.47 in Maidment, D.R. (Editor), *Handbook of Hydrology*, McGraw-Hill, Inc.
- Van Dijk, A.I.J.M. et al. (2002). Rainfall intensity – kinetic energy relationships: a critical literature appraisal. *Journal of Hydrology* **261**: 1-23.
- World Meteorological Organization (1996). *Guide to Meteorological Instruments and Methods of Observation* (6th Edition). *WMO Guide* No. **8**. Secretariat of the World Meteorological Organization, Geneva, Switzerland.
- Yang, D. et al. (1998). Adjustment of daily precipitation data at 10 climate stations in Alaska: Application of WMO intercomparison results. *Water Resources Research* **34**: 241-256 .

On-line information on meteorological equipment and suppliers:

- www.meteo-technology.com
- www.lacrossetechnology.fr (tipping buckets, type WS7048)

Fog

- Bruijnzeel, L.A., Eugster, W. and Burkard, R. (2005). Fog as a hydrological input. Chapter 38 in Anderson, M.G. and McDonnell, J. (Editors), *Encyclopedia of Hydrological Sciences*. John Wiley, Chichester, pp. 559-582.
- Burkard, R., Bützberger, P. and Eugster, W. (2003). Vertical fogwater flux measurements above an elevated forest canopy at the Lägeren research site, Switzerland. *Atmospheric Environment* **37**: 2979-2990.
- Frumau, K.F.A. et al. (2006). Fog gauge performance as a function of wind speed in northern Costa Rica. In: L.A. Bruijnzeel et al. (Editors), *Forests in the mist: Science for Conservation and Management of Tropical Montane Cloud Forests.* University of Hawaii Press, Honolulu (in press).

- Holwerda, F., *Bruijnzeel, L.A.* & Scatena, F.N. (2006). Estimating event fog deposition and duration using passive fog gauges and throughfall measurements at Pico del Este, Puerto Rico. In: L.A. Bruijnzeel et al. (editors), *Forests in the mist: Science for Conservation and Management of Tropical Montane Cloud Forests.* University of Hawaii Press, Honolulu (in press).
- Holwerda, F. et al. (2006). Estimating fog deposition at a Puerto Rican elfin cloud forest site: comparison of the water budget and eddy covariance methods. *Hydrological Processes* (in press).
- Nylander, P. et al. P. (1997). *Present Weather Detector PWD11 - User's Guide.* Vaisala, Helsinki, Finland.
- Tobón, C. et al. (2006). Water dynamics of epiphytic vegetation in a lower montane cloud forest: interception, storage and evaporation of horizontal precipitation. In: L.A. Bruijnzeel et al. (Editors), *Forests in the mist: Science for Conservation and Management of Tropical Montane Cloud Forests.* University of Hawaii Press, Honolulu (in press).

On-line information on equipment or materials for the construction of fog gauges:

- www.asmfg.com/shade.htm (Phifer Shadescreen for Juvik-type gauge)
- www.lacrossetechnology.fr (tipping buckets, type WS7048)
- www.opticalsensors.se (OFS-Mk2 visibility meter)

Throughfall and stemflow

- Holwerda, F., Scatena, F.N. and Bruijnzeel, L.A. (2006). Throughfall in a Puerto Rican lower montane rain forest: a comparison of sampling strategies. *Journal of Hydrology* (in press).
- Lloyd, C.R., Marques-Filho, A., 1988. Spatial variability of throughfall and stemflow measurements in Amazonian rain forest. Agricultural and Forest Meteorology 42, 63-73.
- Schellekens, J. et al. (1999). Modelling rainfall interception by a lowland tropical rain forest in Eastern Puerto Rico. *Journal of Hydrology* 225, 168-184.

Evaporation

- Brutsaert, W.H. (1982). *Evaporation into the Atmosphere*. D. Reidel Publishing, Dordrecht, The Netherlands.
- Calder, I.R. (1990). *Evaporation in the Uplands*. J. Wiley, chichester.
- Garratt, J.R. (1992). The Atmospheric Boundary Layer. Cambridge Atmosphere and Space Science Series, Cambridge University Press, pp. 15-144.
- Holwerda, F. (2005). *Water and energy budgets of rain forests along an elevation gradient under maritime tropical conditions.* PhD Thesis, Vrije Universiteit, Amsterdam, The Netherlands. (available on-line at: www.falw.vu.nl/onderzoeksinstituten/index (Hydrology and Geo-environmental Sciences / Hydrology PhD Dissertations online) .
- Raupach, M.R. and Finnigan, J.J. (1988). Single-layer models of evaporation from plant canopies are incorrect but useful, whereas multilayer models are correct but useless. *Australian Journal of Plant Physiology* **15**: 705-716.
- Shuttleworth, W.J. (1992). Evaporation. pp. 4.1-4.53 in Maidment, D.R. (Editor), *Handbook of Hydrology*, McGraw-Hill, Inc.
- Van der Molen, M.K. (2002). *Meteorological impacts of land use change in the maritime tropics*. PhD Thesis, Vrije Universiteit, Amsterdam, The Netherlands. (available on-line at: www.falw.vu.nl/onderzoeksinstituten/index (Hydrology and Geo-environmental Sciences / Hydrology PhD Dissertations online)

On-line information on meteorological equipment and suppliers:

- www.meteo-technology.com

Soil physical techniques

- Baver., L.D. (1956). *Soil Physics*. J. Wiley and Sons Inc., New York.
- Hillel, D. (1998). *Introduction to Environmental Physics*. Academic Press Inc., California.
- Saigusa, M., Shoji, S. and Nakaminami, H. (1987). Measurement of water retention at 15 bar tension by pressure membrane method and available moisture of Andosols. Japanese Journal of Soil Science and Plant Nutrition **58**: 374-377.
- Tindall, J. et al. (1999). *Unsaturated Zone Hydrology for Scientists and Engineers*. Chapters 4 (Potential and thermodynamics of soil water), 6 (Principles of water flow in soil), 7 (Unsaturated water flow in soil), 11 (Infiltration and drainage), and Appendix 1 (Site characterization and monitoring devices). Prentice Hall US, ISBN 0-13-660713-6.
- Tobón-Marin C. (1999). Monitoring and modelling hydrological fluxes in support of nutrient cycling studies in Amazonian rain forest ecosystems. *Tropenbos Series* no. **17**, TROPENBOS, Wageningen, the Netherlands. 169 pp.
- Tobón, C. et al. (2006). Changes in soil hydraulic properties and soil water status after conversion of tropical montane cloud forest to pasture in northern Costa Rica. In: L.A. Bruijnzeel et al. (Editors), *Forests in the mist: Science for Conservation and Management of Tropical Montane Cloud Forests.* University of Hawaii Press, Honolulu (in press).

On-line information on soil moisture sensors (TDR, tensiometers):

- www.campbellsci.com: products, sensors, soil water
- www.ums-muc.de (automatic tensiometers)
- www.sdec-france.com (manual tensiometers and data logging)
- www.soilmeasurement.com (idem)
- www.soilmoisture.com (idem, tension infiltrometer)
- www.soiltest.com \ ELE International Inc. (Guelph permeameter)

Streamflow measurement

- Bos, M.G. (1989). *Discharge Measurement Structures* (3rd edition), ILRI Publication no. 20, Institute for Land Reclamation and Irrigation, Wageningen, The Netherlands, ISBN 9070754150. Also available on-line at: http://www.alterra.wur.nl/NL/publicaties/ILRI-publicaties/Downloadable+publications/
- Herschy, R.W. (1995). *Streamflow Measurement* (2nd edition). E & FN SPON, an imprint of Chapman & Hall, ISBN 0419194908.
- On-line manual on streamflow measurement: http://www.usbr.gov/pmts/hydraulics_lab/pubs/wmm/

On line information on automatic water level recorders and velocity meters:

- www.campbellsci.com: products, sensors, water level
- www.globalw.com
- www.solinst.com
- www.in-situ.com
- http://www.rickly.com/sm/stage_measurement.htm
- http://www.inmtn.com/html/water/water.htm
- www.vanessen.com (Diver sensors)
- www.ott-hydrometry.de (current-meters).

Appendix 1:
Study sites of the FIESTA-project and summary of equipment used

Measurement sites: an intensive field measurement campaign was conducted between August-September 2002 and August 2004 to obtain quantitative insight into the hydrological functioning of plots or small catchment areas under the chief vegetation types of the study area, viz.: (i) old-growth, tall windward cloud forest, (ii) 30-year-old pasture with scattered remnant trees, (iii) isolated 15-20 year-old secondary woodland blocks surrounded by pasture, and (iv) stunted, wind-swept ridge-top elfin cloud forest. All sites were located within the headwaters of the Caño Negro and Río Chiquito catchments that drain towards the Atlantic side of Costa Rica (see Figure A.1 for locations). In addition, the climate and streamflow for the entire 91.4 km^2 Río Chiquito catchment, which had 63% of its original forest cover converted to pasture by 1992 but has maintained its headwater area largely under cloud forest, were monitored as well for model validation purposes at the operational scale.

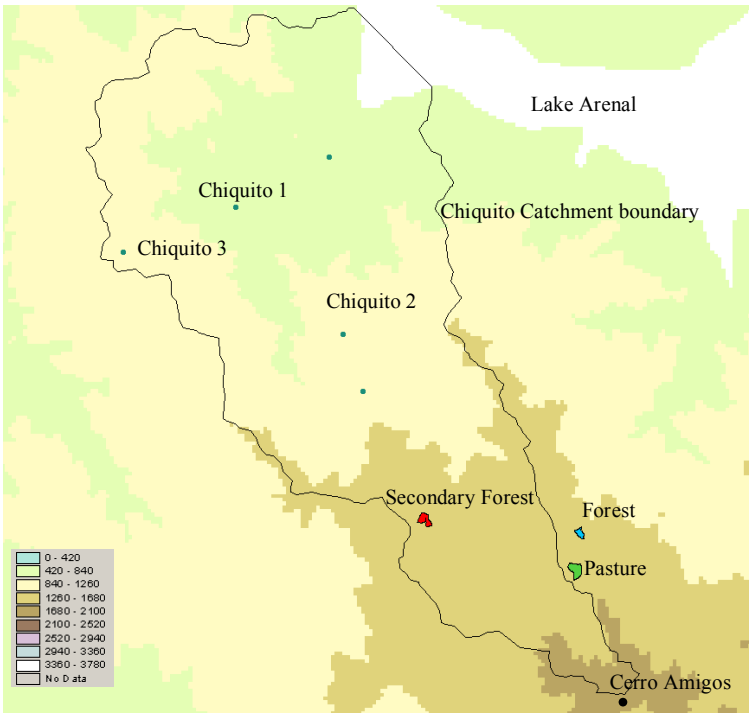

Figure A.1. *Project site locations in and around the Río Chiquito catchment in northern Costa Rica.*

Groups of activities: the overall work can be divided into a series of distinct, yet closely linked successional groups of activities: (i) the collection of detailed topographic climatic, vegetation, soil and hydrological data at the plot- (100-500 m^2), small catchment- (<100 ha), and operational catchment scales (100 km^2), respectively; (ii) the formulation of process-based, spatially distributed hydrological models for use at local, operational, and national scales, respectively; and (iii) the validation of the operational-scale catchment model using both existing and newly collected data as a preliminary to (iv) applying the model to assess the hydrological impacts of various land-cover change scenarios. In a parallel exercise conducted at the (inter)national scale (v), the impacts of similar scenarios for land-cover change, plus those of prescribed changes in climate, were assessed as well. An overview of the chief results of the project can be found in the Final Technical Report, with additional details on the simulations carried out at the operational and national scale being given in Annexes 3 and 4 to the FTR, respectively.

An overview of the micro-catchment (3.5 ha) under cloud forest is given in Figure A.2 whereas Figure A.3 shows the instrumental set-up for the catchment. A similarly heavily instrumented catchment under pasture was situated nearby and shown in Figures A.4 and A.5. Additional details on instrumentation are given in the Table at the end of this Appendix.

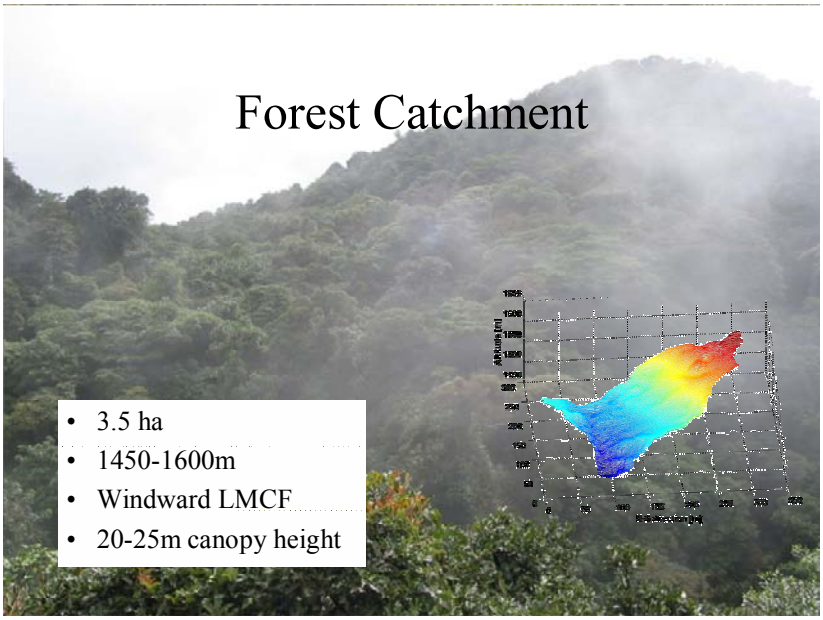

Figure A.2. *Overview of cloud forested micro-catchment, San Gerardo.*

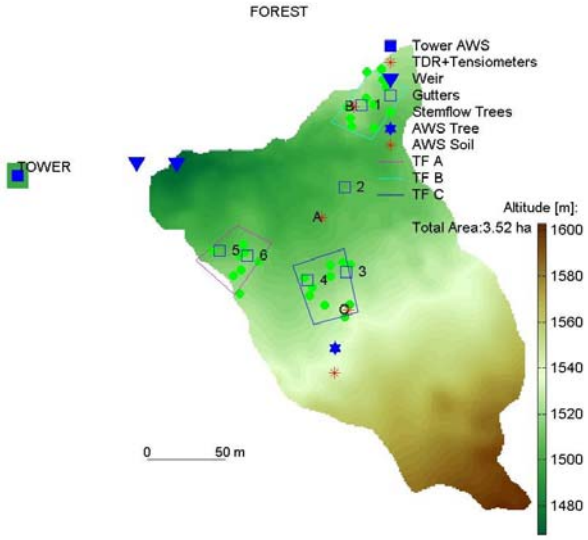

Figure A.3. *Location of meteorological tower, automatic weather stations (AWS), streamflow weirs, soil water (TDR) and throughfall/stemflow plots (TF) in the cloud forest micro-catchment, San Gerardo.*

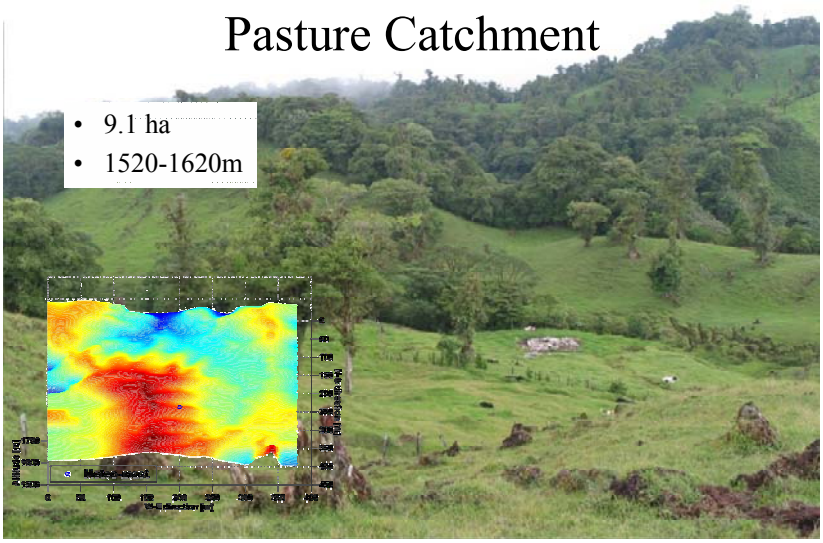

Figure A.4. *Overview of micro-catchment under pasture, San Gerardo.*

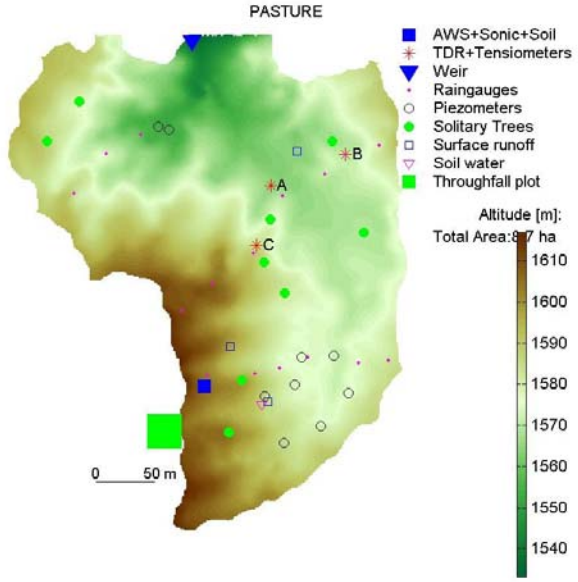

Figure A.5. *Location of automatic weather station (AWS), rain gauges, streamflow weir, soil water (TDR), overland flow and groundwater (piezometer) stations in the pasture micro-catchment.*

The main climatic data collection sites in the two catchments are portrayed in Figure A.6, viz. a 25 m high scaffolding tower for measurements above the cloud forest canopy (left-hand panel), and various masts for measurements at the pasture site (righ-hand panel).

Figure A.6. Climate measurements at San Gerardo: instrumented canopy tower in cloud forest (left) and main pasture station (right).

Similarly intensive measurements were carried out at a secondary forest site (Figure A.7a) located near Monte de Olivos within the Rio Chiquito catchment (see plan view in Figure A.8). In addition, a station for the measurement of precipitation, fog and wind was set-up at Cerro Amigos on the continental divide. Cerro Amigos represents the most extreme situation concerning gustiness and cloudiness in the area (Figure A.7b).

Figure A.7. *Monte de Olivos secondary forest station (left) and Cerro Amigos station (right).*

Finally, three basic climate stations were installed at different elevations within the Rio Chiquito catchment to improve the spatial coverage of climatic information for the area (Figure A.9)

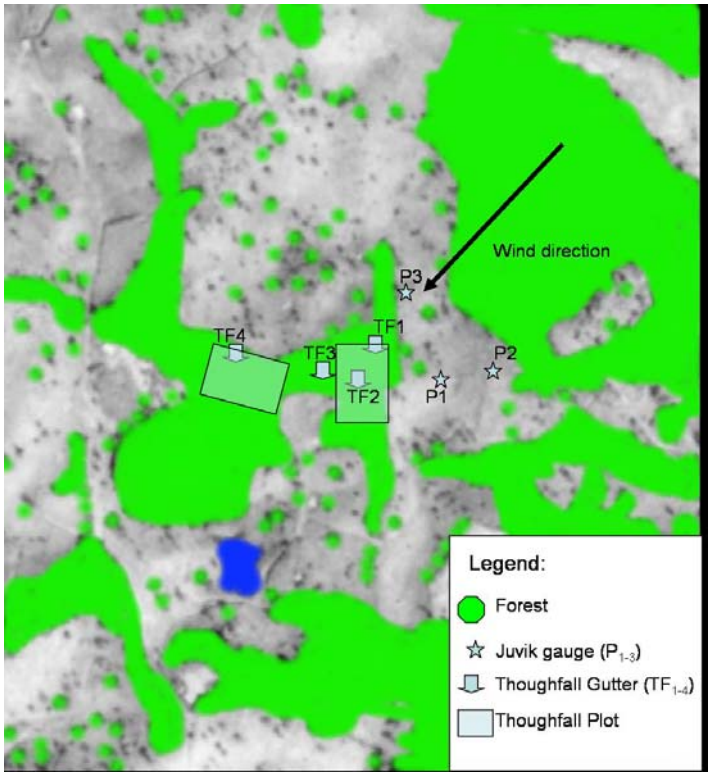

Figure A.8. *Plan view of Monte de Olivos secondary forest site.*

Figure A.9. *Automatic weather stations Chiquito #2 (left) and Chiquito # 3 (right) with Volcan Arenal in the background.*

Table A.1. *Overview of instruments used at the respective measuring stations.*

FOREST SITE

Water Input				Instrument			Datalogging	Measuring	Storage	Data	
Parameter	Plot	Reps.	Height [m]	General	Specification	Brand	Instrument	Frequency	Frequency	start	end
PV	Tower	1	25	Rain gauge	Standard (100cm²)	VUA	Measuring cylinder	Daily	Daily	Oct-02	Aug-04
PV	Tower	1	25	Rain gauge	Standard,shielded	VUA	Measuring cylinder	Daily	Daily	Dec-02	Aug-04
PV	Tower	1	25	Rain gauge	ARG100 (510cm²)	Campbell Scientific, Inc.	Campbell 23x	15sec	1min	Oct-02	Aug-04
PV	Tower	1	22	Rain gauge	Modified Juvik (100cm²)	VUA	Campbell 23x	15sec	1min	Oct-02	May-05
PH	Tower	1	22	Fog gauge	Modified Juvik (540cm²)	VUA	Campbell 23x	15sec	1min	Oct-02	May-05
PH	Tower	3	6,14,22	Fog gauge	Wire Harp (2500cm²)	VUA	Campbell 23x	15sec	1min	Oct-02	Aug-04
PT	Tower	1	25	Rain gauge	Spherical Vanes	VUA	Tinytag TGPR-1201	5 min	5min	Feb-05	May-05
PT	Tower	1	25	Rain gauge	Spherical Cylinders	VUA	Tinytag TGPR-1201	5 min	5min	Feb-05	May-05
PW	Tower	1	25	Fog gauge	Passive Fogbox	VUA	Campbell 23x	15sec	1min	Oct-03	May-05
PF	Tower	1	25	Fog gauge	Passive Fogbox	VUA	Campbell 23x	15sec	1min	Oct-03	May-05
'PF'	Tower	1	25	Fog sensor	OFS-MK1	Lofving Optical Sensors	Campbell 23x	15sec	1min	Oct-02	Aug-04
'PW'	Tower	1	25	Fog sensor	OFS-MK1	Lofving Optical Sensors	Campbell 23x	15sec	1min	Oct-02	Aug-04
PV	Tree	1	35	Rain gauge	Modified Juvik (100cm²)	VUA	Campbell 23x	15sec	1min	May-03	Oct-03
PH	Tree	1	35	Fog gauge	Modified Juvik (540cm²)	VUA	Campbell 23x	15sec	1min	May-03	Oct-03
PTF	A,B,C	2	1	Gutter	Steel (1.2m²)	VUA	Tinytag TGPR-1201	1min	1min	Oct-02	May-05
PTF	A,B,C	20	0.5	Rain gauge	Standard (100cm²)	VUA	Measuring cylinder	Daily	Daily	Oct-02	Oct-03
PTFemergent	3 Trees	24	0.5	Rain gauge	Standard (100cm²)	Local funnel	Measuring cylinder	Daily	Daily	May-03	Jul-03
PTFemergent	2 Trees	20	0.5	Rain gauge	Standard (100cm²)	Local funnel	Measuring cylinder	Daily	Daily	Dec-03	Mar-04
PSTF	C	1	1	Stemflow	Tube	None	Campbell 23x	15sec	1min	May-03	Oct-03
PSTF	A,B,C	10	1	Stemflow	Tube	None	Measuring cylinder	Daily	Daily	Apr-03	Oct-03

PASTURE SITE

Water Input				Instrument			Datalogging	Measuring	Storage	Data	
Parameter	Plot	Reps.	Height [m]	General	Specification	Brand	Instrument	Frequency	Frequency	start	end
PV	Meteo	1	0.3	Rain gauge	Standard (100cm²)	VUA	Measuring cylinder	Daily	Daily	Oct-02	Nov-04
PV	Meteo	1	0.3	Rain gauge	Standard,shielded	VUA	Measuring cylinder	Daily	Daily	Dec-02	Nov-04
PV	Pasture	14	0.3	Rain gauge	Standard (100cm²)	VUA	Measuring cylinder	Daily	Daily	Jun-03	Nov-04
PH	Meteo	3	0.5	Fog gauge	Modified Juvik (540cm²)	VUA	Measuring cylinder	Daily	Daily	Dec-03	Nov-04
PV	Meteo	1	0.3	Rain gauge	ARG100 (510cm²)	Campbell Scientific, Inc.	Campbell 23x	15sec	1min	Oct-02	Aug-04
PV	Meteo	1	0.3	Rain gauge	VUA (510cm²)	VUA	Campbell 23x	15sec	1min	Sep-04	May-05
PV	Meteo	1	2.3	Rain gauge	VUA (510cm²)	VUA	Campbell 23x	15sec	1min	Dec-03	Aug-04
PV	Meteo	1	2.3	Rain gauge	Modified Juvik (100cm²)	VUA	Campbell 23x	15sec	1min	Oct-02	May-05
PH	Meteo	1	2	Fog gauge	Modified Juvik (540cm²)	VUA	Campbell 23x	15sec	1min	Oct-02	May-05
PH	Meteo	1	2	Fog gauge	Modified Juvik, double	VUA	Campbell 23x	15sec	1min	Mar-03	Aug-04
PH	Meteo	1	2	Fog gauge	Wire Harp (2500cm²)	VUA	Campbell 23x	15sec	1min	Oct-02	Aug-04
PTF	A	25	0.5	Rain gauge	Standard (100cm²)	Local funnel	Measuring cylinder	Daily	Daily	Dec-02	Sep-03
PTFsolitary	10 Trees	T=94	0.5	Rain gauge	Standard (100cm²)	Local funnel	Measuring cylinder	Daily	Daily	May-04	Nov-04

P=Precipitation, V=vertical, W=Wind-driven, F=Fog, H=W+F=horizontal, T=f(V,H)=Total, STF=stemflow, TF=throughfal

SECONDARY FOREST

Water Input				Instrument			Datalogging	Measuring	Storage	Data	
Parameter	Plot	Reps.	Height [m]	General	Specification	Brand	Instrument	Frequency	Frequency	start	end
PV	All	13	0.3	Rain gauge	Standard (100cm²)	VUA	Measuring cylinder	Daily	Daily	Nov-03	Oct-04
PV	Meteo	1	0.3	Rain gauge	Standard (100cm²)	VUA	Measuring cylinder	Daily	Daily	Nov-03	Oct-04
PV	Meteo	1	2.3	Rain gauge	Modified Juvik (100cm²)	VUA	Campbell 23x	15sec	1min	Nov-03	Oct-04
PH	Meteo	1	2	Fog gauge	Modified Juvik (540cm²)	VUA	Campbell 23x	15sec	1min	Nov-03	Oct-04
PV	Corner	1	2.3	Rain gauge	Modified Juvik (100cm²)	VUA	Campbell 23x	15sec	1min	Nov-03	Aug-04
PH	Corner	1	2	Fog gauge	Modified Juvik (540cm²)	VUA	Campbell 23x	15sec	1min	Nov-03	Aug-04
PV	Treeline	1	2.3	Rain gauge	Modified Juvik (100cm²)	VUA	Campbell 23x	15sec	1min	Nov-03	Aug-04
PH	Treeline	1	2	Fog gauge	Modified Juvik (540cm²)	VUA	Campbell 23x	15sec	1min	Nov-03	Aug-04
PTF	A,B	2	1	Gutter	Steel (1.2m²)	VUA	Tinytag TGPR-1201	1min	1min	Nov-03	Nov-04
PTF	A,B	20	0.5	Rain gauge	Standard (100cm²)	VUA	Measuring cylinder	Daily	Daily	Nov-03	Oct-04
PTFemergent	2 Trees	20	0.5	Rain gauge	Standard (100cm²)	Local funnel	Measuring cylinder	Daily	Daily	Nov-03	Oct-04
PTFsolitary	2 Trees	3&7	0.5	Rain gauge	Standard (100cm²)	Local funnel	Measuring cylinder	Daily	Daily	May-04	Oct-04
PSTF	A,B	10	1	Stemflow	Tube	None	Measuring cylinder	Daily	Daily	Nov-03	Nov-04

CHIQUITO STATIONS				Instrument			Datalogging	Measuring	Storage	Data	
Parameter	Plot	Reps.	Height [m]	General	Specification	Brand	Instrument	Frequency	Frequency	start	end
PV	1,2,3	1	0.5	Rain gauge	Funnel (510cm²)	Local, plastic	Measuring cylinder	2 Weekly	2 Weekly	Apr-03	Jul-04
PV	1,2,3	1	2.3	Rain gauge	Modified Juvik (100cm²)	VUA	Campbell BDR320	15sec	10 min	Apr-03	Jul-04
PH	1,2,3	1	2	Fog gauge	Modified Juvik (540cm²)	VUA	Tinytag TGPR-1201	10 min	10 min	Apr-03	Jul-04

CERRO AMIGOS STATION				Instrument			Datalogging	Measuring	Storage	Data	
Parameter	Plot	Reps.	Height [m]	General	Specification	Brand	Instrument	Frequency	Frequency	start	end
PV	1	1	2.5	Rain gauge	Modified Juvik (100cm²)	VUA	Tinytag TGPR-1201	10 min	10 min	Apr-03	May-04
PH	1	1	2.2	Fog gauge	Modified Juvik (540cm²)	VUA	Tinytag TGPR-1201	10 min	10 min	Apr-03	May-04

P=Precipitation, V=vertical, W=Wind-driven, F=Fog, H=W+F=horizontal, T=f(V,H)=Total, STF=stemflow, TF=throughfal